Charged Block Copolymers with Phosphonate Anchor Groups for Antibacterial Polymer Brushes

D I S S E R T A T I O N

Zur Erlangung des akademischen Grades des
Doktor rerum naturalium (Dr. rer. nat.)

vorgelegt
der Fakultät für Naturwissenschaften
Universität Paderborn

Eingereicht von
M.Sc. Rafael Methling

Paderborn 2023

Gutachter Prof. Dr. Dirk Kuckling

Prof. Dr. Jan Paradies

Eingereicht am: 6.2.2023

Datum der Verteidigung: 16.3.2023

Diese Arbeit wurde in einem Zeitraum vom 1. Januar 2020 bis zum 31. Dezember 2022 im Fachbereich Organische und Makromolekulare Chemie der Universität Paderborn unter der Leitung von Prof. Dr. Dirk Kuckling angefertigt.

Abstract

For several decades dental implants have ranked among standard treatments in healthcare and gain more and more relevance due to aging demographics and demands for therapies which ensure a high quality of life. Since the integration of artificial teeth constitutes a severe intrusion in the patient's tissue and bone structure, the procedure is linked to secondary diseases caused by infections of the implant. Proliferation of bacteria can lead to destruction of tissue, bone loss and eventually implant failure. Thus, current research is focused on developing preventive strategies by optimizing the interface between implant and endogenous structures. New approaches encompass either impeding bacterial proliferation or facilitating the desired attachment of host tissue. Using functional polymer coatings, the implant surface can be functionalized to feature one of these properties or even both.

In this work, linear block copolymers with anchoring segments and polycationic, antibacterial segments were developed using RAFT polymerization. The block structure allows the construction of polymer brushes with one segment linked to a metal surface and the other towering into the supernatant solution, rendering the surface contact-killing towards bacteria. Phosphonic acid groups were employed in the anchor block to allow the grafting of ready-made polymers onto the surface from solution. This approach allows a convenient coating of arbitrary geometries, making it particularly suitable for implant functionalization. By varying the number of anchoring groups, the effect on grafting density on titanium oxide was investigated. Coated substrates were further examined regarding physicochemical and biological properties, verifying brush formation and its antibacterial effect.

Furthermore, a series of adsorbable polymers with improved biocompatibility was synthesized by tuning the amphiphilic balance of the antibacterial block. Hydrophobic groups were incorporated in the otherwise polycationic chain at different ratios to elucidate the optimal block composition. To facilitate the adhesion of human cells even more, an electrophilic moiety was introduced in a terminal polymer block, allowing the incorporation of adhesion promoting biomolecules in "click"-like reactions.

Moreover, the synergy of antibacterial/polycationic and antifouling/polyzwitterionic properties in polymer brushes based on anchorable linear polymers was explored. Due to opposite solubility with regards to ionic strength of aqueous solutions, a polymer brush featuring both moieties exhibited salt-responsive behavior. It was demonstrated that the surface of coated substrates could be switched by adjusting the salt concentration and inhibited colonization of bacteria when tested against Gram-positive and -negative strains.

Kurzzusammenfassung

Zahnimplantate gehören seit mehreren Jahrzehnten zum Standardrepertoire in der Dentalmedizin und gewinnen aufgrund der alternden Bevölkerung und dem Bedarf an Therapien, die eine hohe Lebensqualität gewährleisten, immer mehr an Bedeutung. Da das Einsetzen von fest verankertem Zahnersatz einen schwerwiegenden Eingriff in Gewebe und Knochenstruktur des Patienten darstellt, ist das Verfahren häufig mit Folgeerkrankungen verbunden, die durch Infektionen des Implantats verursacht werden. Der Befall mit Bakterien kann zur Zerstörung des umliegenden Gewebes, zu Knochenverlust und schließlich zur Abstoßung des Implantats führen. Daher konzentriert sich aktuelle Forschung auf die Entwicklung von Präventivmaßnahmen durch Optimierung der Grenzfläche zwischen Implantat und körpereigenen Strukturen. Neue Strategien verhindern beispielsweise die Vermehrung von Bakterien oder beschleunigen den Bewuchs mit humanen Zellen. Mit funktionellen Polymerbeschichtungen kann die Implantatoberfläche so modifiziert werden, dass sie eine dieser Eigenschaften oder sogar beide aufweist.

In dieser Arbeit wurden lineare Blockcopolymere mit Ankersegmenten und polykationischen, antibakteriellen Segmenten durch RAFT-Polymerisation dargestellt. Die Blockstruktur ermöglicht die Herstellung von Polymerbürsten, bei denen das Ankersegment an eine Metalloberfläche gebunden ist und das andere in die überstehende Lösung ragt, wodurch die Oberfläche gegenüber Bakterien kontaktabtötend wirkt. Im Ankerblock wurden Phosphonsäuregruppen eingesetzt, um das Aufpfropfen fertiger Polymere aus der Lösung auf die Oberfläche zu ermöglichen. Dieser Ansatz ermöglicht die Beschichtung beliebiger Geometrien und eignet sich daher besonders für die Funktionalisierung von Implantaten. Durch Variation der Anzahl der Ankergruppen wurde der Einfluss auf die Pfropfdichte auf Titanoxid analysiert. Die beschichteten Substrate wurden außerdem auf ihre physikochemischen und biologischen Eigenschaften hin untersucht, um die Ausbildung der Schichten und ihre antibakterielle Wirkung nachzuweisen.

Um die Biokompatibilität solcher Polymere zu verbessern, wurde das amphiphile Gleichgewicht des antibakteriellen Blocks eingestellt, indem mit variierendem Anteil hydrophobe Gruppen in die polykationische Kette eingebaut wurden. Darüber hinaus soll die Anbindung menschlicher Zellen erleichtert werden, indem adhäsionsfördernde Biomoleküle in "click"-ähnlichen Reaktionen am Polymerende angebracht werden.

Zuletzt wurde die Synergie von antibakteriellen/polykationischen und antiadhesiven/polyzwitterionischen Eigenschaften in Polymerbürsten auf der Grundlage von verankerbaren linearen Polymeren untersucht. Aufgrund der gegensätzlichen Löslichkeit der Segmente in wässrigen Lösungen mit unterschiedlicher ionischer Stärke zeigte eine Polymerbürste, die beide Komponenten enthielt, ein salzresponsives Verhalten. Es wurde gezeigt, dass die Oberflächeneigenschaften der beschichteten Substrate durch Anpassung der Salzkonzentration verändert sowie Wachstum und Anhaftung von Bakterien gehemmt werden.

Eidesstattliche Erklärung

Hiermit versichere ich, die vorliegende Arbeit selbständig angefertigt und keine anderen als die von mir angegebenen Hilfsmittel verwendet zu haben. Alle Stellen, die aus anderen Quellen entnommen wurden, sind als solche kenntlich gemacht worden. Diese Arbeit wurde in gleicher oder ähnlicher Form noch keiner Prüfungsbehörde vorgelegt.

Paderborn _____

Rafael Methling

Anerkennung der Promotionsordnung

Hiermit erkenne ich die Promotionsordnung der Fakultät für Naturwissenschaften der Universität Paderborn, welche am 31. März 2021 von der Universität erlassen wurde, an. Bisher wurde weder an der Universität Paderborn noch an einer anderen Hochschule im In- oder Ausland ein Promotionsversuch unternommen.

Paderborn

_____

Rafael Methling

Danksagung

Eine Thesis wie diese ist nie das Werk einer einzelnen Person. Vielen Menschen gebührt Dank für ihren Beitrag an den Ergebnissen, die ihren Weg in diese Arbeit gefunden haben.

Zunächst danke ich Herrn Prof. Dr. Dirk Kuckling, der mir dieses interessante Thema zur freien Verfügung gestellt und mich in seinem Arbeitskreis aufgenommen hat. Herrn Prof. Dr. Jan Paradies danke ich für die bereitwillige Übernahme des Zweitgutachtens.

Bei Frau Prof. Dr. Sabine Fechner und Herrn PD Dr. Hans Egold bedanke ich mich dafür, dass sie sich bereiterklärt haben, das Ende dieser Promotion als Teilnehmer der Prüfungskommission zu begleiten.

Im Folgenden bedanke ich mich bei allen, die mich vor Ort an der Uni Paderborn unterstützt haben: bei Dr. Artjom Herberg, auf dessen Anleitung und Hilfestellung in Sachen GPC-Messungen zahlreiche Ergebnisse dieser Thesis aufbauen. So verhält es sich auch mit dem Team für NMR-Analytik, Frau Karin Stolte und Herr PD Dr. Hans Egold, deren Arbeit unerlässlich für den Forschungsbetrieb ist. Dr. Adam Neuba, Christiane Gloger und Andrea Harbarth danke ich für das Aufnehmen von MS- und IR-Spektren. Annette Lefarth, Daniela Kästing, Claudia Berkemeier und Mariola Zukowski gebührt Dank dafür, dass sie den betrieblichen Ablauf in Labor und Verwaltung gewährleisten.

Darüber hinaus danke ich allen aktuellen und ehemaligen Mitgliedern des AK Kuckling, die ich kennenlernen durfte und die Anteil hatten an der ausgelassenen Atmosphäre, wegen derer ich stets gerne zur Arbeit gegangen bin. Dazu zählen Matthias van der Linde, Maksim Rodin, Katharina Völlmecke, Sebastian Peschtrich, Dr. Naresh Killi, Dr. Carsten Schmiegel, Dr. Tarik Rust, Dr. Dimitri Jung, Dr. Patrik Berg, Dr. Marie Berg und viele weitere, die uns für Tage, Wochen oder Monate besucht haben. Florian Pakusch, Oliver Dückmann und Robert Salewski danke ich für ihre praktischen Beiträge als Abschlussstudenten. Auch den zahlreichen weiteren Mitgliedern der organischen Chemie möchte ich für die schöne Zeit danken.

Ein interdisziplinäres Thema wie das meinige lässt sich nicht ohne die Hilfe von Experten anderer Fachbereiche bewältigen. Ich danke den Kooperationspartnern aus Dresden, Dr. Cornelia Wolf-Brandstetter und Dr. Frank Simon, sowie von der Universität Siegen, Michael Greiter, Jiwar Al Zawity, Dr. Mareike Müller und Prof. Dr. Holger Schönherr, herzlich für die Zusammenarbeit.

Zu guter Letzt möchte ich mich bei meiner Familie und meinen Freunden bedanken. Ihr wart und seid mir eine große Stütze und sicherlich wären weder Studium noch Promotion in dieser Form möglich gewesen, hättet ihr mich nicht auf diesem Weg begleitet.

Table of Contents

1 Introduction 1

1.1 Scope and goal 2

2 Theoretical background 4

2.1 Free and controlled radical polymerization 4

2.2 Antibacterial polymers 9

2.3 Contact-killing surfaces 12

2.4 Antifouling surfaces and surface regeneration 13

2.5 Salt-responsive polymers 15

2.6 Biocompatibility of antibacterial polymers 17

2.7 Polymer brushes 19

2.8 Phosphonic acid as anchor group 22

3 Preparation of antibacterial polymer brushes on titanium via “grafting to” method 25

3.1 Phosphonate monomers and derived polymers 25

3.2 Block copolymers with anchor groups 29

3.3 Effect of anchor block length on grafting density 32

3.4 Brush stability against acid and base 35

3.5 Physicochemical properties of coated titanium samples 37

3.6 Microbiological and cell biological investigations of coated titanium samples 41

3.7 Conclusions 44

4 Amphiphilic block copolymers with enhanced biocompatibility 45

4.1 Tuning the amphiphilic balance 45

4.2 End functionalization for improved cell adhesion 49

4.3 Conclusions 55

5 Salt-responsive polymer brushes with antibacterial and antifouling properties 56

5.1 Synthesis of zwitterionic and cationic copolymers 58

5.2 Adsorption on titanium oxide particles 61

5.3 Antifouling behavior and switchability of brushes 62

5.4 Physical characterization of coated substrates 66

5.5 Biological evaluation of polymer coatings 69
5.6 Conclusions 72
6 Experimentals 75
6.1 Materials 75
6.2 Instrumentation and methods 76
6.2.1 Conducted at Paderborn University 76
6.2.1.1 NMR spectroscopy 76
6.2.1.2 Calculation of molecular weight 76
6.2.1.3 Dialysis and lyophilization 77
6.2.1.4 IR spectroscopy 77
6.2.1.5 Mass spectrometry (MS) 77
6.2.1.6 UV/vis spectroscopy and adsorption isotherms 77
6.2.1.7 Size exclusion chromatography (SEC) 77
6.2.1.8 SPR sample preparation and measurement 78
6.2.2 Conducted at IPF Dresden and TU Dresden 78
6.2.2.1 Contact angle measurements 78
6.2.2.2 Streaming potential measurements 78
6.2.2.3 Analysis of attachment and biofilm formation under starving conditions 79
6.2.2.4 Biocompatibility assessment 79
6.2.2.5 Statistical analysis 79
6.2.2.6 Live/dead staining 80
6.2.2.7 X-ray photoelectron spectroscopy (XPS) 80
6.2.3 Conducted at the University of Siegen 80
6.2.3.1 Atomic Force Microscopy (AFM) 81
6.2.3.2 Contact angle measurements 81
6.2.3.3 Ellipsometry 81
6.2.3.4 Tests with Gram-positive and Gram-negative bacteria 81
6.2.3.5 Scanning electron microscopy (SEM) 82
6.2.3.6 X-ray photoelectron spectroscopy (XPS) 82
6.3 Syntheses 83

6.3.1 Diethyl 4-vinylbenzyl phosphonate (DEVBP) 83
6.3.2 Dimethyl 4-vinylbenzyl phosphonate (DMVBP) 84
6.3.3 4-vinylbenzyltrimethyl ammonium chloride (TMA) 84
6.3.4 *N*-acryloyl-2-methylalanine 85
6.3.5 2-Vinyl-4,4-dimethylazlactone (VDMA) 85
6.3.6 P($DEVBP_{17}$) 86
6.3.7 P($DMVBP_{12}$) 86
6.3.8 P(VP_{64}) 87
6.3.9 P(VP_{64}-b-$DMVBP_{14}$) 87
6.3.10 P($VPPr_{65}$-b-$DMVBP_{6}$) 88
6.3.11 P($VPPr_{65}$-b-PA_{6}) 88
6.3.12 P($DMVBP_{12}$-b-TMA_{171}) 89
6.3.13 P($VBPA_{16}$-b-TMA_{101}) 89
6.3.14 P($DMVBP_{12}$-b-TMA_{89}-b-Sty_{23}) 90
6.3.15 P($VBPA_{12}$-b-TMA_{89}-b-Sty_{23}) 90
6.3.16 P($DMVBP_{12}$-b-Sty_{89}-co-TMA_{74}) 91
6.3.17 P($VBPA_{12}$-b-Sty_{89}-co-TMA_{74}) 91
6.3.18 P($DMVBP_{12}$-b-Sty_{39}-co-TMA_{64}-b-$4FBA_{19}$) 92
6.3.19 P($MVBP_{12}$-b-TMA_{167}-b-$Biotin_{2}$) 93
6.3.20 P($DMVBP_{12}$-b-TMA_{167}-b-RGD_{5}) 94
6.3.21 P($MVBP_{12}$-b-TMA_{167}-b-RGD_{5}) 94
6.3.22 P(VSP_{63}-b-$DMVBP_{13}$) 95
6.3.23 P(VSP_{63}-b-PA_{13}) 95
6.3.24 P(VP_{64}-b-$DMVBP_{14}$-b-TMA_{64}) 96
6.3.25 P(VSP_{64}-b-$DMVBP_{14}$-b-TMA_{64}) 96
6.3.26 P(VSP_{64}-b-PA_{14}-b-TMA_{64}) 97
7 References 98
8 Appendix 107
8.1 Antibacterial polymer brushes on titanium via “grafting to” 107
8.2 Salt-responsive polymer brushes with antibacterial and antifouling properties 113

1 Introduction

Implantology is a fundamental part in today's healthcare. Prospectively, its relevance will only increase in view of the demographic change, as an aging population will have a greater demand for medical procedures to retain quality of life. Exemplary, 1.3 million dental implants are inserted each year in Germany alone which is more than three times the amount of twenty years prior.[1] Successful implant integration plays the central role in the longevity of the implant and ensures minimal secondary treatment, which is important for both the patient's wellbeing and from an economic point of view.[2] In contrast to natural teeth, a long-lasting, artificial paragon is anchored directly into the bone ("osseointegration"). Thus, multiple interfaces to the host biological system are created: from the bone-to-implant-junction over the gingival soft tissue interface to the abutment or crown, exposed to the oral cavity.[3] In particular, the surfaces in contact with bone and soft tissue are vulnerable just after the surgical procedure. Here, what is called the "race to the surface" begins.[4] The desired attachment of endogenous cells is competing with the proliferation of bacteria at the vulnerable areas. Up to 90 % of all implants have been reported to show first signs of inflammation as a result from primary attachment of bacterial cells.[5] Consequently, the implant can become severely infected ("peri-implantitis"), which leads to bone loss and even implant failure. The combat of peri-implantitis is exacerbated by the formation of a dense biofilm which encapsulates and shields bacterial colonies.[6] It promotes resistance against antibiotics and is hardly accessible due to the nature of the implant-host-interface.

Therefore, prevention of bacterial colonization and acceleration of integration into the host tissue is a primary target in the development of next-generation implant systems.[7] Researchers aim to utilize the progress in physical and chemical surface modification techniques in order to give endogenous cells a leg up. The gold-standard for manufacturing dental implants is titanium which shows good biocompatibility, mechanical strength and corrosion resistance, but does not exhibit intrinsic antibacterial properties.[8] Strategies to improve the material encompass nano-modification,[9] optimization of surface roughness and wetting behavior,[10] utilization of different titanium oxide modifications[11] and treatment to modify surface hydrophilicity.[12] Moreover, the chemical toolbox offers a wide variety of bioactive compounds the implant can be coated with, paving way to contact-killing surfaces,[13] easy-to-clean surfaces[14] or surfaces that facilitate the attachment of desired cells instead of bacteria.[15] Since the majority of cutting-edge systems still suffers from several drawbacks, most approaches have not yet found their way into clinical trial. Fundamental research currently tackles challenges regarding effectivity, biocompatibility and stability of surface modifications.

1.1 Scope and goal

The aim of this thesis is the synthesis and investigation of polymers that address the insufficient antibacterial and adhesion-promoting properties of titanium implants. Polycationic polymer brushes, that is surface tethered polymer chains made of cationic subunits, emerged as a particularly effective measure against the proliferation of bacteria by rendering the respective surface contact-killing. Following the example set by ground-breaking works of Tiller et al.,[13] poly(*N*-alkyl pyridinium) should be employed as an antibacterial polymer block in this work (Figure 1.1). Using RAFT polymerization as a controlled technique to access macromolecular block structures, a second block was to be introduced in order to anchor the chain to the surface. Hereto, a monomer containing phosphonic acid groups was employed. These moieties are known to form stable bonds with titanium oxide surfaces, making them predestined for the application on implants.

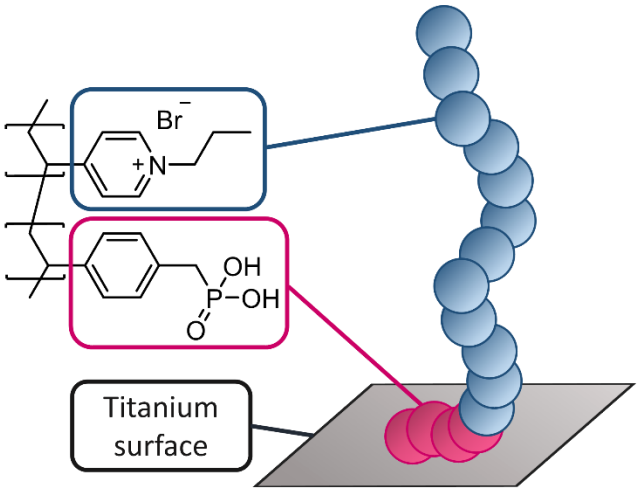

Figure 1.1: Representation of a surface tethered block copolymer chain on titanium via phosphonic acid anchor groups.

Compared to surface-initiated polymerization techniques, the “grafting to” approach is less covered in literature on antibacterial polymer brushes. Since it relies on preformed polymers that attach onto a surface from solution in a dip coating process, the targeted structure can be precisely synthesized and investigated before brush formation. There is only little information on how a block copolymer with an anchoring segment should be designed for optimal adsorption. Thus, after establishing the synthesis of the targeted structure, the effect of the anchor block length on the grafting density of the polymer brush should be investigated. Moreover, the coating stability as well as the physicochemical and biological properties of coated titanium substrates should be investigated using surface analytics and cell assays.

In the next step, adsorbable polymers with enhanced cytocompatibility should be targeted. Studies on dissolved antibacterial polymers with different composition regarding the ratio of hydrophobic and cationic units uncovered a dependency of hemolytic activity on the amphiphilic balance.[16] Thus, a series of block copolymers should be synthesized comprising

an anchor block and a mixed segment of cationic and hydrophobic monomers at different ratios. The biological evaluation should aid in designing both efficient and cytocompatible polymer brushes. Based on this system, the (in the brush state) outward-facing terminus of the polymer should be modified with a biomolecule that enhances cell attachment, namely the RGD sequence. Hereto, a monomer should be incorporated that allows the incorporation of the biomolecule in a “click-like” fashion.

Lastly, the synergy of antibacterial and easy-to-clean/antiadhesive should be explored based on the adsorbable polymer system. Research suggests that purely antibacterial surface modifications suffer from deactivation over time due to the attachment of bacterial debris.[17] Thus, the sustainable prevention of biofilm formation demands a more sophisticated mechanism. Utilizing the antiadhesive properties of polyzwitterions, a class of polymers derived from monomers carrying both a positive and a negative charge, a recoverable surface should be designed. When both polycationic and polyzwitterionic chains are present on a surface, each functionality could be switched off and on by adjusting the salt concentration of the supernatant solution. In this work, a responsive polymer brush system should be explored synthetically based on the “grafting to” of the respective multiblock copolymer. Using reference polymers for comparison, the responsiveness of the system should be probed via surface plasmon resonance (SPR) spectroscopy, a technique which allows the monitoring of surface phenomena in situ. Further surface analytics like X-ray photoelectron spectroscopy (XPS) and contact angle measurements should be utilized to investigate the surface properties in detail. Lastly, the biological properties should be examined in bacterial assays.

2 Theoretical background

2.1 Free and controlled radical polymerization

Nearly 200 years after the discovery of polystyrene, which back then was not recognized as a product of radical polymerization and only received its correct name until Staudinger's theory on macromolecules gained approval in the scientific community, the synthetic technique nowadays accounts for roughly 40-45 % of all industrial polymers.[18] It allows the synthesis of a wide variety of major polymers, for example poly(acrylamide), poly(ethene), poly(vinyl chloride) and many more. Moreover, its tolerance to many solvents, functional groups and the presence of trace impurities like water or stabilizers makes it a very attractive process from an economic point of view. The polymerization can be conducted in bulk, in solution and in dispersive media, using batch type reactors or even flow reactors.

Like in any chain polymerization, the formation of large molecules from monomers is possible due to the repeated reaction of an active site with a bifunctional group, resulting in the addition of one unit, which then carries the active end. In radical polymerization, the active species are organic radicals, mostly sp^2-hybridized carbon atoms.[19] In the first step, radicals are formed from homolytic bond cleavage, usually by means of a small amount of initiator based on azo or peroxo compounds, which decompose when supplied with energy in form of heat, radiation or mechanical force. Some classes of monomers are susceptible to thermal self-initiation, for example styrene. While theoretically each molecule of initiator yields two radicals, in practice, the initiator efficiency lies in the range of 0.5 to 0.7 since a share of the reactive species forms inert side products due to an irreversible termination reaction with their solvent cage. Next, the chain growth is initiated by reaction of the free radical with a monomer. The attack of the vinyl group occurs at the sterically less hindered carbon atom to form the more stable free radical, which can be further stabilized by resonance and polar effects.

In the propagation step, the active chain ends react with free monomer repeatedly to form long polymer threads. Despite the high reactivity of radicals, the radical polymerization proceeds with good regio- and chemoselectivity, which is evident by the high degree of head-to-tail structures in the polymers formed. The reaction rate is dependent on the concentration of monomer and of the concentration of propagating radicals:

$$v_p = k_p[M][M\cdot] \quad (1)$$

v_p = reaction rate of propagation
k_p = rate constant of propagation
$[M]$ = monomer concentration
$[M\cdot]$ = concentration of propagating radicals

Termination occurs by recombination of radicals or disproportionation, which both follow a second order rate law with respect to the radical concentration:

$$v_t = 2k_t[M\cdot]^2 \quad (2)$$

v_t = reaction rate of termination
k_t = rate constant of termination

Comparably, radical transfer reactions are slow at low temperatures since they require a high activation energy. In accordance to rate laws (1) and (2), the radical concentration must be held very low in order to favor chain propagation over termination. This, however, also decreases the polymerization rate, leading to extended reaction times.

Owing to the short lifetime of a radical (about 1 s), this polymerization technique is not suited for targeted end group modification or the synthesis of complex structures like block copolymers. Within a limited frame, the molecular weight of the resulting products can be influenced by using chain transfer agents, however, the molecular weight distribution is generally broad and cannot be adjusted arbitrarily. The desire to overcome these limitations sparked the development of new techniques for chain growth polymerization, whose first representative was the living anionic polymerization introduced by M. Szwarc.[20] Since then, more convenient techniques based on radical mechanisms, so called controlled radical polymerizations, have been explored who rely on the reversible deactivation of the active chain. By keeping the concentration of the radical concentration, i.e. the active species low, the termination reaction is slowed down. Simultaneously, a dynamic equilibrium between propagating and dormant chains allows the even growth of all chains.

Nitroxide-mediated polymerization (NMP) and atom transfer radical polymerization (ATRP) make use of the persistent radical effect to establish this equilibrium. Stable radicals like nitroxides or organometallic species are used to trap propagating chain ends.[21] The resulting dormant species is constantly reactivated to react with free monomer and deactivated again (Scheme 2.1). The persistent radicals X cannot react which each other but only with active radicals and accumulate in the solution early on due to radical-radical termination reactions. Thus, propagating chains react either with free monomer or the persistent radicals, keeping the concentration of active radicals low.

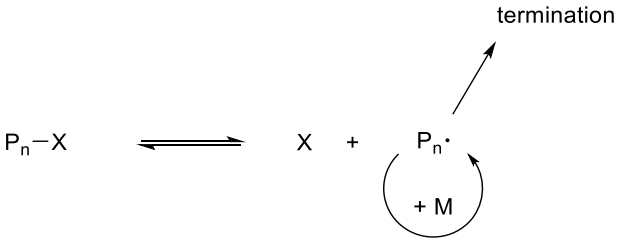

Scheme 2.1: Schematic representation of a reversible-deactivation mechanism based on the use of a persistent radical species X with the dormant polymer chain P_n-X and the propagating chain P_n·.

The third widely used method of controlled polymerization is the reversible-addition-fragmentation chain-transfer (RAFT) polymerization.[22] Its controlled nature relies on the degenerative chain transfer to transfer agents which are utilized in concentrations much larger than that of the initiator. Here, this very agent forms the dormant species which releases and captures polymer chains by reacting with the propagating ends (Scheme 2.2). If this transfer happens much faster than the propagation reaction, all chains grow evenly and exhibit a narrow molecular weight distribution. The overall radical concentrations correspond to the amount of initiator used and is kept low, so that termination is largely suppressed.

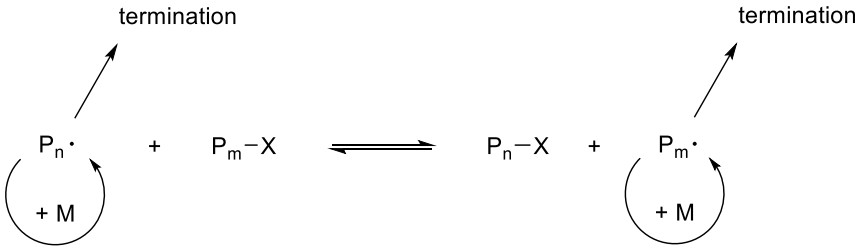

Scheme 2.2: Schematic representation of the controlled polymerization by degenerative chain transfer with the propagating chain ends $P_n\cdot/P_m\cdot$ and the dormant chains bound to the transfer agent P_n-X/P_m-X.

The breakthrough in the utilization of the degenerative chain transfer occurred in 1998 when the RAFT process was presented to the scientific community and marks a milestone in the development of controlled radical polymerizations.[23] The handling differs only little from a conventional radical polymerization, but exhibits the key features of controlled polymerization procedures:[24]

- The lifetime of growing chains is extended from about 1 s to more than 1 h.
- The correlation between molecular weight and monomer conversion is linear.
- The molecular weight can be adjusted by the ratio of monomer to transfer agent.
- Polymers have high end group fidelity with a low percentage of dead chains.
- Fast initiation and suppression of termination reactions lead to very low dispersites, typically under 1.3, which decrease with increasing monomer conversion.

The mechanism of the RAFT process is depicted in Scheme 2.3. The initiation (a) is equal to conventional radical polymerization. Upon stimulus, the reagent decomposes into two radicals, some of which add to monomers and form a propagating chain. In the next step, the role of the chain transfer agents (CTA) becomes evident. CTAs for RAFT are either dithioesters, trithiocarbonates, dithiocarbamates or xanthates, all of which share one structural feature: they possess a C-S-double bond that is susceptible to addition by a radical. The propagating end $P_n\cdot$ can either react with monomers M for chain elongation or attack at the doubly bound sulfur atom of the CTA to yield an intermediate species that can decompose into a dormant chain with a transfer agent terminus and a new radical R· (b). Reaction of this radical R· with monomers M yields another propagating end $P_m\cdot$ (c). When both the radicals derived from the initiator and from the CTA are consumed, the main equilibrium (d) is established. During the

polymerization, active polymer chains $P_n\cdot$ and $P_m\cdot$ are rapidly exchanged with the dormant thiocarbonylthio compounds. Ideally, this exchange proceeds fast in comparison to the monomer addition, ensuring that all chains grow equally. The concentration of CTA is high in comparison to the concentration of initiator so that the majority of polymer chains is in the dormant state. Radical-radical coupling (e) is largely suppressed since the overall radical concentration is low and steady. Except for small percentage of active polymer chains which corresponds to the number of initiating radicals, the thiocarbonylthio end group is retained at the polymer terminus at the end of polymerization.

a) initiation

b) reversible chain transfer/propagation

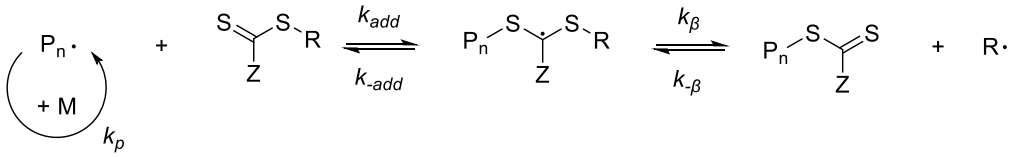

c) reinitiation

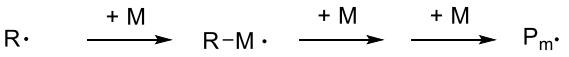

d) main equilibration/propagation

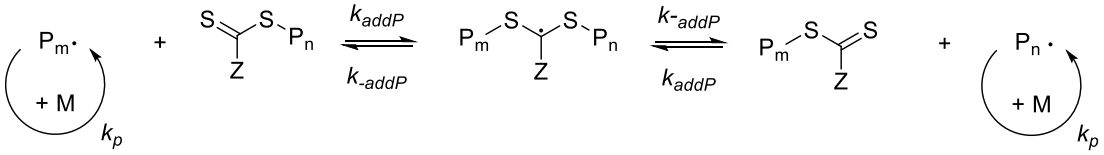

e) termination

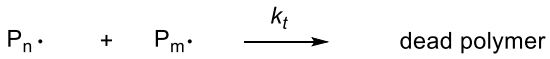

Scheme 2.3: General RAFT mechanism.[25]

The Z group of the CTA determines the stability of the intermediate radical and thus affects the rate of addition to the C-S-double bond k_{addP}, which must be high to obtain good control over molecular weight and dispersity.[26] This is the case when the formation of the intermediate radical is encouraged, yet it also needs to be sufficiently unstable to release a propagating chain. Therefore, the structure of the RAFT agent must be chosen with respect to the reactivity of the monomer. Similarly, the R group should exhibit a comparable reactivity as the initiating radicals. Nowadays, a wide range of monomers is covered by commercially available CTAs.

Neglecting the initiator derived chains, the molecular weight of the polymer can be calculated from the ratio of the converted monomer to CTA by the following simplified equation:[27]

$$M_{n,theory} = \frac{\rho[M]_0 MW_M}{[CTA]_0} + MW_{CTA} \quad (3)$$

$M_{n,theory}$ = theoretical molecular weight
ρ = monomer conversion
$[M]_0$ = initial monomer concentration
MW_M = molecular weight of the monomer
$[CTA]_0$ = initial concentration of CTA
MW_{CTA} = molecular weight of the CTA

When a higher concentration of initiator is used, its impact on the theoretical molecular weight can be approximated assuming an initiator efficiency of 0.5 with the following equation:

$$M_{n,theory} = \frac{\rho[M]_0 MW_M}{[CTA]_0 + 2[I]f} + MW_{CTA} \quad (4)$$

$[I]$ = initiator concentration yielding two radicals
f = initiator efficiency

In controlled radical polymerizations, the concentration of radicals during the reaction can be assumed to be steady. Thus, the kinetics of the propagation reaction for free radical polymerizations (equation 1) can be simplified to a pseudo first order rate law (equation 5). With a semi-logarithmic plot according to the integrated rate law the apparent rate constant k_a can be determined (equation 6).

$$v_c = k_a[M] \quad (5)$$

v_c = reaction rate of chain propagation for controlled radical polymerization
k_a = apparent rate constant

$$ln\frac{[M]_0}{[M]_t} = k_a t \quad (6)$$

$[M]_o$ = initial monomer concentration
$[M]_t$ = monomer concentration at reaction time t
t = reaction time

The retention of the thiocarbonylthio group in RAFT polymers provides the opportunity for post modifications of the ω-end.[28] Via secondary reactions, it can be converted to thiols, hydroxyl groups, alkenes and more. Most notably, it allows the block extension with a second type of monomer by isolating the polymer and utilizing it as a macro-RAFT agent. By careful experimental design, the fraction of dead chain ends can be kept low, however, especially in the synthesis of multiblock copolymers the lower molecular weight contaminations accumulate in the product which becomes evident through higher dispersities and tailing of SEC traces. More recent advancements of the technique aim to avoid these problems by

utilizing (photocatalyzed) iniferter processes.[29] This has also helped to overcome limitations regarding the maximum molecular weight to produce well-defined ultra-high-molecular-weight polymers.[30] Moreover, there have been advances regarding the development of oxygen-tolerant RAFT techniques or utilization of sulfur-free RAFT for the synthesis of sequence-controlled polymers.[31] These examples depict a small excerpt of the recent developments following the introduction of this controlled polymerization technique which are reviewed in more detail in literature.[32]

2.2 Antibacterial polymers

The evolution of living organisms has long-since spawned tactics to combat the proliferation of undesired bacteria, one of them being antimicrobial peptides (AMPs). This class of substances is broadly spread among multicellular organisms and comes in a magnitude of different forms, for example in regards to size, as AMPs with less than 10 and more than 100 amino acids are known.[33,34] Despite their diversity, several main characteristics have been identified: virtually every antimicrobial peptide comprises spatially organized hydrophobic and cationic groups. Lysine and arginine are a vital ingredient in AMPs as they carry a positive charge under physiological conditions owing to their amine and guanidine group, respectively. The three-dimensional conformation of the peptide results in the characteristic alignment of cationic to hydrophobic moieties (Figure 2.1).[35]

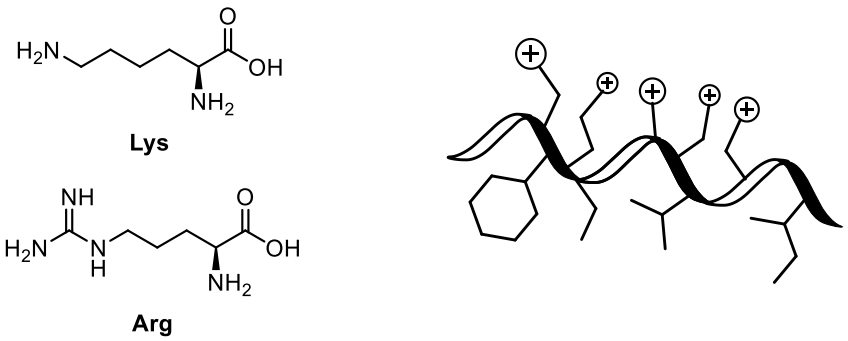

Figure 2.1: Left: Amino acids lysine and arginine which are positively charged under physiological conditions. Right: sketch of an antimicrobial peptide comprising cationic and hydrophobic compartments.

The importance of the combination of cationic charges and hydrophobic groups issues from the target of AMPs, namely the structure of bacterial membranes.[36] They are largely composed of phospholipids, carrying a negatively charged head-group and hydrophobic, mostly aliphatic tails. Due to the aqueous environment, they constitute a double layer where the polar head groups form the outward surface and the lipophilic parts align on the inside of the layer. The opposite charges of membrane surface and cationic AMPs result in attractive forces which promote the adsorption of the peptide onto the bacterium. Several mechanisms for how bacteria are killed by AMPs have been identified (Figure 2.2).[37]

In the barrel-stave model, the AMPs insert into the membrane, effectively forming a tunnel where the hydrophobic regions align with the lipid layer and the cationic groups point inwards. This uncontrolled permeability of the membrane leads to cell death.[34] The toroidal pore model differs in regards to the pore structure: adsorbed AMPs aggregate and cause the head groups of the phospholipids to align with the inner part of the gap, leading to a torus-like appearance.

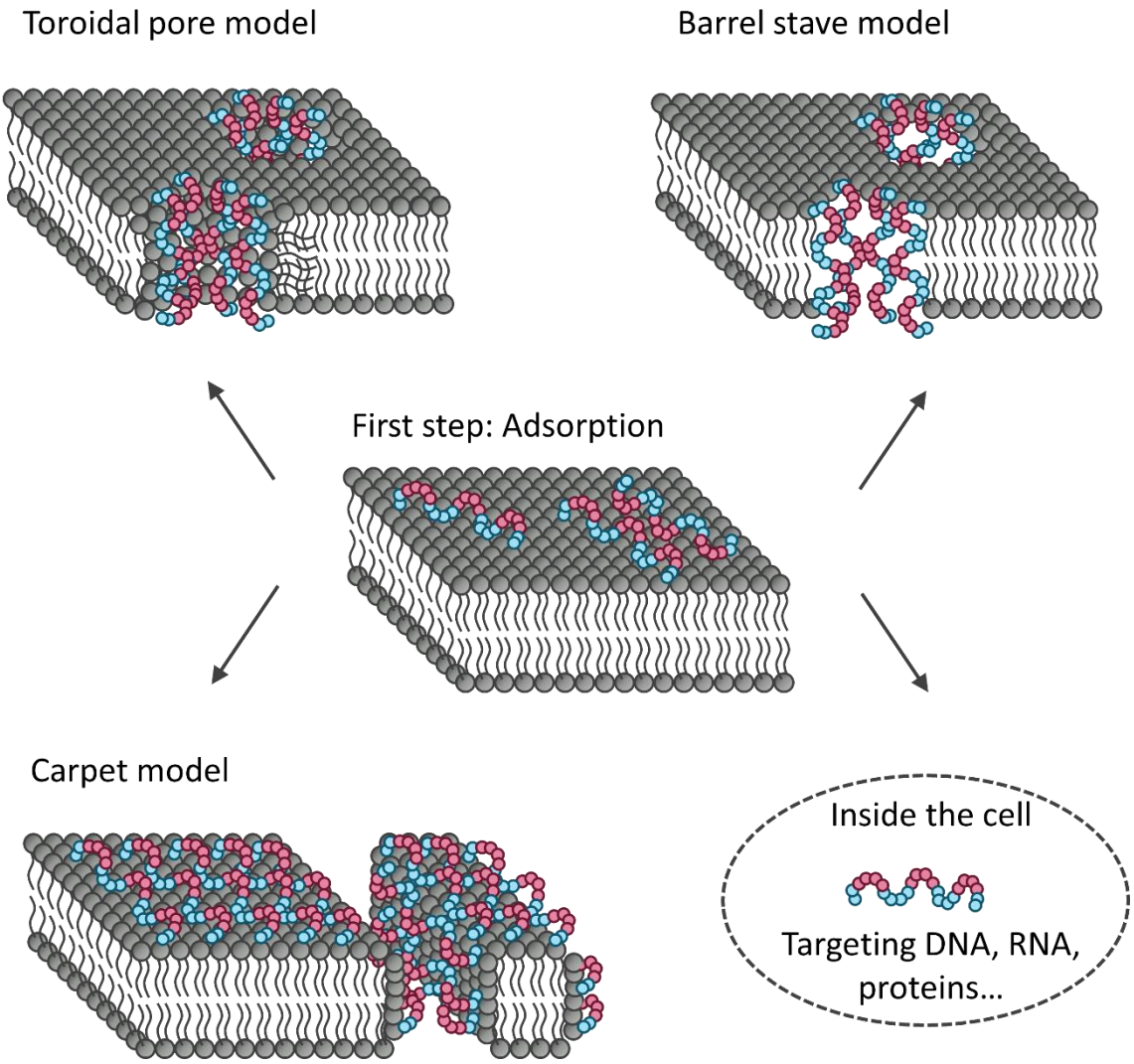

Figure 2.2: Different mechanisms of antibacterial peptides (red: cationic, blue: hydrophobic) targeting bacteria.[37]

The carpet model describes the accumulation of AMPs on the membrane surface which is eventually breached at a critical concentration. Phospholipids are capsuled in micelles and large gaps are formed, again leading to cell death. The inlying components of the bacteria can also be targeted by hindering the synthesis of DNA, RNA and proteins as well as other delicate intracellular processes. Which mechanism is dominant is highly dependent on the specific AMP. It should be noted that the composition of the cell membrane is more complex than outlined in these mechanistic discussions, especially considering the different membrane composition of Gram-positive and Gram-negative strains.[36] The latter exhibit two

phospholipid bilayers separated by a thin peptidoglycan layer, while Gram-positive bacteria possess only one lipide bilayer with a thick peptidoglycan network on the outside.

Compared to conventional antibiotics, the physical nature of these mechanisms makes it less likely for bacteria to develop a resistance which usually results from smaller changes like modification of enzymes or target mutations.[35] Some bacteria have been found to modify their membranes to reduce the negative charge or use efflux pumps to remove inserted AMPs. Generally, these strategies reduce the sensitivity towards AMPs but do not lead to immunity.[38]

Despite their advantages over conventional antibiotics AMPs have not found widespread use as drugs or disinfectants due to costly synthesis and poor proteolytic stability.[39] These findings, however, sparked the development of synthetic polymers mimicking the natural paragon to overcome these drawbacks. Scientists explored the use of different cationic moieties, for example phosphonium salts[40], protonated amines[41], guanidinium[42] and alkylated pyridinium[43] (Figure 2.3). The types of backbones are just as diverse. Among others, there are antimicrobial polysaccharides[44], polyacrylamides[45], polynorbornenes[42], nylon-3 copolymers[46] and polycarbonates[47].

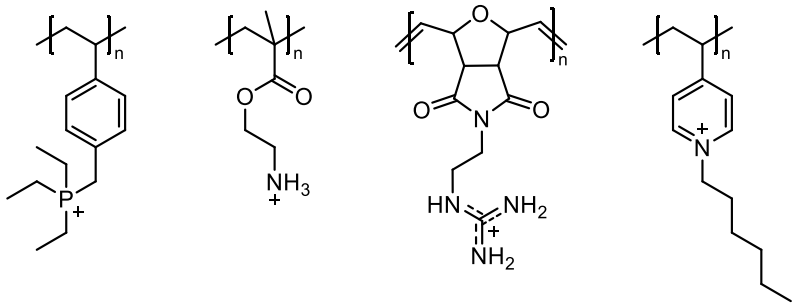

Figure 2.3: Functional groups used in synthetic antibacterial polymers emulating AMPs.

By systematically varying parameters in synthetic antimicrobial polymers, structure-activity relationships have been elucidated to an extent. Increasing the molecular weight, for example, has been shown to enhance the antimicrobial activity in some cases.[48] Charge density and the balance of hydrophobic and hydrophilic groups have also been a subject of discussion. Beyond the fact that the polymer should contain cationic and hydrophobic groups, an absolute rule for designing the perfect material has not been found yet and the efficacy remains highly specific to combination of antibacterial polymer and the tested strains.[45,49]

Since the application in human patients is one major goal, cytocompatibility is a central issue. Oftentimes, there is only poor selectivity between mammalian and bacterial cells so that a particularly effective antimicrobial polymer is too harmful for the medicated organism. It has since been established that the “amphiphilic balance” is essential in order to join biocompatibility and efficacy.[50] It is suggested that the right combination of functionalities can be employed to manage both properties. Boyer et al. conducted a series of screening tests

to optimize the composition of cationic/hydrophobic/hydrophilic copolymers regarding hemolytic and antibacterial activity.[16,45,51] The optimization proved challenging and the researchers concluded that secondary parameters like structural compatibility of monomers also have to be taken into account.

Moreover, although they offer advantages over conventional antibiotics regarding drug resistance in bacteria, antibacterial polymers are less active than their low molecular counterparts and require higher doses for a successful therapy.[52] However, the application in combinatorial therapy along with traditional antibiotics is a promising approach.[53] Their membrane disrupting properties can aid in overcoming some strategies of bacteria to avoid accumulation of drugs inside the cell, for example outer membrane impermeability or removal of antibiotic agents with efflux pumps.

2.3 Contact-killing surfaces

In seminal works, Tiller et al. modified glass slides with linear pyridinium-based polyelectrolytes in order to transfer the bactericidal action of polycations from solution to surfaces.[13,54] They exposed the coated glass to suspensions of different bacterial colonies and showed that up to 99 % of deposited bacteria were killed on the dried material. Moreover, they investigated the effect of the pendant alkyl chain on the pyridinium groups: among the evaluated chain lengths, three, four and six carbon atoms proved to be most effective (Figure 2.4). At ten and more carbon atoms the efficacy was as low as non-functionalized poly(vinyl pyridine) which the authors attributed to the aggregation of the more hydrophobic polymers and less interactions with the cell membrane. These groundbreaking results provided a working hypothesis to the scientific community, which spawned a tremendous amount of research in this field.[55-58] It also identified structural parameters like charge density as crucial for the interactions between surface-bound polymers and bacteria.

The underlying mechanisms of contact killing are still matter of intensive discussion.[58] Penetration of the cell membrane by surface bound chains was considered by Tiller et al.[13], but is deemed unlikely to be the only or even dominant mechanism since it requires very long and stretched chains at low grafting densities to disrupt the membranes like conventional AMPs. In fact, some systems with shorter brushes[59] or even networks[60] also show excellent antibacterial properties.

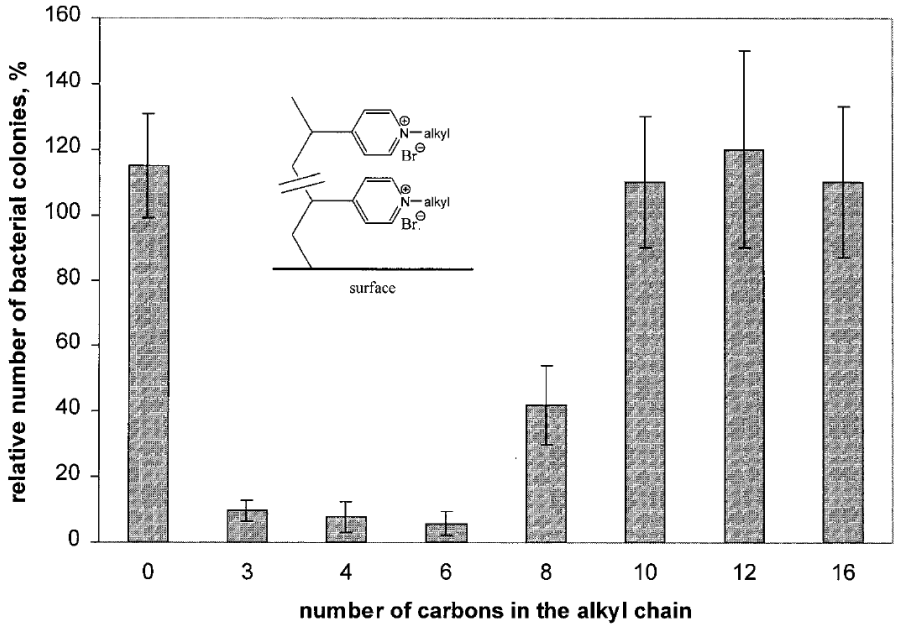

Figure 2.4: Effectivity of contact-killing surfaces coated with alkylated poly(vinyl pyridine) in dependence on the alkyl chain length. Figure reproduced from reference [13]. Copyright 2001 National Academy of Sciences.

Some authors suggest that bacteria can be impeded in their ability to grow and proliferate due to the strong adhesion to cationic polymer coatings, eventually resulting in cell death.[61] Hereto, the charge density has to exceed a certain threshold to exert sufficient force and prohibit the deformation of the membrane which is necessary for cellular division. It has also been proposed that polycationic surfaces may act as an "anion sponge", removing phospholipids from the membrane and thus damaging it.[62] Since the membranes rely on bivalent cations (Mg^{2+} and Ca^{2+}) for stabilization, removal of those by entropically favored exchange with the surface bound polyelectrolytes is assumed to impair the cell membrane.[63]

2.4 Antifouling surfaces and surface regeneration

Antibacterial non-regenerating surfaces lose their efficacy due to a shielding effect by bacterial debris of killed bacteria. Similarly, drug-releasing surfaces are only active until the antibacterial compound is consumed.[6,17,64] Once a biofilm has formed on a surface, it screens bacteria and overcoming the infection with conventional antibiotics becomes extremely difficult. There have been advances in the use of degradable multi-layer systems which regenerate through a shedding mechanism, still, the lifetime is limited by the number of layers.[65]

The identification of this issue gave rise to the application of low- or antifouling surface modifications which refers to the property of a material to resist non-specific adsorption of (bio)molecules.[66] Such systems exploit the pronounced hydration layer surrounding surface-tethered molecules, impeding the adhesion of material from solution which includes bacteria (Figure 2.5A).[67] PEG and other hydrophilic materials bind water molecules via hydrogen

bonding and thus prevent the close contact and attachment of larger molecules as they cannot penetrate the dense hydration shell. An even stronger hydration shell can be formed by moieties which induce order through electrostatic interactions, namely zwitterionic compounds.[66]

Zwitterions (also betaines or inner salts) carry an equal number of positively and negatively charged groups which are linked by covalent bonds.[68] The spatially separated charges induce a high dipole moment while the molecule itself is electrically neutral. Structurally, the most common zwitterions are carboxybetains, phosphobetaines and sulfobetaines.[69] Depending on the nature of charged groups, the molecules are only in their zwitterionic state in a specific pH range. Amino acids are zwitterionic at neutral pH but can be converted to their cationic form by protonation and their anionic form by deprotonation, respectively (Figure 2.5B). In contrast, sulfobetaines with quaternary ammonium groups are zwitterionic over a broad pH range owing to the strong acidity of sulfonic acids and the inert ammonium group.[70]

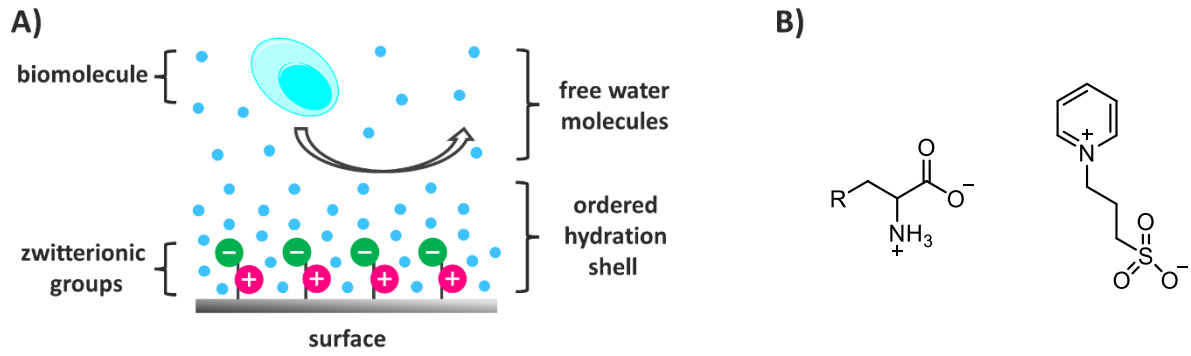

Figure 2.5: A) Sketch of an antifouling surface equipped with zwitterionic groups. B) Structural examples for zwitterionic groups: carboxybetaine (left) and pyridinium based sulfobetaine (right).

Self-assembled monolayers of zwitterions were identified to render the surface antifouling in the early 2000s.[14] More recently, the macromolecular equivalent in form of polyzwitterions has attracted attention due to the possibilities polymer chemistry offers regarding multifunctionality and control over architecture.[71] They have since been employed in various areas like antifogging surfaces, reduction of cellular association ("stealth") or antifouling coatings for marine and biomedical applications.[72] These surface modifications do not exhibit antibacterial effects, though, so several of polymer-based systems have been published exploiting the synergy of antifouling and contact-killing. Earlier works combine polycationic and polyzwitterionic moieties by block copolymerization or grafting of antifouling polymers onto antimicrobial networks.[57,73] Both bactericidal effect and decreased fouling were detected, which offers an improvement compared to purely contact-killing surfaces.

An even more promising approach are stimuli-responsive systems, which can be switch between both bactericidal and antifouling modes and thus offer a theoretically unlimited number of kill-and-release-cycles. Possible triggers are pH[74], aqueous/dry conditions[75],

light[76], which rely on chemical reactions of the respective moieties, or ionic strength,[60] which exploits changes in solubility of certain segments. Lienkamp et al. investigated surface-bound and pH-responsive networks utilizing carboxybetaines (Scheme 2.4).[74] They observed that the networks act protein-repellent at neutral pH, owing to their zwitterionic nature since the carboxylic acid is deprotonated. In acidic media the carboxylate is protonated, which results in a positively charged surface. The authors argue that this switching can be triggered by bacterial metabolites which are known to decrease the pH compared to physiological conditions, making the system suitable for in vitro applications.

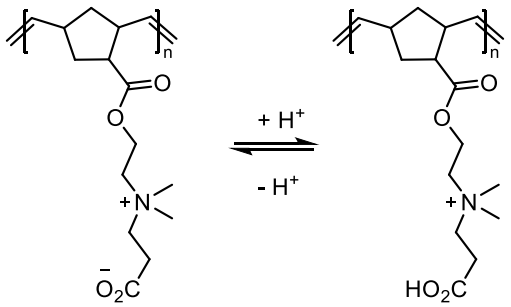

Scheme 2.4: pH-responsive norbornene based polymer for surface applications combining polycationic/bactericidal and polyzwitterionic/antifouling properties.[74]

2.5 Salt-responsive polymers

Ionic strength as a trigger seems particularly interesting for applications in sensitive areas, for example in dental implantology since it is compatible with the oral flora and easily applicable. It does not rely on changes in the chemical structure of the material, so both cationic and zwitterionic groups are present permanently. The underlying effect that allows the (de)activation of one functionality is the solubility of polymer chains in dependence of the salt concentration.

Polycations (as well as polyanions) exhibit a characteristic behavior in water: compared to neutral polymers, they assume a more stretched conformation because of the intramolecular repulsion of charged groups.[77] This is also the reason for the so called “polyelectrolyte effect” which describes the increase of the viscosity of polyelectrolyte solutions with decreasing concentration of polyelectrolyte.[78] In a diluted system, the charges of the polymer chains are less screened by counterions and compensate by expanding further, resulting in a higher viscosity. This also illustrates the importance of the ionic strength of the solvent: addition of salt to a water-polyelectrolyte-system will cause the polymer chains to adopt a more relaxed conformation because dissolved ions screen the repulsion between chains (Figure 2.6). The salt-dependent change in conformation is sometimes also referred to as polyelectrolyte effect, especially in the context of salt-responsive systems.[79]

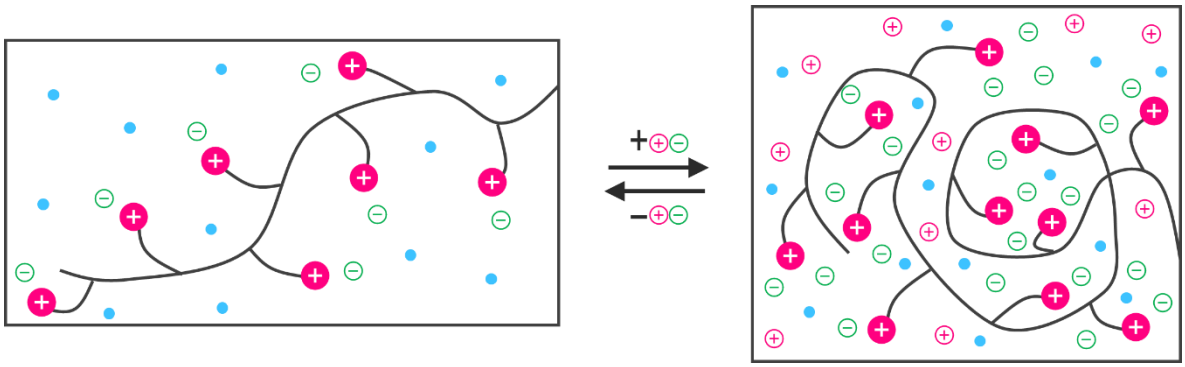

Figure 2.6: Schematic representation of the polyelectrolyte effect concerning the expansion of a polycationic polymer in absence of salt in water and the relaxed conformation in presence thereof.

The remaining class of charged polymers, polyzwitterions, shows the opposing behavior in aqueous solution. Without electrolyte present, the strong electrostatic forces between intermolecular and intramolecular chains make the bulk polymer collapse into an insoluble solid (Figure 2.7).[79] Upon addition of salt, however, the charges between zwitterionic moieties are shielded and allow the chains to extend into solution, which is referred to as "antipolyelectrolyte effect". The concentration needed to solve a specific amount of polyzwitterionic polymer is polymer specific and dependent on the concentration as well as the type and charge of the ions.[80] Beyond that, it has been observed that most polyzwitterions show an upper critical solution temperature (UCST) because the electrostatic forces can be overcome with thermal energy as well.[81]

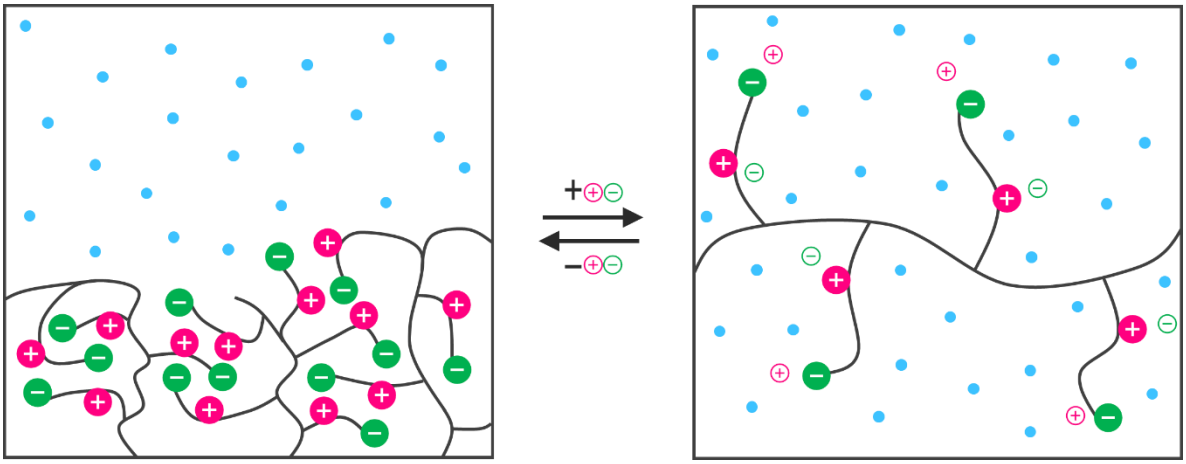

Figure 2.7: Schematic representation of the anti-polyelectrolyte effect showing insoluble polyzwitterions due to intra and intermolecular attraction in low-salt water and the dissolution upon addition of ions.

Huang et al. designed an interpenetrating network exploiting the polyelectrolyte and anti-polyelectrolyte effect to change between antibacterial and antifouling modes.[60] The hydrogels were prepared by first polymerizing a monomer carrying a tertiary amine and 4 mol % of crosslinker to yield the polycationic and densely crosslinked gel. Afterwards, it was swollen in a solution of the zwitterionic monomer and 0.02 % crosslinker to form a loosely crosslinked gel within the cationic network. They observed changes in optical, rheological and morphological properties depending on the ionic strength of the solution used for swelling the

hydrogel. Moreover, a bactericidal efficiency of over 80 % and a bacteria release rate of 96 % after washing with 1 M NaCl solution were determined. Most notably, they showed that the system was able to kill and release bacteria in five repeated cycles with only little decrease in efficacy.

2.6 Biocompatibility of antibacterial polymers

Due to the manifold structural types of cell membranes, antibacterial polymers show selectivity between bacterial and mammalian cells.[82] In general, the latter are less vulnerable to membrane disruption since they are stabilized by cholesterol and feature a higher share of neutral (zwitterionic) lipids, which decreases the attractive forces between antibacterial polymer and membrane. Yet, in physiological interfaces like they occur in implantology, biocompatibility has to be understood as more than just non-hemolytic.[83] Once an artificial surrogate is implanted into an organism, what is called the “race to the surface” begins. The from a medical perspective desired adhesion of host tissue competes with biofilm formation and proliferation of harmful bacteria.[4] In principle, this leaves two strategies: defend the implant or encourage tissue cell attachment.[84] The employment of antibacterial agents or surfaces usually also impairs the functionality of mammalian cells and even after optimization of the hemolytic activity, the adhesion of desired cells is only less hindered but not facilitated.[16,51] To promote implant integration, the surface chemistry has to be designed to selectively address desirable cells.

Cell adhesion receptors, such as integrin, mediate the contact of cells and the extracellular matrix in multicellular organisms. Moreover it plays a vital part in governing the multistep process of new cell adhesion.[85] The RGD-sequence has been identified as the minimal essential motif to be recognized by integrins (Scheme 2.5) and is composed of the three amino acids arginine, glycine and aspartic acid. Since this discovery it has proven to be the most effective peptide sequence for stimulated cell adhesion on synthetic surfaces and can be integrated into molecules using its primary amine group, for example via carbodiimide chemistry or electrophilic moieties.[15,86,87] Beyond that, there has been work on more active species like RGD-cyclopeptides and more selective derivatives.[88]

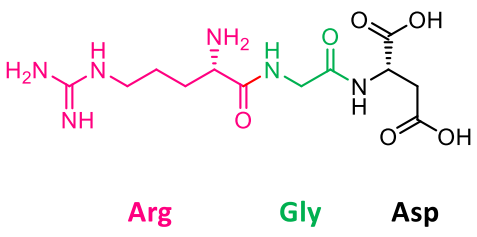

Scheme 2.5: Structure of the tripeptide RGD made of arginine, glycine and aspartic acid.

It was highlighted in published reports that several aspects have to be taken into account when designing such bioconjugates for surface modifications.[87] Naturally, the RGD sequence has to be accessible which should reflect in the spatial arrangement of different functionalities. Thus, when considering a brush structure, it should be located on the chain end to maximize exposure to the surrounding environment. Despite the careful design, polymer chain conformation may screen and inhibit the activity of the peptide sequence.[89] Moreover, it has to be considered that the addition of a large amount of immobilized biomolecules may alter the brush structure due to changes in polarity and size.[90] Since microorganisms like bacteria are smaller than the desired mammalian cells, it is suggested that the surface density of RGD can be considerably lower than the actual brush density.[91] Still, it has been found that a threshold surface concentration of the binding motif is necessary for improved cell proliferation for the example of human corneal epithelial cells.[92]

Schönherr et al. equipped titanium surfaces with polymer brushes made of poly(di(ethylene glycol)methyl ether methacrylate) (PDEGMA) via surface initiated RAFT polymerization and investigated the attachment of NIH 3T3 mouse embryonic fibroblasts.[87] This cell line plays an important role in tissue formation and integration but was observed not to adhere to the modified surfaces at 25 nm brush thickness, owing to the antifouling properties of the hydrophilic polymer bristles. After end modification with a peptide containing the RGD-sequence (Figure 2.8), it was demonstrated that the cell attachment was significantly improved despite the otherwise unaltered brush composition. These results underline the importance of the outward facing groups: although they make up only a fraction of the overall molecular weight, the binding motif had a tremendous impact on the cytocompatibility. Furthermore, a negative control experiment using RAD (arginine-alanine-aspartic acid) as end group modification did not result in improved cell-surface-interactions, confirming that the effect could be ascribed to the specific peptide sequence of RGD.

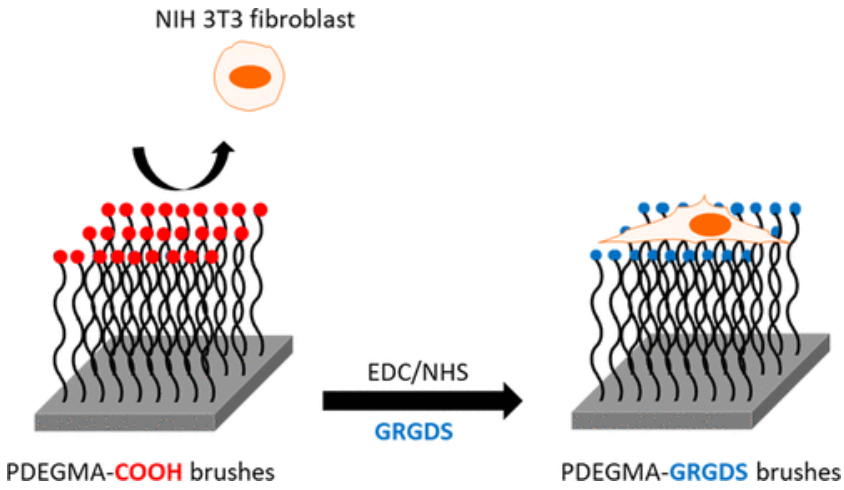

Figure 2.8: PDEGMA-brushes with COOH end group showing antifouling behavior but good fibroblast attachment after end-modification with RGD. Reprinted (adapted) with permission from [87]. Copyright 2021 American Chemical Society.

2.7 Polymer brushes

The term polymer brush denotes surface tethered (usually linear) polymer chains whose conformation is altered in comparison to the undisturbed molecule in a good solvent.[93–95] At high grafting densities, neighboring strains obstruct each other and instead of a random-walk conformation, the polymer stretches along its backbone and away from the surface which comes with an entropic penalty. The consequences for properties regarding polymer, surface and interface have been extensively addressed in literature, still, recent studies reveal yet unknown fundamental principles, for example regarding grafting and degrafting mechanisms.[96]

For a vivid perception of the system, the findings of Genzer et al. can be considered, who observed different regimes for linear, terminally anchored polyacrylamides depending on the grafting density.[97] At great distances between anchor points, the polymers assume a conformation not too different from the freely solved state if the constrictions by the surface are neglected (Figure 2.9). Due to the resemblance in shape, this state is called “mushroom regime”. The closer the anchor points are moved together, the more chains are restricted by neighboring strands and forced into a more stretched conformation, resulting in the “brush regime”. The reduced grafting (or tethered) density Σ is commonly used to characterize the state of a given system. It denotes the area that would be occupied by a free unhindered polymer chain under the same experimental conditions (temperature, solvent) and is defined as

$$\Sigma = \sigma \pi R_g^2$$

with the grafting density σ (number of chains per area) and the radius of gyration R_g.[95] Brittain et al. argue that it is essential to control the grafting density (and with it the regime) in tethered polymer systems since the entropic penalty is fundamental to behavior and interactions, for example with biological systems. The transition to the “true brush” regime is depending on the specific system since parameters like molecular weight, polymer structure and brush environment play a vital role. It can be difficult to investigate Σ for complex polymers since R_g is hard to obtain in these cases, which is also why it is rarely reported in literature.

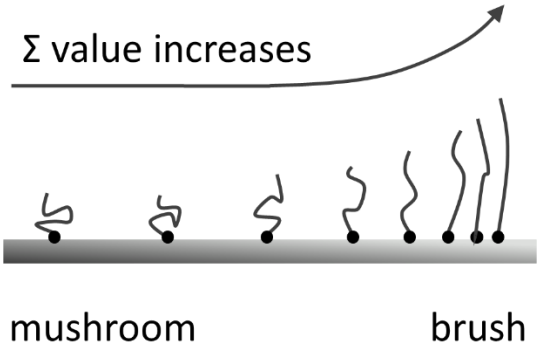

Figure 2.9: Schematic representation of mushroom-to-brush regimes depending on the reduced grafting density Σ of surface tethered polymers.

Brushes can be used to generate surfaces for a wide range of applications, for example for stabilization of colloids[93,98,99], bioactive and antifouling surfaces[87,100,101] or responsive surfaces[102,103]. Figure 2.10 illustrates the importance of controlling the grafting density: for colloidal systems, a certain threshold is needed for the chains to overcompensate the attractive forces between particles and facilitate solvent-particle interactions (Figure 2.10A). Using responsive polymers, a dispersion of the coated particles can be switched between stable and instable, for example, depending on whether the chains are swollen with solvent or not.[99] Moreover, polymer brushes can be employed to moderate the interactions of secondary particles or species with a surface (Figure 2.10B). Here, the control of the grafting density is also essential, and the optimum is again depending on the size, chemistry, and desired outcome of the complex interplay of involved compartments. In real systems, correlations between the grafting density and the solvent interaction enthalpy or the brush stability have been observed.[104]

Within grafted polymers, polyelectrolyte brushes make for a special case due to their inherent expanded conformation compared to their neutral peers.[77] They experience strong intramolecular repulsion due to adjacent charged groups which is exacerbated by the intermolecular forces when the chains are forced into a confined space on a surface. Additionally, polar solvents like water exert strong osmotic forces, pulling the polymer chain away from their anchoring points. It was shown that surface-near bonds are likely to break, especially in high stress conditions like high grafting density, good solvent or at elevated temperatures causing significant degrafting within minutes until the system stabilizes at lower grafting densities owing to a more relaxed regime.[77]

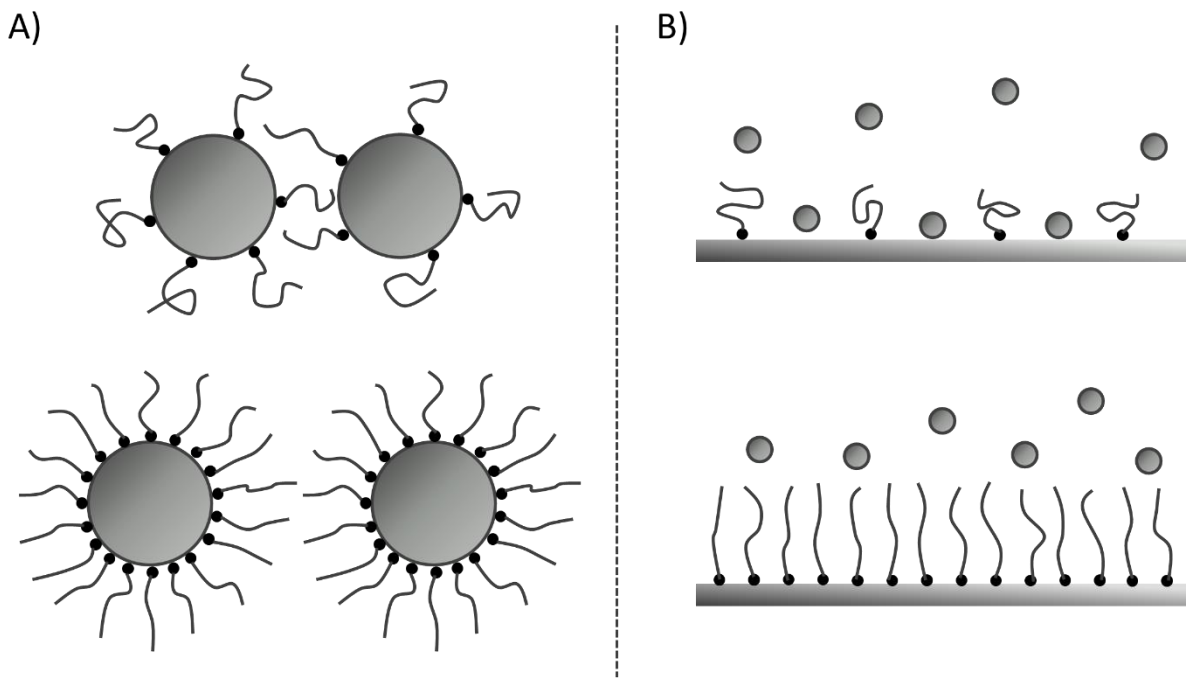

Figure 2.10: A) Particle stabilization by grafted linear polymer chains. B) Mediation of surface-particle interactions depending on the grafting density of surface tethered polymer chains.

For the construction of polymer brushes, two general approaches are possible. “Grafting from” denotes the polymerization of the chosen monomer from a surface where a low-molecular weight initiator has been deposited before.[105] This method yields high grafting densities since the small molecules that are grafted as initiating sites allow a dense occupation of the surface. Even at low initiating rates, the resulting chain density is high, reaching well into the “true brush” regime. Oftentimes, the layer thickness can simply be controlled by adjusting the reaction time.

The analysis of the actual polymer on the surface is challenging as the chains either have to be degrafted to use solution-based methods or surface analytics must be employed. Free polymer which has been initiated by the cleaved radical that is not attached to the surface can be collected and analyzed as well. It has been reported that the properties are in good agreement with those of the actual chains forming the brush for surface-initiated ATRP.[106] The inconvenient synthesis involving solid material from the very first step is another drawback, especially when considering transfer and upscaling.

Alternatively, polymers can be prepared independently using established polymerization methods and subsequently grafted to the surface via one or more terminal groups.[107] This gives precise control over polymer architecture which can be easily verified using analytical methods suitable for dissolved analytes. Thus, there is a very good understanding of the polymer regarding molecular weight, structure, solubility or thermal properties independent from the surface application. Since the polymers are not yet confined to a small space, even demanding post modification reactions can be employed which may otherwise be impaired

due to steric effects. Harsh reaction conditions may also damage pregrafted brushes which are sensitive to heat-induced degrafting. The final grafting step can be accomplished by dipping the desired object into the polymer solution which is convenient for the coating of complex geometries and flexible regarding the upscaling and transfer between different shapes and sizes.

Compared to “grafting from”, however, the grafting densities are low since it is energetically unfavorable for the ready-made chains to stretch to a great extent and diffuse through the layer of bound polymer, even considering the enthalpy resulting from the bond formation between polymer and surface.[108] Moreover, it has to be considered that the grafting to process discriminates species with regards to their molecular weight, so that polymer brushes do not necessarily reflect the properties of the free polymer, especially in disperse samples.[96] Ultimately, the decision between the two approaches needs to be decided by what the targeted application is demanding and which drawbacks can be tolerated.

For the construction of stable polymer brushes, the chains require one moiety or section which is able to form one (e.g. thiols[109], silanes[77]) or more (e.g. catechols[100,110], phosphonic acids[111]) covalent bonds with the surface, sometimes aided by hydrogen bonding. Binding groups can also be incorporated by polymerizing monomers carrying the respective moiety, forming “anchoring” blocks. Naturally, this approach demands controlled polymerization conditions, since randomly distributed binding sites along a polymer chain do not form polymer brushes but layers where the backbone is close to the surface along the whole chain. Upon consideration of published systems that make use of blocks comprising binding groups, it becomes evident that there is little information on why a specific quantity of such groups or a specific anchor block length is chosen.[101,112] At this juncture, more research is necessary to uncover correlations between segment length and adsorption behavior.

2.8 Phosphonic acid as anchor group

Organophosphonic acids have been shown to form stable bonds with metallic surfaces or particles: in an early example, Reven et al. used octadecylphosphonic acid to form self-assembled monolayers on zirconium oxide and titanium oxide.[113] They are suitable for surface applications not only because they feature a stable P-C-bond, but also due to the good hydrolytic stability of the surface bonds, which even exceeds that of siloxanes.[114-116] The exact modes of surface binding are still under discussion and heavily influenced by the concrete nature of the substrate, nevertheless, different studies suggest a preference of bidentate, tridentate or a mixture of both states (Scheme 2.6).[117] Organophosphonic acids are well-accessible through Michaelis-Arbuzov or Michaelis-Becker reactions, for example, allowing an efficient synthesis of polymerizable building blocks.[118]

Scheme 2.6: Bi- and tridentate binding modes of organophosphonic acids on titanium (oxide) surfaces.

Metal oxides are suitable materials for grafting of phosphonic acid containing molecules which includes the native oxide layer of aluminum and titanium, for example.[116] The occurrence of oxygen on such surfaces is not limited to metal oxide but hydroxyl groups exist as well. Their quantity and acidity can vary depending on the type of alloy, manufacturing processes and pretreatment of the surface. These factors then affect the mechanism of how the P-O-M-bonds are formed. Generally, it is suggested that the doubly bound oxygen of the phosphonic acid coordinates to Lewis acid sites, which facilitates the nucleophilic attack of hydroxyl groups (or hydroxide anions in cases of ionic Ti-O-bonds) and subsequent condensation of water, yielding a bidentate phosphonic acid surface complex (Scheme 2.7A).[119] Some studies indicate the occurrence of hydrogen bonding between adjacent phosphorous species as well.[120] It has been found that the grafting density is not limited by surface hydroxyl content, since the Ti-O-Ti-bonds can be cleaved in the presence of phosphonic acids. Hereto, the titanium oxide is activated due to the coordination of the oncoming phosphorous species (Scheme 2.7B).[115,119] This allows the deprotonation of one phosphorous bound hydroxyl group by titanium oxide, which is subsequently cleaved from one titanium atom in favor of a surface hydroxyl group and a phosphonic acid metal ester.

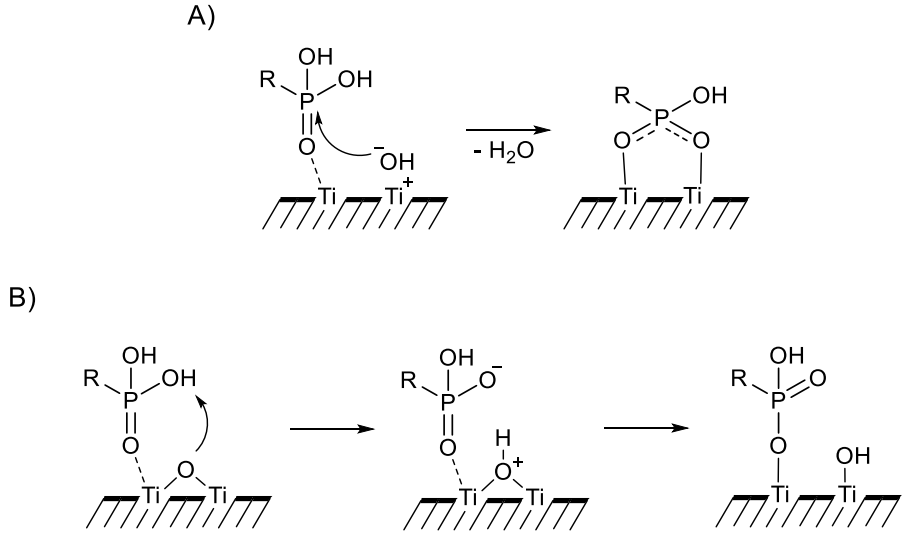

Scheme 2.7: A) Mechanism of covalent bond formation of organophosphonic acid with titanium oxide surface after Lewis-acidic activation. B) Mechanism of cleavage of Ti-O-Ti-bonds in presence of organophosphonic acid.

Silyl and alkyl phosphonates can react with titanium oxide as well under cleavage of the respective silanols and alcohols.[121] In some cases, this offers advantages regarding the coating process, as the respective acids are usually less soluble in organic solvents, however,

the binding efficiency compared to the free acid is decreased, leading to less densely grafted surfaces.[122] After allowing the physisorption from solution onto the desired material, tempering facilitates the condensation reaction and concludes the covalent linking.[119]

3 Preparation of antibacterial polymer brushes on titanium via “grafting to” method

In parts, this chapter constitutes a manuscript which has been accepted for publication.[123]

At the outset of working on antibacterial and adsorbable polymers for combating postoperative infections on titanium implants, the access to fundamental building blocks and the derived polymers needed to be explored. First and foremost, this involves the adsorbing (or anchoring) block comprising phosphonate groups, which has already been worked on in the Kuckling group and elsewhere.[124,125]

3.1 Phosphonate monomers and derived polymers

Diethyl 4-vinylbenzyl phosphonate (DEVBP) was synthesized according to published procedures by both Michaelis-Arbuzov and Michaelis-Becker reactions (Scheme 3.1).[125,126]For the Michaelis-Becker product, the yield (41 %) is about 30 % lower than reported in the literature[124] (Table 3.1), which is mostly due to losses during purification via column chromatography. The synthesis via Michaelis-Arbuzov reaction afforded the product with 41 % yield which is about 50 % lower than reported in the literature.[127] Here, the low yield is caused by the conversion of only 56 % after three days at 90 °C. Higher temperatures facilitate product formation, however, batches tend to polymerize at high conversions even in the presence of radical scavengers. Still, the Michaelis-Arbuzov pathway proved more convenient since the reactions were carried out in a homogenous system and can be upscaled easily, while the reaction of sodium hydride with diethyl phosphite in the case of Michaelis-Becker demanded closer monitoring due to the formation of a foaming suspension.

The methyl derivate (DMVBP) was synthesized by reacting vinylbenzyl chloride with trimethyl phosphite at 110 °C for 44 h and was isolated with 30 % yield. Again, this is low in comparison to the previously reported value of 72 %[125], but the established conditions provided a reproducible and reliable access to the monomer which oftentimes showed itself sensitive to self-initiated polymerization.

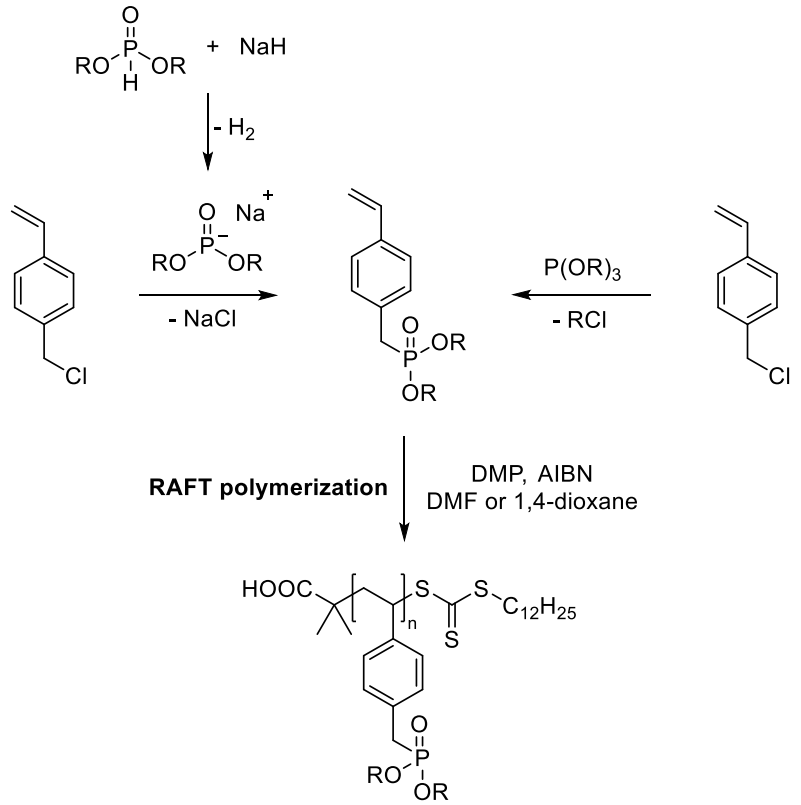

Scheme 3.1: General pathways to dialkyl 4-vinylbenzyl phosphonate monomer with R = Me (DMVBP); Et (DEVBP) via Michaelis-Becker (top left) and Michaelis-Arbuzov (top right) reactions. RAFT polymerization of the afforded monomer (bottom).

Table 3.1: Monomer yields for different reaction pathways compared to literature.

monomer	method	yield	yield reported in literature
DEVBP	Michaelis-Becker	47 %	73 %[124]
DEVBP	Michaelis-Arbuzov	41 %	90 %[127]
DMVBP	Michaelis-Arbuzov	30 %	72 %[125]

Both monomers could readily be polymerized via RAFT process using 2-(dodecylthiocarbonothioylthio)-2-methylpropionic acid (DMP) as chain transfer agent, AIBN as initiator and DMF or 1,4-dioxane as solvents (Scheme 3.1 and Table 3.2). The solid products were isolated by precipitation from cold diethyl ether and analyzed using NMR spectroscopy and SEC. The conversion was determined from ^{1}H NMR spectroscopy of quenched samples after the given reaction time by comparing signal integrals from the monomer to broad polymer peaks. Remarkably, while the monomer conversion for P(DEVBP) was >80 % in all cases, the conversion of the methyl derivate under the same conditions rarely exceeded 60 %. This suggests that the reaction conditions are not optimal, for example regarding the choice of CTA or solvent. Published studies on the RAFT polymerization of DMVBP show that conversions over 90 % are possible, when a suitable CTA (e.g. Z group = benzyl) in toluene are used.[128] Nevertheless, the dispersities of the phosphonate polymers synthesized in this work

laid well within the ranges of a controlled polymerization with values of 1.22 and lower. SEC analyses (THF as eluent for P(DEVBP), HFIP for P(DMVBP)) provide significantly lower average molar weights compared to the determination via NMR spectroscopy, but both methods are consistent regarding the comparison of polymers with different degrees of polymerization among themselves.

Table 3.2: Data for polymers with phosphonate groups synthesized via RAFT polymerization.

polymer	conv.	M_n(NMR) /gmol^{-1}	P_n (NMR)	M_n(GPC) /gmol^{-1}	*D*	solvent	reaction time /h
P(DEVBP)	84 %	2700	9	1800	1.10[a]	1,4-dioxane	45
P(DEVBP)	89 %	4200	15	2500	1.13[a]	DMF	22
P(DEVBP)	88 %	4600	17	2600	1.15[a]	1,4-dioxane	19
P(DMVBP)	40 %	3100	12	1800	1.19[b]	DMF	19
P(DMVBP)	55 %	4100	16	2000	1.19[b]	DMF	22
P(DMVBP)	64 %	7000	29	3800	1.22[b]	DMF	21

[a] SEC with THF as eluent, [b] SEC with HFIP as eluent

The end group retention of the trithiocarbonate was verified by detection of the respective signals of the polymer-bound dodecyl-group in ^{1}H NMR spectra and by block extension experiments. The block formation by employing the polymers as macro-RAFT agents were demonstrated with DEVBP as comonomer in case of P(DEVBP) (self-blocking experiment) and 4-vinyl pyridine (VP) in case of P(DMVBP). The SEC analysis reveals that the majority of chains had grown in both cases and the dispersity increased only slightly (Figure 3.1). Although the self-blocking of P(DEVBP) was found to be possible, it was not compatible with VP in this block order under the investigated conditions. By contrast, P(DMVBP) and P(VP) blocks could be combined either way based on the respective macro-CTA. Although incompatibility of monomers in RAFT is not uncommon, this is surprising, since the nature of the ester was not expected to affect the polymerization reaction which takes place at the vinyl group. Still, several iterations of the experiment confirmed this result. The flexibility regarding the block order of phosphonate monomer and VP was deemed vital for further studies on this system, which is why only the methyl derivate DMVBP was considered in the following experiments.

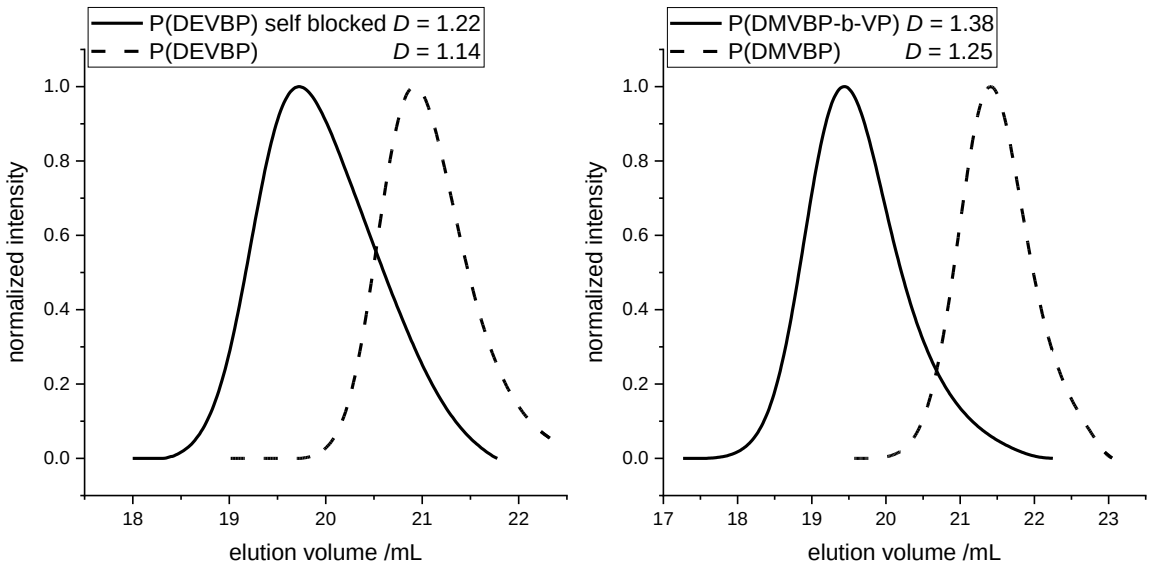

Figure 3.1: SEC traces of self-blocking experiment of P(DEVBP) in THF (left) and block copolymerization of P(DMVBP) with VP in HFIP (right).

The kinetics of the homopolymerization of DMVBP with [M]:[DMP]:[AIBN] = 100:1:0.25 in DMF were investigated. Samples were taken over the course of 24 h and analyzed using ^{1}H NMR spectroscopy and SEC. At low conversions, it was not possible to isolate polymer by precipitation from diethyl ether, which is why not all samples could be analyzed via SEC. The behavior of $\ln([M]_0/[M]_t)$ with the reaction time derives significantly from the ideal linearity: an induction period can be observed in the first 120 min, which is sometimes observed in RAFT systems, especially at high concentrations of CTA (Figure 3.2 left).[129] After a conversion of 20 %, the apparent reaction rate decreases, resulting in a decreasing slope of the curve, which indicates that the free radical concentration is not constant. With an averaged value of 0.056 h^{-1} it is in the same order of magnitude of RAFT polymerizations of styrene with a comparable CTA, owing to a similar reactivity of the vinyl group.[130] The theoretical average molecular weight calculated from the monomer conversion was considerably higher than the values derived from SEC due to the deviating structure of the polymer used for calibration (Figure 3.2 right). In well-controlled polymerizations, the dispersity decreases with ongoing chain growth, which was not the case for this system, especially after 40 % conversion. This suggests limited control and possibly chain termination, probably also due to contamination with oxygen from sampling. Apart from testing a more suitable CTA, the molecular weight distribution could be optimized by stopping the reaction at about 30-40 % conversion. Despite the derivation from ideal kinetics, the data from the isolated and chain extended polymers (Table 3.2 and Figure 3.1) showed that the system is suitable for the synthesis of multiblock copolymers. For the goal of this work, high end group fidelity and compatibility of the macro-RAFT agent with the chosen comonomers resulting in efficient block extension were the most important parameters, which is why the system was not modified further.

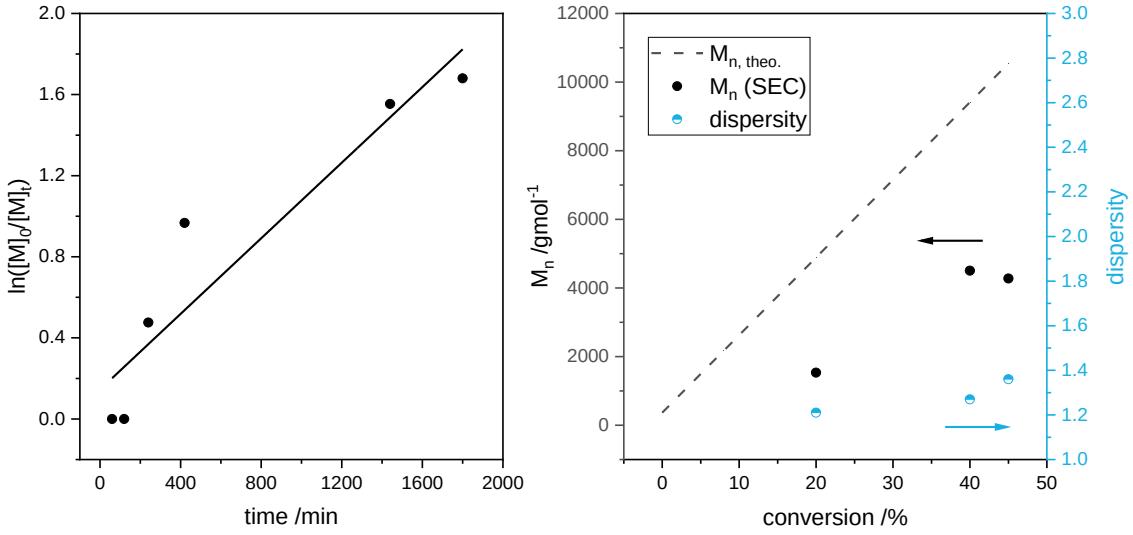

Figure 3.2: Kinetic investigation of RAFT polymerization of DMVBP with [M]:[DMP]:[AIBN] = 100:1:0.25. $ln([M]_0/[M]_t)$ against time with linear fit (left) and evolution of Mn with monomer conversion with polymer dispersity (right).

3.2 Block copolymers with anchor groups

In general, block copolymers of VP and DMVBP are accessible in any order by consecutive RAFT polymerization with DMP and AIBN in DMF and were isolated by precipitation in diethyl ether or toluene. SEC analyses proved block formation in any case with dispersities ranging from 1.3 to 1.8, which suggests derivation from ideal conditions in some cases. To afford the envisioned structure of a diblock copolymer with one anchoring segment and a cationic antibacterial block, the precursor polymer P(DMVBP-b-VP) had to be modified by post-polymerization reactions. Compared to a conversion of functional groups before the polymerization, this comes with the disadvantage of the oftentimes reduced solubility of the polymer compared to its monomer. Moreover, the reaction needs to be efficient to ensure (near) complete conversion, since unreacted moieties cannot be removed from the chain. Coiling or phase separation of the polymer chains may screen the desired reaction site from the reactant, so elevated temperatures may be needed to facilitate swelling or disrupt chain interactions. In the case of multifunctional polymers, the reaction must be compatible with adjacent segments as not to impair other functional groups.

For the system of this work, the pyridine moieties were reacted with 1-bromopropane in nitro methane to yield the positively charged pyridinium moieties (VPPr) (Scheme 3.2). These polycations have been used to render surfaces strongly antibacterial when applied as a brush coating, as demonstrated in seminal work of Tiller et al.[13] The procedure was based on published reports on the quaternization of pyridine-containing polymers with alkyl halides.[55,131] The reaction proceeded with quantitative conversion after 2 d at 70°C which

was verified using ^{1}H NMR spectroscopy by reference to the broad signals caused by the alkyl groups as well as the shift of the aromatic protons of the heterocycle. The polymers were purified by precipitation from toluene and obtained in good yields of >80 %. The respective monomer, alkylated vinyl pyridinium, cannot be isolated since it undergoes self-initiated anionic polymerization, which is why it is necessary to perform this reaction after polymerization.[132]

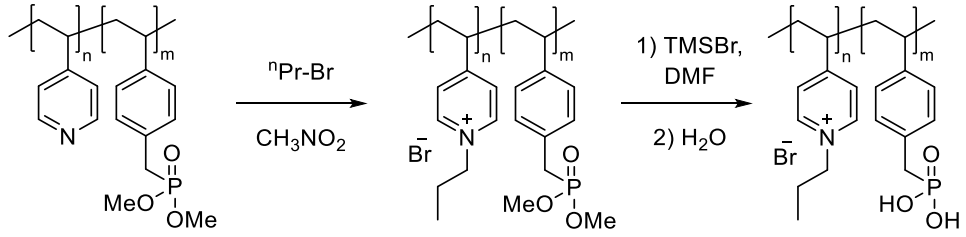

Scheme 3.2: Post modification of P(VP-b-DMVBP) to obtain alkylated pyridinium moiety and free phosphonic acid.

Lastly, the vinylbenzyl phosphonic acid units (PA) were liberated by silylation with excess TMSBr in dry DMF and treatment with water or methanol afterwards. The polymers were isolated by dialysis and subsequent lyophilization with >60 % yield. At complete conversion to the phosphonic acid, the resonance of the phosphorus atom undergoes a characteristic shift from 29 ppm to 26 ppm in the ^{31}P NMR spectrum. Remarkably, although the polymer is soluble in DMSO-*d6*, the peaks caused by the anchor block are only visible upon acidification of the sample. This is probably due to the formation of hydrogen bonds between partly deprotonated phosphonic acid groups, which result in aggregation and poor swelling of the respective segments of the polymer, thus being invisible in NMR spectra. Upon protonation of the phosphonic acid moieties, the solvation is enhanced, and the resonances appear (Figure 3.3). The same phenomenon was observed in ^{31}P NMR spectra regarding the resonance of the phosphonic acid.

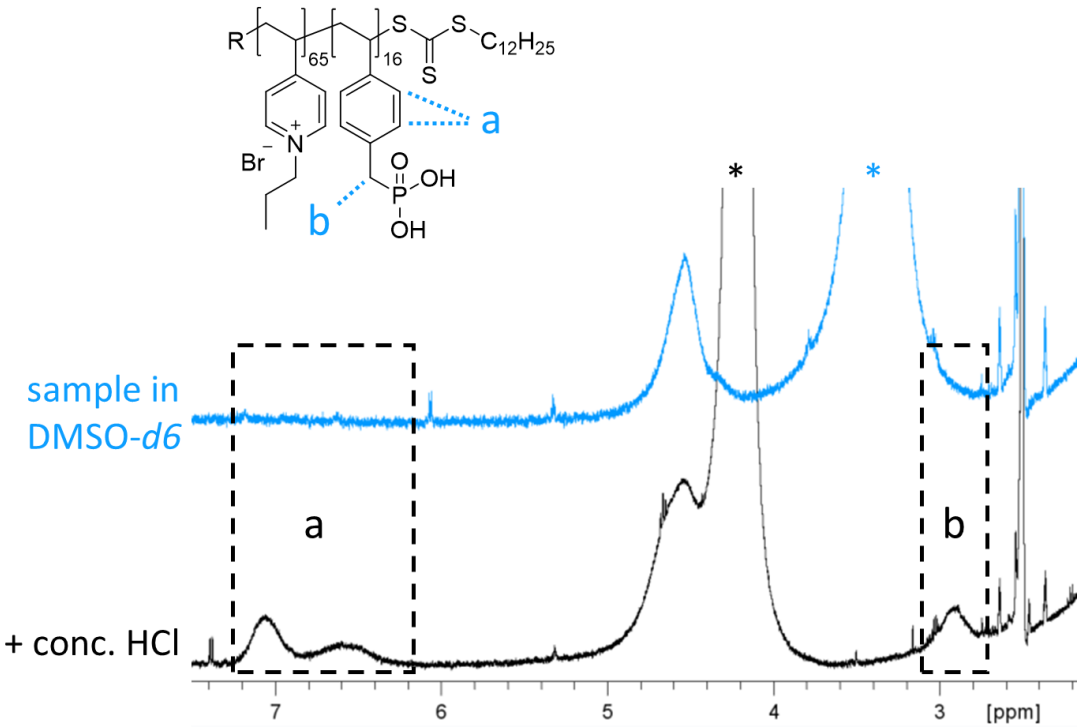

*Figure 3.3: Representative ^{1}H NMR spectra of P(VPPr$_{65}$-b-PA$_{16}$) in DMSO-d6 with and without traces of conc. HCl. a and b denote aromatic and methylene group peaks, respectively, which are visible after acidification. * denotes the water signals which shift upon change of pH.*

The trithiocarbonate end group is most likely retained under these conditions, as the broad resonance of the dodecyl group at 1.24 ppm in the ^{1}H NMR spectrum is still present. However, its characteristic absorption band at 320 nm in UV/vis spectra was not observed due to superposition of more intensive signals.

In Figure 3.4, representative SEC traces of the four-step synthesis of P(VPPr$_{65}$-b-DMVBP$_{16}$) are displayed. The maximum was shifted to lower elution volumes after each step and maintained its characteristic shape, indicating block formation and homogenous transformation by the post modification reactions. The dispersity increased from 1.30 to 1.79 after the block extension of P(VP) with DMVBP, which may be due to some free radical polymerization indicated by the slight shoulder at 21.0-22.5 mL. In the subsequent steps, the dispersity decreased again, because the lower molecular weight fractions were removed in the purification processes. Even though the molecular weight decreased due to the cleavage of alkyl groups from the phosphonate, the elution volume is shifted to lower volume. This can be explained by the severe change in polarity affecting the hydrodynamic volume which overcompensated the loss of two methyl groups.

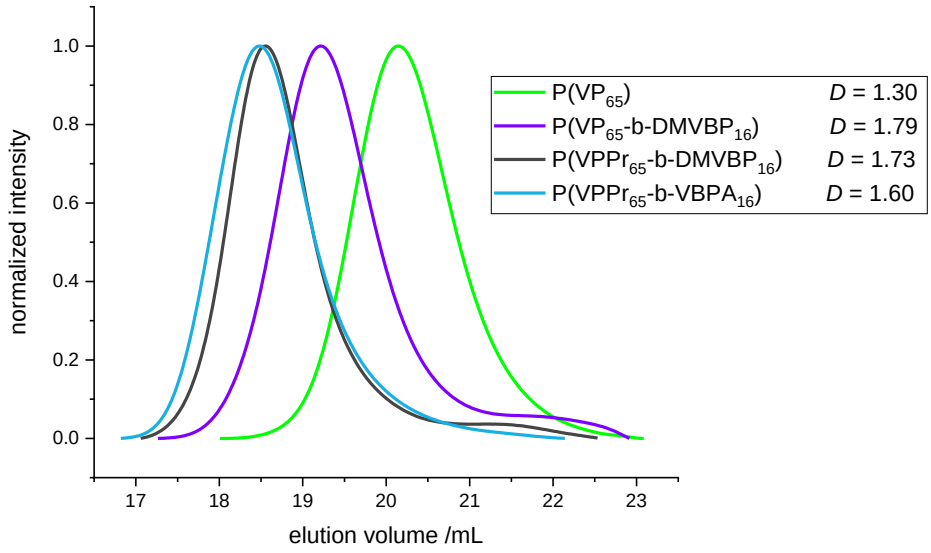

Figure 3.4: Representative SEC (HFIP) traces of the products of the four step synthesis of P(VPPr$_{65}$-b-PA$_{16}$).

3.3 Effect of anchor block length on grafting density

When considering published studies on comparable systems comprising a linear anchoring block with a certain number of binding groups, there is little information on why a specific block length is chosen.[99,101,112] Beside the more obvious consequences regarding molecular weight, solubility and polarity of the polymer, it can be assumed that the quantity of surface binding groups also affects the grafting density and other surface specific properties. Since the grafting density is a key parameter for the construction of polymer brushes and more specific for antibacterial surfaces, a series of block copolymers with the general structure P(VPPr-b-DMVBP) was synthesized and compared regarding their chemical properties and surface affinity (Table 3.3).

The quantity of VP was fixed to 65 and 66 units based on published research on related systems with good antibacterial effectiveness in that range.[112] The anchor block length was varied by adjusting the amount of DMVBP in the block extension of P(VP) and one polymer P(PA$_{11}$-b-VPPr$_{66}$) was synthesized in reversed order to investigate possible effects of block sequence. SEC measurements showed monomodal distributions through every synthetic step and the derived molecular weights were in good agreement with the values calculated from NMR spectra. With dispersities ranging from 1.38 to 1.60 the molecular weight distribution of the final polymers was slightly broader than to be expected from polymers synthesized under optimized RAFT-conditions except for P(PA$_{11}$-b-VPPr$_{66}$) which exhibits a value of 1.89, owing to poor control during the polymerization. Still, no negative impact on the desired function of the brush was expected since all necessary groups were present in the polymer. The overall solubility in polar solvents decreased with increasing number of phosphonic acid groups in the

anchor block resulting in P($VPPr_{65}$-b-PA_{21}) not being soluble in water and P($VPPr_{65}$-b-PA_{48}) and P($VPPr_{65}$-b-PA_{114}) not being soluble in water or alcohols at all.

Table 3.3: Molecular weights (NMR and SEC), dispersities D and solubility in methanol and water for diblock copolymers.

polymer	M_n(NMR) /gmol^{-1}	M_n(SEC) /gmol^{-1}	*D*	sol. in MeOH/H_2O
P($VPPr_{65}$-b-PA_3)	16,000	15,500	1.38	✓ / ✓
P($VPPr_{65}$-b-PA_6)	16,400	15,400	1.52	✓ / ✓
P(PA_{11}-b-$VPPr_{66}$)[a]	17,500	18,700	1.89	✓ / ✓
P($VPPr_{65}$-b-PA_{16})	18,300	17,200	1.60	✓ / ✓
P($VPPr_{65}$-b-PA_{21})	19,700	15,900	1.44	✓ / *X*
P($VPPr_{65}$-b-PA_{48})	24,600	insoluble	-	*X* / *X*
P($VPPr_{65}$-b-PA_{114})	37,000	insoluble	-	*X* / *X*

[a] reverse block order

As titanium samples carry a native oxide layer, titanium oxide particles were used to investigate the affinity of polymer to the metal surface from methanolic solutions at different concentrations.[99] Phosphonic acid groups react with surface hydroxyl groups to form M-O-P bonds, covalently anchoring the polymer to the particle. Visually, the adsorption became evident as the coated particles behaved like a stable dispersion for several hours up to days, whereas the pristine titanium oxide particles settled without stirring in a shorter timeframe. In order to determine the amount of adsorbed polymer, the coated particles were filtered off and the residual dissolved polymer was detected via UV/vis spectroscopy. A Lambert-Beer calibration plot was recorded for each polymer beforehand which allowed to calculate the concentration after the adsorption process from the adsorption bands of the aromatic systems at 227 nm and 257 nm (Figure 3.5). Similar bands have been observed for quaternized pyridinium polymers with methyl or ethyl groups.[133] Note that the characteristic UV band of the trithiocarbonate group which is expected at 305-310 nm could not be observed due to superposition with the more intensive signals.[134]

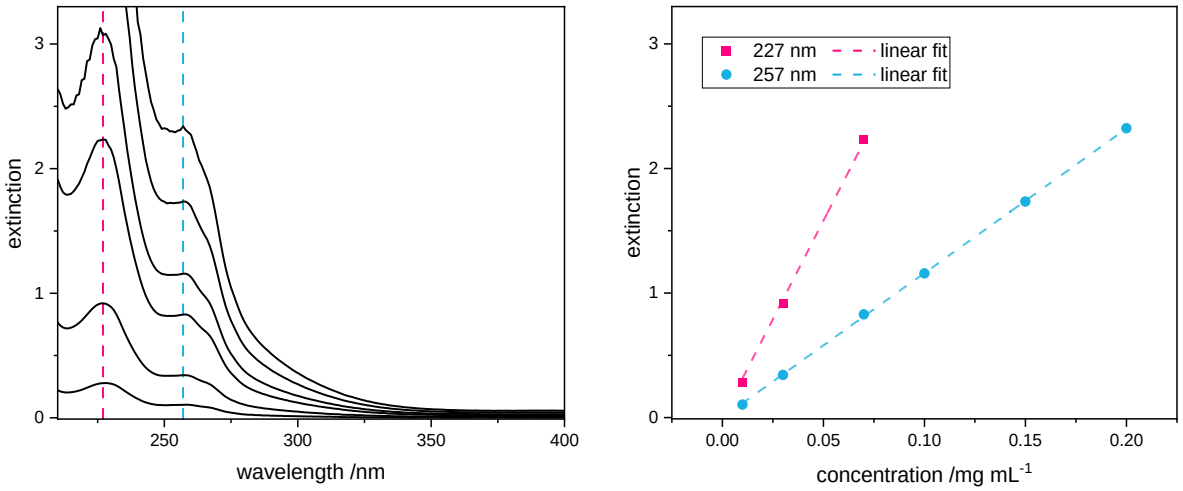

Figure 3.5: Left: representative UV/vis spectra of P(VPPr$_{65}$-b-PA$_{16}$) at different concentrations in methanol. Right: respective Lambert-Beer calibration plots for aromatic bands at 227 nm and 257 nm.

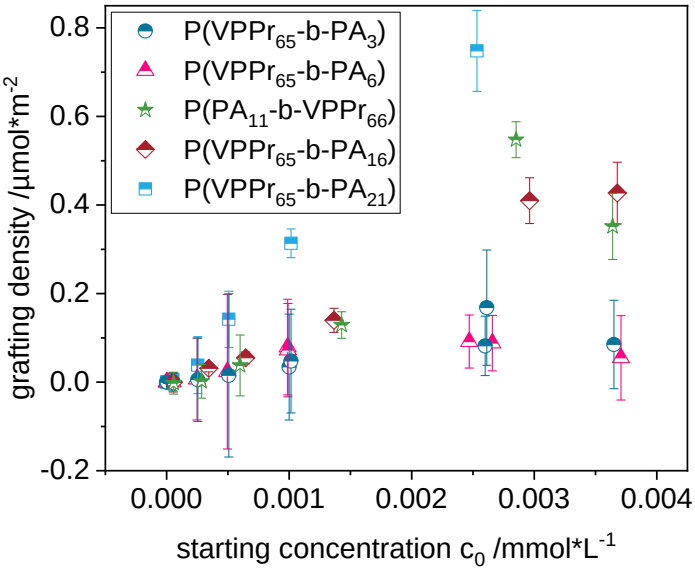

Figure 3.6: Grafting density of adsorbable diblock copolymers on titanium oxide particles at different concentrations.

Generally, higher polymer concentrations lead to higher grafting densities (Figure 3.6). Samples with 3, 6, 11 and 16 PA-units plateaued at about 2.5 to 3.0 mmol/L (about 50 mg/mL). This agrees with the notion that there were no multilayers formed but saturation of the surface was reached at a certain threshold. Changing the block order did not have a significant effect on the adsorption efficacy as demonstrated by the data for P(PA$_{11}$-b-VPPr$_{66}$). Grafting densities up to 0.75 µmol/m² were reached, which is in the same order of magnitude of reported values for polymer brushes formed by the “grafting to”-mechanism.[77,96,135,136] A comparison of different block lengths demonstrates that the adsorption efficacy is dependent of the anchor block length with P(VPPr$_{65}$-b-PA$_{21}$) performing best. This, however, goes at the cost of solubility in water (and other solvents at even higher content of PA) which should be

considered when designing polymers for coating titania as this may be a critical factor in the treatment process of implant surfaces.

Noticeably, the polymers with higher molecular weights yielded the highest grafting density which contradicts the common observation that the grafting density is partly controlled by the polymer weight, i.e. shorter polymer chains allow for a denser occupation.[137] In this “diffusion limited” model, it is suggested that the diffusion of new chains to the surface is facilitated when the neighboring polymer strands occupy less space, resulting in more chains per area. However, recent findings indicate that grafting and degrafting is not only limited by diffusion but also by intricate processes at the reactive site with involvement of the binding groups.[136] Since the polymers reported here contain more than one binding site, the effect of polymer weight may well be overcompensated by this.

3.4 Brush stability against acid and base

The formation of a polymer brush prepared with P(VPPr$_{65}$-b-PA$_{16}$) on titanium surfaces as well as its stability towards acidic and basic conditions were investigated via surface plasmon resonance (SPR) spectroscopy. This method allows the in-situ investigation of thin layers on metal coated wafers regarding their thickness and refractive indices. Conducting time-dependent measurements, kinetic phenomena like adsorption and desorption can be monitored.[99,138] The substrate is LaSFN9-glass coated with chromium (ca. 1 nm), gold (ca. 50 nm) and titanium oxide (ca. 4 nm) by atomic layer deposition (ALD). The brush is then prepared by grafting the polymer onto the metal layer from methanol solution and annealing at 120 °C. Subsequently, the substrate is cleaned with water and methanol to remove unbound polymer.

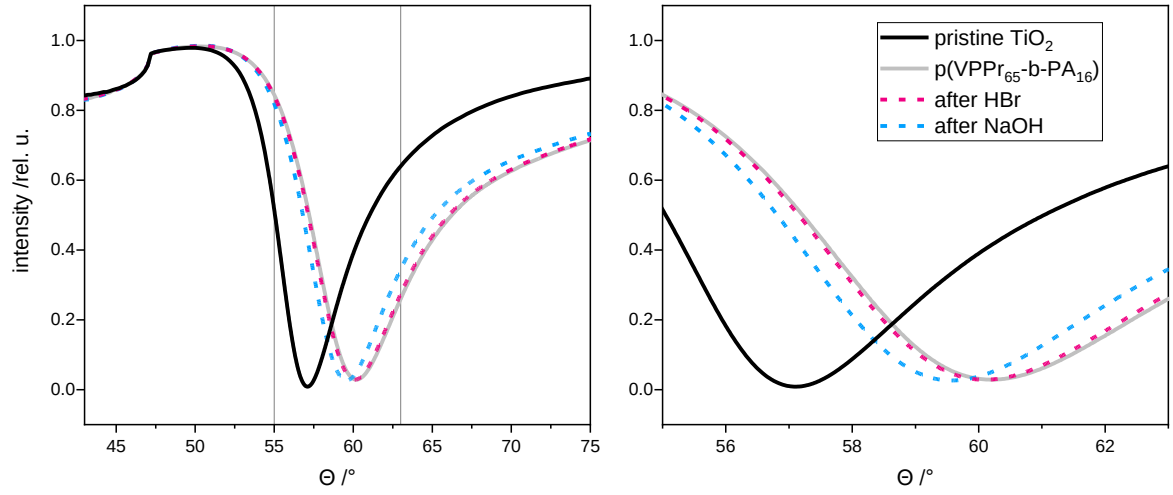

Figure 3.7: SPR measurements. full reflectivity scans of titanium oxide surface coated with P(VPPr$_{65}$-b-PA$_{16}$) before and after exposure to HBr/NaOH.

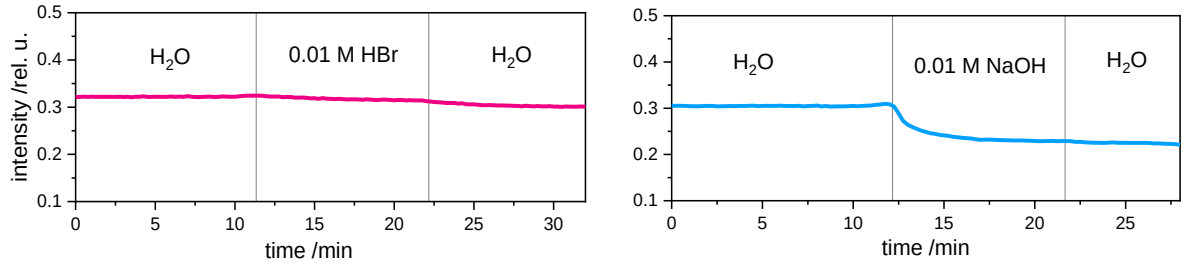

Figure 3.8: SPR measurements. Stability test of P(VPPr$_{65}$-b-PA$_{16}$)-coated substrates against water and 0.01 M HBr (left) and NaOH (right) in kinetic mode.

The significant shift in the plasmon minimum from 57.1° to 60.2° after the coating process proves the formation of an additional layer (Figure 3.7). The thickness of the polymer adlayer is derived from fitting the angle-dependent reflectivity to the edge of total internal reflection and the plasmon minimum assuming a refractive index of the swollen polymer layer of 1.435 (ε’=2.06, detailed parameters in appendix Table 8.1 and Table 8.2). Thus, a layer thickness of 9 nm was determined which is in the expected range for grafted polymer brushes in good solvents.[136]

The brush stability was probed in aqueous media using a flow cell by observing changes in reflectivity over time (Figure 3.8). After equilibration, a stable baseline is afforded, which suggests that there is no desorption in water. Dental implants are exposed to considerable chemical stress due to food intake, which is why acidic and basic conditions were used to probe the sample. Exposure to aqueous hydrobromic acid (pH 2) over 10 min does not affect the layer thickness significantly. Injection of aqueous sodium hydroxide (pH 12), however, causes a considerable drop in reflectivity, corresponding to a shift of the plasmon minimum to lower angles. Fitting the resulting curves reveals a decrease in thickness from 9 nm to about 5 nm. Remarkably, the chains are only partly removed from the surface. It has been established that polyelectrolyte brushes are inherently more strained than their non-charged counterparts: due to intramolecular repulsion of adjacent cationic groups the polyelectrolyte assumes a more stretched conformation which results in a loss of entropy and decreases the energy necessary for mechanical failure of the surface-polymer-bonds.[77] Particularly, high grafting densities decrease the thermodynamic stability of polyelectrolyte brushes due to intermolecular repulsion of neighboring strands. The suggested mechanism is displayed in Figure 3.9: starting from a densely grafted polymer brush (A), a fraction of phosphonic acid metal esters is hydrolyzed in basic solution (B). After a certain number of chains has been cleaved, the hydrolytic stability is improved owing to a more relaxed (“mushroom”) conformation of the remaining molecules (C).

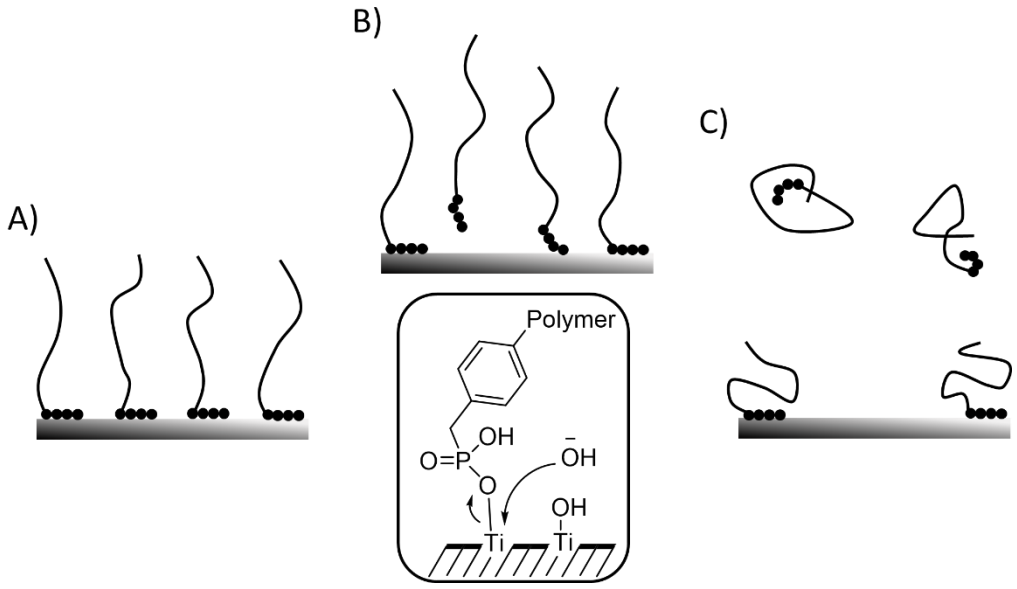

Figure 3.9: Suggested mechanism for brush cleavage by hydrolysis. A) Dense brush with stretched chains. B) Chains are removed via basic hydrolysis. C) Coiling of the remaining chains as well as of the removed chains becomes more pronounced due to less intermolecular repulsion of adjacent chains.

The following experiments were conducted, evaluated and discussed by Dr. Frank Simon (XPS measurements) from Leibniz-Institut für Polymerforschung Dresden and Dr. Cornelia Wolf-Brandstetter (surface wettability, streaming potential, microbiological investigations) from TU Dresden and are reproduced with minor adjustments in text and figures in order to convey the complete investigations on the polymers presented here. For the physicochemical and biological characterization of coated substrates, three water soluble polymers were chosen: comparing P(VPPr$_{65}$-b-PA$_3$) and P(VPPr$_{65}$-b-PA$_{16}$), conclusions can be drawn regarding higher or lower grafting densities. Since P(VPPr$_{65}$-b-PA$_{16}$) and P(PA$_{11}$-b-VPPr$_{66}$) form polymer brushes of similar density, they allow insights into the effect of reverse block order.

3.5 Physicochemical properties of coated titanium samples

Intermediate hydrophilicity for the titanium reference was observed with advancing water contact angles of about 45° (Figure 3.10). All polymer coated surfaces revealed even lower contact angles but the difference to the reference was significant only for P(VPPr$_{65}$-b-PA$_3$). For this coating type, the shorter length of the hydrophobic anchor block might affect the final wettability of the coated surfaces. However, the differences between all coated samples were not significant. It has to be highlighted that the variability among coated samples was much higher than for the reference samples, indicating a heterogeneous coating outcome.

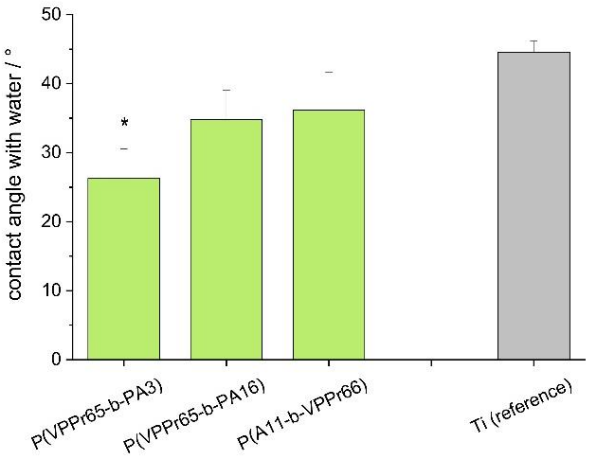

Figure 3.10: Advancing contact angles on coated and uncoated titanium samples determined with water.

Coated and identically treated reference samples were analyzed by means of X-ray photoelectron spectroscopy (XPS) after identical treatment steps as for all further physicochemical and biological characterizations. A typical wide scan as well as high resolution spectra of C and N region of the reference and one polymer coated sample are shown in Figure 3.11. The atomic percentages of the components most relevant for the interpretation of coating results are shown in Table 3.4**,** while complete analysis is given in the appendix (Table 8.3 and Table 8.4).

The high-resolution element spectra were deconvoluted into component peaks having different binding energy values (BE). The shapes of N 1s spectra recorded from the copolymer-coated samples are very characteristic for the P(VPPr$_m$–b–PA$_n$) polymer. The two well separated component peaks indicate the presence of two differently bonded nitrogen species. On first look these findings are in contrast to the suggested chemical structure of the synthesized polymers showing only one species of nitrogen as well as NMR data revealing complete quaternization. Photoelectrons from these protonated nitrogen species (C–^{M}N^{+}=C ↔ C=^{M}N^{+}–C) led to component peak *M* at BE ≈ 402.39 eV. The binding energy values of the second component peak *L* (BE ≈ 399.93 eV) is characteristic for organically bonded nitrogen atoms do not carry a charge, such as C–^{L}N=C ↔ C=^{L}N–C. However, the amount of charge of a quaternary nitrogen can also be compensated by strong electrostatic interactions with an electron donor, e.g. titanates (Ti-O$_y$) from the titanium oxide surface. Similar peak splittings of quaternary ammonium compounds partially interacting with surfaces have been found on silanoates (Si-O$_y$).[139]

Care should be taken when interpreting the calculated atomic percentages, as it is well known that the native titanium oxide layer can be contaminated with a number of hydrocarbon impurities from the laboratory atmosphere or from the solutions used for the cleaning and coating steps. Typically, a variety of different compounds containing alcohols, ethers, ketones,

and carboxyl groups are found. During coating process, the polymers are expected to adsorb in addition to already existing contaminations or to partially replace them. The resultant C content thus is based on remaining contaminations as well as on presence of adsorbed polymers. In contrast, the N and P can be regarded as marker elements for the success of polymer adsorption. As shown in Table 3.4, a clear increase of the P content was observed for the three polymers having the same block order and differing only in the anchor block length (P($VPPr_{65}$-b-PA_3), P($VPPr_{65}$-b-PA_{16}), P($VPPr_{65}$-b-PA_{21})). With increasing P content in the polymers also increasing P was found on coated samples. As the pyridinium block was of constant length, the increasing N content indicates a higher polymer coating density for the polymers with longer phosphonate anchor block in accordance with the adsorption experiments shown in Figure 3.6. The behavior of the polymer P(PA_{11}-b-$VPPr_{66}$) with reversed block order was obviously different. While the P content fits to the relative percentage of P within the molecule, less N was found in adsorbed state. However, this sample was also found to have higher Ti and O content and lower C content, making this coating in parts more similar to the uncoated reference sample than the other coated samples. Hence a different orientation of adsorbed molecules might be expected. A different behavior of this compound is also seen when comparing molecular weight specified by size exclusion chromatography, revealing highest hydrodynamic radius although NMR studies revealed a molecular weight according to sum formula.

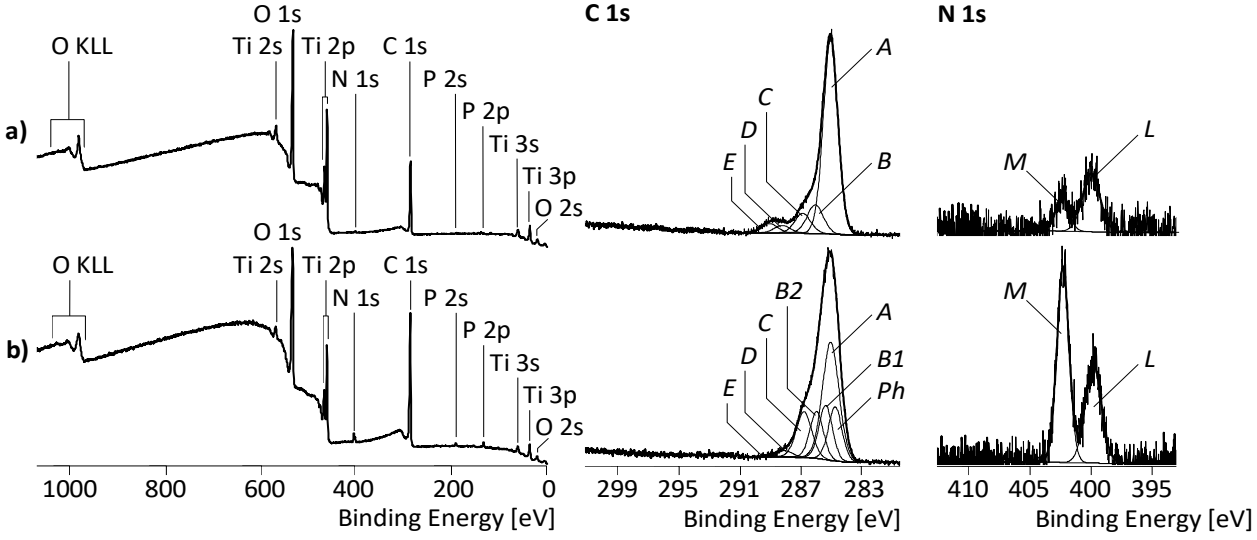

Figure 3.11: XPS wide-scan (left column), C 1s (middle column) and N 1s (right column) spectra for a) uncoated titanium reference and b) polymer-coated sample p($VPPr_{65}$-b-PA_{16}). The assignment of the component peaks (Ph, A, B, etc.) to the structural units can be found in appendix Figure 8.3.

Table 3.4: Relative elemental compositions of reference and polymer coated samples as derived from XPS survey spectra. More data on elemental composition derived for other elements be found in appendix Table 8.3 and Table 8.4.

Peak	C 1s /At%	N 1s /At%	O 1s /At%	P 2p /At%	Ti 2p3/2 /At%
Reference (Ti)	48.25	1.01	37.26	0.38	11.94
p($VPPr_{65}$-b-PA_3)	58.84	2.35	29.05	1.03	7.35
p($VPPr_{65}$-b-PA_{16})	59.73	2.97	27.56	1.49	6.70
p($VPPr_{65}$-b-PA_{21})	64.78	2.93	23.79	2.02	5.45
p(PA_{11}-b-$VPPr_{66}$)	55.12	2.56	31.05	1.31	8.41

Titanium reference samples as well as polymer coated samples were further characterized by streaming potential measurements. The calculated zeta potential shows a nearly linear slope in the region close to the isoelectric point (IEP) which suggests chemically inert surfaces for all types of samples (Figure 3.12). For the polymer coated samples this is in agreement with the expected behavior of the polycationic blocks, i.e. the part that extends into the surrounding solution, as alkylated pyridinium as well as the polymer backbone is generally unreactive. For the reference surface IEPs between pH 3.3 and 3.8 were determined in repeated measurements. This value is slightly lower compared to published values of titanium surfaces by streaming potential measurement reporting an IEP of about 4.0.[140] This difference in surface properties can be attributed to the pre-treatment by autoclaving within ultrapure water, resulting in a much more hydrophilic surfaces with contact angles of only 45°. The autoclaving of titanium is known to increase the native oxide layer[141], which then dominates at the surface, while titanium surfaces stored at air tend to adsorb hydrocarbon contaminations. In consequence, a higher content of dissociable acidic OH-groups is expected comparable to the observed increase, when titanium surfaces were heated in water vapor.[142] The behavior of the polymer coated surface is obviously dominated by the positively charged VPPr-block, as all three coatings with the identical VPPr-block result in very similar zeta potential curves with identical IEP and slope. The IEP is significantly shifted by roughly 3 pH units towards higher pH compared to the uncoated reference with values ranging between pH 6.5 and 7. The surface charge properties were neither affected by the different length of the anchor groups nor by the order of the two blocks (P($VPPr_{65}$-b-PA_{16}) vs. P(PA_{11}-b-$VPPr_{66}$)).

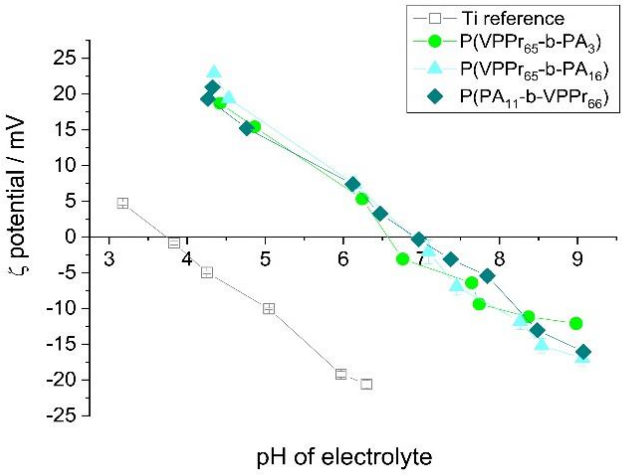

Figure 3.12: Streaming potential measurements at different pH values allowing calculation of zeta potential of coated samples.

3.6 Microbiological and cell biological investigations of coated titanium samples

Data on amounts of detached viable bacteria shown in Figure 3.13, represent the extent of bacteria able to survive at the surface after 17 h of biofilm formation. Respective bacteria were detached by combined sonification and vortexing for subsequent quantification. In contrast, the live/dead staining images (Figure 3.14) reflect conditions directly on the samples immediately after biofilm formation.

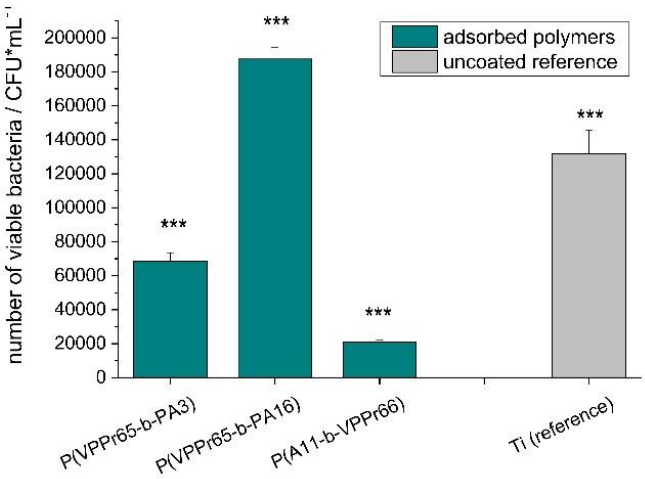

Figure 3.13 Characterization of coated titanium samples with respect to their antibacterial potential. Number of viable bacteria attached to the surfaces after 17 h cultivation under starving conditions promoting biofilm formation (Asterisks denote significant differences to all other sample types).

Bacterial adhesion and subsequent biofilm formation at the titanium surfaces was significantly reduced ($p < 0.001$) at samples coated with P($VPPr_{65}$-b-PA_3) or P(PA_{11}-b-$VPPr_{66}$), while antibacterial effect was limited for coatings with P($VPPr_{65}$-b-PA_{16}). Here, viability of detachable bacteria was even slightly higher than on uncoated reference surfaces (Figure 3.13), although obviously a higher number of dead cells was also found in contact with this surface compared to the reference (Figure 3.14). In general, a higher percentage of dead cells was observed for all coated polymers compared to the uncoated reference, but complete killing was not achieved.

The difference in the antibacterial properties of P($VPPr_{65}$-b-PA_3) and P($VPPr_{65}$-b-PA_{16}), was surprising, as both differ solely in the length of the anchor block, but not in quaternized pyridinium block. These findings are in line with the outcomes of the cytotoxicity assays described further below. However, when redissolved polymers were in contact with planktonic bacteria (Figure S6) similar antimicrobial efficacy was observed for both polymers differing in anchor block length but with identical quaternized block.

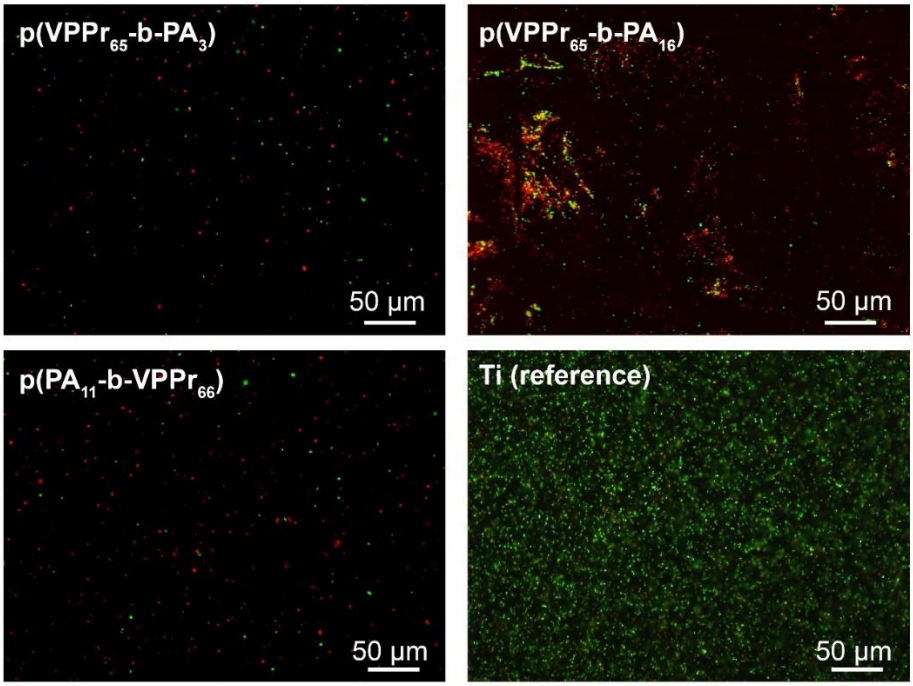

Figure 3.14: Live/dead staining of attached biofilm directly after dynamic cultivation.

A very interesting finding is the significantly different behavior of bacteria to polymers with comparable length of both blocks but a reversed block order, P(PA_{11}-b-$VPPr_{66}$) vs. P($VPPr_{65}$-b-PA_{16}), which was observed in adsorbed state as well as for dissolved polymers (Figure 3.13 and appendix Figure 8.1). Interpretation of the XPS spectra indicate a different orientation as P content was comparable but the higher Ti and O content could be explained by a thinner coating. Due to the reversed synthesis of blocks, the polymer brushes carry different end groups facing the solution. As a result from the macro-RAFT agent, P(PA_{11}-b-$VPPr_{66}$) features

a terminal aliphatic dodecyl chain, whereas the polycationic block of P($VPPr_{65}$-b-PA_{16}) is terminated with a carboxylic acid group. The difference in hydrophilicity may affect the orientation on the surface and thus the interaction with biological systems and are subject of ongoing research.

In addition to the polymer based effects, it has to be highlighted that the biofilm adhesion at reference surfaces, that were polished and stored under wet conditions prior to all experiments, was already comparatively low with an approx. 2-log reduction compared to machined and grinded surfaces used in previous investigations for identical cultivation conditions.[143] By additional functionalization with the polymers the adhesion of viable bacteria could be further reduced in particular by P(PA_{11}-b-$VPPr_{66}$).

Cell biocompatibility was assessed with polymer coated samples (Figure 3.15) as well as with polymer solutions directly diluted in cell culture medium (appendix Figure 8.2). Cell adhesion and cell spreading was impaired in a manner that goes in line with the antibacterial properties: only slight changes in cellular behaviour was seen for P($VPPr_{65}$-b-PA_{16}), while reduced cell attachment as well as less expressed cell spreading are seen for coatings with P($VPPr_{65}$-b-PA_3) or P(PA_{11}-b-$VPPr_{66}$). This correlation between antimicrobial activity and cytotoxicity is known for a series of other antimicrobial substances such as polymers based on (2-methacryloyloxyethyl) phosphonate (DMMEP) and dipicolyl aminoethyl methacrylate (DCAMA) copolymers.[144]

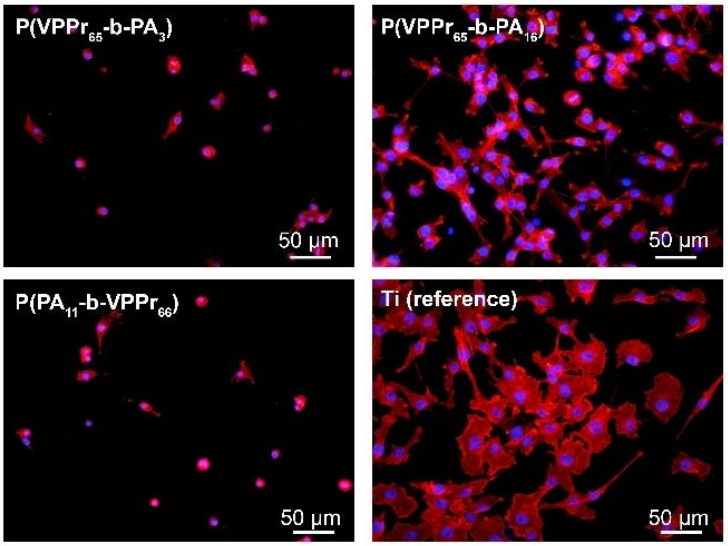

Figure 3.15: Fluorescence images of human gingival fibroblast after 24 h cell adhesion to coated titanium samples with staining for nuclei (blue) and actin (red).

3.7 Conclusions

Seven linear block copolymers containing polycationic pyridinium segments and phosphonic acid anchor blocks were synthesized via RAFT polymerization and post modifications. Using a “grafting to” process to form polymer brushes on titanium substrates, it was observed that the grafting density depends on the number of phosphonic acid groups present in the anchoring block. The brushes proved stable in neutral and acidic conditions, while basic conditions diminished the grafting density to a certain degree.

The antimicrobial activity of the polymers could be verified for all three selected water-soluble molecules but was depended on actual design and immobilization status. When exclusively the anchor block length was changed an equal antimicrobial effect was seen for dissolved polymers in contact with planktonic bacteria.

In contrast, for adsorbed polymers antimicrobial efficacy was greater for the shorter anchor block, although a higher surface density was achieved for the longer anchor block length. Final explanations for this behavior are not possible with actual available data, but might be related higher flexibility of the cationic VPPr-block of the molecule with shorter anchor block in adsorbed state. Another interesting impact factor was identified, as the reversed block chain order of phosphonic anchor and cationic VPPr-block had tremendous effect on antimicrobial efficacy but cytotoxic properties as well, although an identical shift of the IEP was obtained, and thus overall surface chemistry should be comparable. Of particular high interest is to find out the reasons for this complete different biological behavior. Potential effects might be attributed to the specific conformation of polymers in immobilized state, as the molecular weight order was reversed in NMR and size exclusion experiment, indicating a higher hydrodynamic radius of the polymer with the reversed block order. Different binding status was also derived from XPS measurements. For this aspect further investigations to specify surface orientation are required to discriminate physicochemically based effects from additional impact factors.

4 Amphiphilic block copolymers with enhanced biocompatibility

4.1 Tuning the amphiphilic balance

As was confirmed for the polymer brushes of the general structure P(VPPr-b-PA) presented above, good antibacterial properties of cationic polymers are often associated with poor cytocompatibility. One way to manage toxicity towards human cells is the copolymerization with monomers containing hydrophobic or uncharged hydrophilic groups.[16,51] Thus, a series of adsorbable polycations was synthesized incorporating styrene (Sty) as hydrophobic comonomer to tune the amphiphilic balance. Again, P(DMVBP) was used as anchor block precursor. Based on the findings regarding the block length (chapter 3.3), a degree of polymerization of 12 was chosen to ensure a high surface affinity and good solubility in water. In order to slim down the synthesis, an inherently cationic monomer was used for the antibacterial block, saving one post modification step. 4-Vinylbenzyltrimethyl ammonium chloride (TMA) is a strong electrolyte and its effectiveness in antibacterial applications was already proven in different studies.[145]

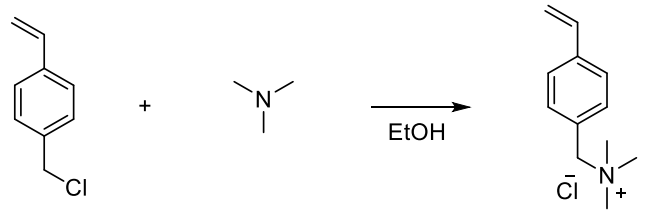

Scheme 4.1: Synthesis of TMA.

TMA was synthesized by reacting 4-vinylbenzyl chloride with trimethyl amine in ethanol and purified by recrystallization from acetonitrile which afforded the product as hygroscopic, colorless crystals in 57 % yield (Scheme 4.1). The monomer proved compatible with the macro-RAFT agent P(DMVBP) derived from DMP when polymerized in DMF/water mixtures with AIBN as initiator at 70 °C. The monomer conversion was >90 % and the polymer was isolated either by dialysis or precipitation in isopropanol. Although the molecular weight of the polymer was over one magnitude higher than the molecular weight cutoff of the membrane, a significant portion was lost during dialysis resulting in a yield of only 57 %. Precipitation affords the product in a higher yield, however, DMF and isopropanol were not removed entirely.

The kinetics of the copolymerization of TMA and Sty with [TMA]:[Sty]:[P(DMVBP$_{12}$)]:[AIBN] = 100:90:1:0.2 were investigated. The reaction was performed with about 0.6 M monomer concentration in DMF/water (3/2 v/v) at 70 °C. It must be noted that the removal of oxygen was conducted by three freeze-pump-thaw cycles, because it was observed that purging with

argon removed significant amounts of the volatile Sty from the reaction mixture, leading to distorted results. While the samples for NMR studies were retrieved according to the standard procedure (freezing under air and dilution in deuterated solvent), the SEC samples had to be isolated via dialysis. It was observed that the removal of solvent in vacuo at 40 °C caused free Sty to polymerize, resulting in bimodal distributions in SEC that were not representative. The first order kinetic plot for the total monomer concentration revealed a linear dependence up to a total conversion of 84 % indicating the absence of termination reactions (Figure 4.1 left). The reaction then reached a total conversion of 91 % after 24 h with a slight drop in reaction rate. Although the reactive site is the same for both monomers, Sty was incorporated significantly faster than TMA (Figure 4.1 right). It is known that the overall polarity can exert severe influence on the reaction rate in copolymerizations: the local concentration of a monomer at the active center depends on the preferential sorption of the polymer coil.[146] This affects the relative reactivity and leads to derivations from random incorporation of two competing species. Due to the pronounced difference in polarity of the monomers at hand, such a mechanism is also conceivable, although no further experiments were conducted to support this assumption.

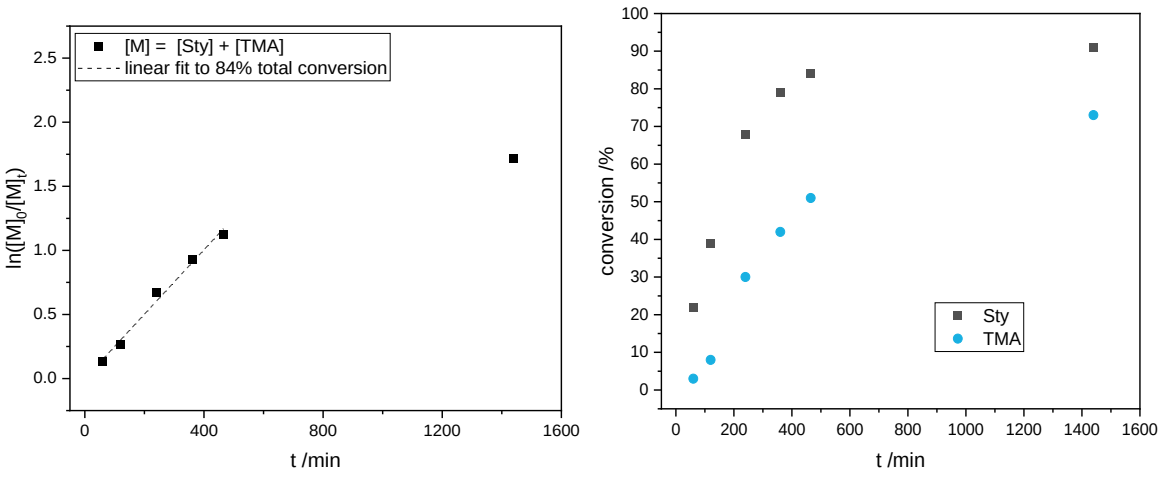

Figure 4.1: Kinetic investigations of [TMA]:[Sty]:[CTA]:[I] = 100:90:1:0.2 DMF/H_2O (1:1 v/v). Left: Pseudo-first-order kinetic plot for total monomer conversion. Right: Conversion determined via ^1H NMR sampling of Stye and TMA against time.

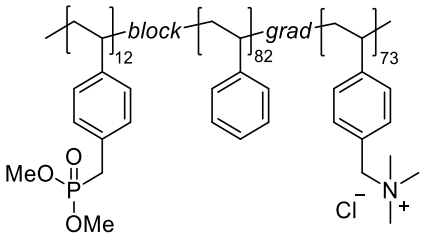

P(DMVBP-b-Sty-grad-TMA)

Scheme 4.2: Structure amphiphilic copolymer with P(DMVBP) as precursor for the anchor block and a Sty-TMA-gradient segment.

The resulting structure exhibits a gradient composition of the second polymer block with a Sty-rich beginning and successively more TMA-units towards the end (Scheme 4.2). At 25 % total conversion, the block is nearly completely composed of Sty, whereas the overall composition after 24 h is close to the feed ratio. The final monomer conversion corresponds to the relative reactivities and amounts to 91 % for Sty (P_n = 82) and 73 % for TMA (P_n = 73). The uneven incorporation also reflects in the average molar weights derived from SEC: an increase with a gradually steepening slope can be observed which can be explained with the higher molar mass of TMA compared to Sty (Figure 4.2 left). This is in good agreement with the theoretical values derived from NMR spectroscopy. The dispersity decreases at first, then increases after 40 % total conversion and finally amounts to 1.51 which is slightly higher than expected for optimized RAFT polymerizations but satisfactory considering the chain extension with monomers of severely different polarities.

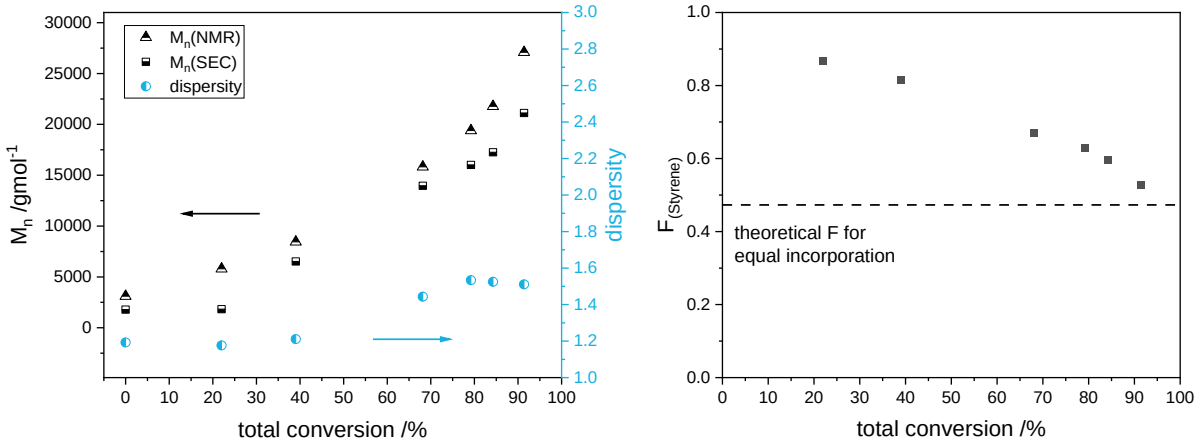

Figure 4.2: Left: Evolution of molecular weight derived from NMR spectroscopy and SEC as well as dispersity against total conversion for kinetics of P(DMVBP-b-Sty-grad-TMA). Right: Fraction of Sty F against total conversion.

Based on the investigated system, five polymers with varying hydrophobicity were synthesized by chain extension of P(DMVBP$_{12}$) (Table 4.1) in order to screen for the optimum between bactericidal effect and cell toxicity. The ratio of Sty to TMA in the final polymer was varied from zero to 2.04. The triblock copolymer P(PA$_{12}$-b-TMA$_{89}$-b-Sty$_{23}$) was obtained by isolation of P(DMVBP$_{12}$-b-TMA$_{89}$) and subsequent chain extension with Sty. It has been shown that a blocked structure as opposed to a random copolymer has an effect on selectivity in amphiphilic antibacterial polymers.[147] The conversion of TMA was determined from ^{1}H NMR samples of the quenched reaction mixture. Since oxygen was removed prior to the polymerization by purging with argon, which was ascertained to also remove some Sty, the respective fraction of this monomer was calculated from the purified polymers by comparing the aromatic signals with signals of TMA. All polymers were treated with ca. 6 M hydrochloric acid at 115 °C overnight to hydrolyze the phosphonic acid ester. 1,4-Dioxane was added as cosolvent in case of P(PA$_{12}$-b-Sty$_{47}$-co-TMA$_{23}$) and P(PA$_{12}$-b-TMA$_{89}$-b-Sty$_{23}$) in order to obtain clear solutions. This is remarkable for the latter since it has a comparably low fraction of the

hydrophobic monomer with Sty/TMA = 0.26. This suggests that the TMA-Sty-block structure has a more significant effect on the overall behavior of the polymer chain in solution compared to a mixed composition. This also reflects in the severe deviation of the average molecular weights of this polymer derived from NMR spectroscopy and SEC (24,000 g/mol (NMR) vs 40,000 g/mol (SEC)).

Although there is no sign of degradation observed in ^{1}H NMR spectra, after hydrolysis the dispersities of each polymer increase by 0.1-0.2 which may be attributed to the harsh reaction conditions. The treatment with TMSBr (cf. chapter 3.2) was not possible for these polymers since no suitable solvent was found that was compatible with the reactant and able to dissolve the polymer. The complete removal of methoxy groups was confirmed by the characteristic shift from 31.8 to 19.3 ppm in ^{31}P NMR spectra and the absence of the respective signals in ^{1}H NMR spectra.

Table 4.1:Polymers with different fractions of Sty synthesized by block extension of P(DMVBP$_{12}$) in DMF/H$_2$O mixtures at 70 °C with AIBN as initiator and subsequent hydrolysis of DMVBP-units with HCl in water or water/1,4-dioxane.

polymer	M_n(NMR) /gmol^{-1}	M_n(SEC) /gmol^{-1}	*D*	Sty/TMA
P(PA$_{12}$-b-TMA$_{171}$)	39,000	46,000	1.62	0
P(PA$_{12}$-b-Sty$_{14}$-co-TMA$_{111}$)	28,000	38,000	1.55	0.13
P(PA$_{12}$-b-Sty$_{82}$-co-TMA$_{74}$)	27,000	32,000	1.55	1.11
P(PA$_{12}$-b-Sty$_{47}$-co-TMA$_{23}$)	13,000	16,000	1.53	2.04
P(PA$_{12}$-b-TMA$_{89}$-b-Sty$_{23}$)	24,000	40,000	1.64	0.26

The results demonstrate that the system Sty/TMA is suitable for the use as amphiphilic antibacterial block: it allows the chain extension of the anchor block with both cationic and hydrophobic moieties simultaneously. Thus, the amphiphilic balance can be tuned by varying the monomer feed. The slight gradient may affect the antimicrobial activity, but it is sufficient to focus on the overall ratio of Sty to TMA and the effect of block structure for preliminary studies. The results should aid in optimizing the antimicrobial block for the application as contact-killing brushes and have yet to be evaluated in biological testing.

4.2 End functionalization for improved cell adhesion

To be able to promote the biocompatibility even further, the synthetic access to an end functionalization of the polymer was targeted. One example for a suitable terminus is the RGD sequence which has been shown to play a vital role in mammalian cell adhesion and proliferation and was used before in comparable surface modifications.[87,92] Among others, prior works of the Kuckling work group have demonstrated the use of 2-vinyl-4,4-dimethylazlactone (VDMA) as monomer in RAFT polymerizations in order to introduce an electrophilic moiety that selectively reacts with nucleophiles in a click-like manner (Scheme 4.3).[148,149] Here, the base polymer composed of anchor block and antibacterial block is to be chain extended with a small quantity of VDMA and subsequently modified with the RGD sequence. Thus, it is oriented towards the solution after brush formation. The fraction of this end functionalization was kept small as not to compromise the brush conformation, because the introduction of a more hydrophobic group at the end most likely decreases the swelling and stretching of the surface tethered chains.

VDMA was synthesized in a two-step procedure according to literature with 29 % overall yield which is slightly lower than the reported value of 36 % (Scheme 4.3).[148] It was not necessary to optimize the yield since one iteration afforded the required amount of the monomer needed for this work.

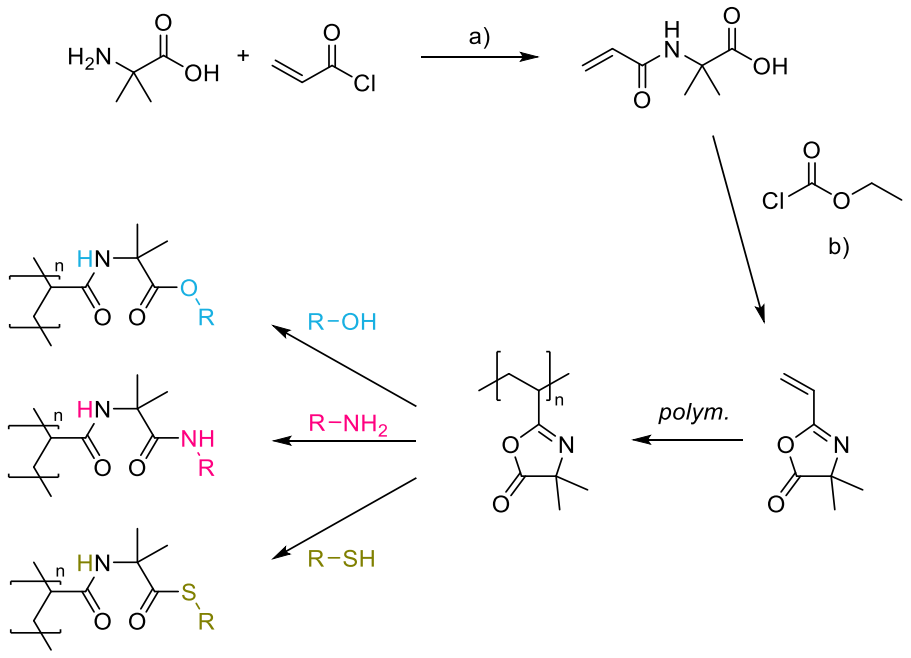

Scheme 4.3: Two-step synthesis of VDMA with reaction conditions: a) NaOH, BHT, H_2O, 0 °C to rt, 3 h. b) TEA, acetone, 0 °C, 3 h. Polymerization and reactivity of P(VDMA) with various nucleophiles, namely alcohols, amines and thiols.

Since the fraction of end-attached groups was kept low, it was obvious that the analysis and verification of the obtained structure would be challenging. In order to prove both the block extension of the macro-RAFT agent and the incorporation of the chosen nucleophile, a model

system was investigated at first using a fluorinated nucleophile as probe. P(PA_{12}-b-Sty_{39}-co-TMA_{64}) was chain extended with VDMA in dry DMSO and AIBN as initiator at 70 °C for 5 h (Scheme 4.4). The reaction mixture was quenched and a conversion of 38 % was determined via ^{1}H NMR spectroscopy by comparing the integral of methyl groups of free and polymerized VDMA. 4-Fluorobenzylamine (4FBA) was added as ring-opening agent and the polymer was isolated via dialysis and lyophilization. The comparison of SEC traces of precursor and product reveal a uniform shift to higher molecular weight which verified the block extension. The emergence of a broad peak at 24.8 ppm next to the diethyl phosphonate signal at 29.2 ppm (traces of HCl were added to protonate the acidic groups) in the ^{31}P NMR spectrum revealed that the phosphonate groups were partly dealkylized. It has been reported that the reaction of phosphonate esters with nucleophilic amines selectively yields the onefold dealkylized monoester.[150] A broad resonance in the ^{19}F NMR spectrum at -116.8 ppm proved the incorporation of the fluorinated compound and the absence of low-molecular residual nucleophile (Scheme 4.4). Upon addition of 4FBA to the NMR sample, its sharp resonances were observed next to the broad peak caused by the fluorine containing polymer. In the ^{1}H NMR spectrum, broad superimposing peaks of the aromatic protons at 6.8-7.5 ppm and the benzylic methylene group at 4.0-4.5 ppm could be assigned to polymer-bound 4FBA. This experiment validates the overall concept by proving both that the macro-RAFT agent can readily be chain extended with VDMA and also reacts with the chosen nucleophile.

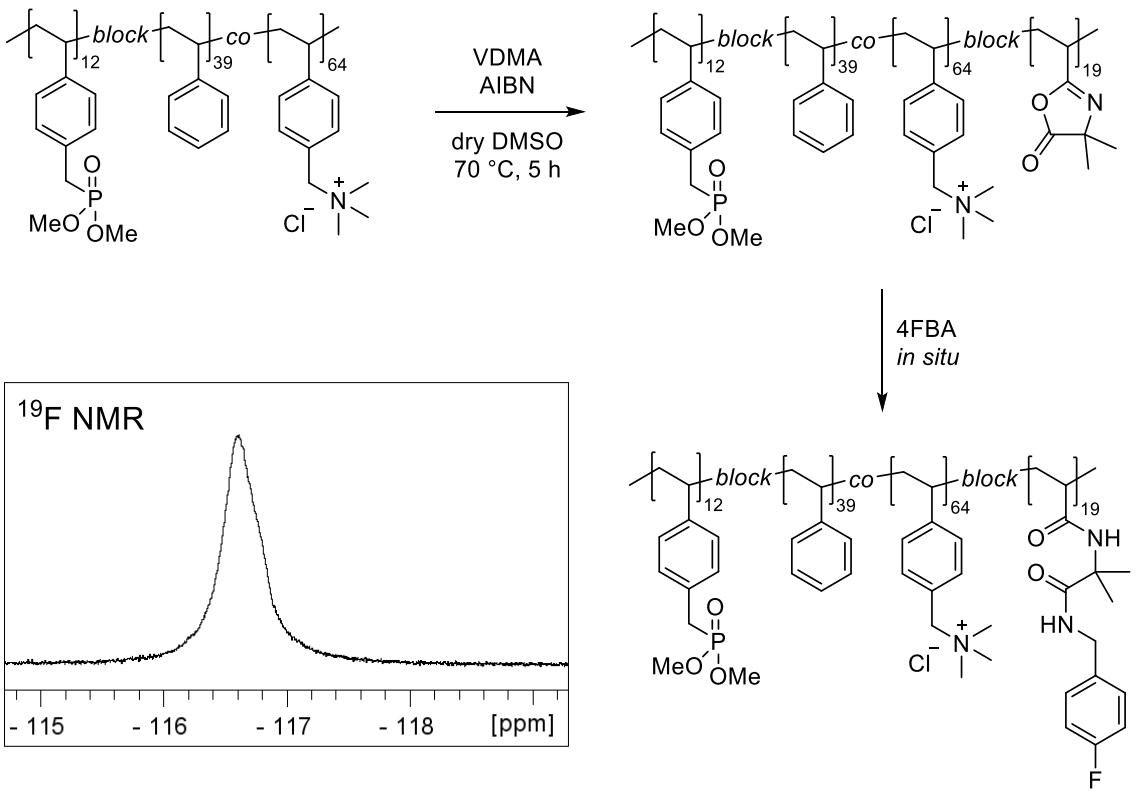

Scheme 4.4: Reaction scheme of block extension of P($DMVBP_{12}$-b-Sty_{89}-co-TMA_{23}) with VDMA and subsequent ring-opening with 4FBA. The ^{19}F NMR spectrum proves the incorporation of the fluorine-containing nucleophile.

It is noted that the polymer was deliberately not isolated after quenching the block extension with VDMA, which has the disadvantage of free VDMA being attacked by the added nucleophile as well. It is assumed that the reaction rate of VDMA in the polymer backbone and of free VDMA is equal. However, since the heterocycle is sensitive to ring-opening by water and other somewhat nucleophilic substances, dialysis and the precipitation in alcohols or wet solvents are not suitable for the isolation of the VDMA-containing polymer. Although a considerable amount of side product is generated, all these species are low molecular and can be removed via dialysis after conducting the ring-opening.

With the concept validated, it was transferred to the incorporation of biomolecules. Besides the RGD sequence, biotin-PEG2-amine was used to generate a biotin end functionalization. This molecule is frequently used for biochemical labelling or recognition due to its specific and strong affinity to certain proteins.[151] This is potentially beneficial for surface analytics of the applied polymer brush. For both variants, P(DMVBP$_{12}$-b-TMA$_{167}$) was used as precursor and reacted with VDMA and AIBN as initiator in dry DMSO at 70 °C (Scheme 4.5). The ^{1}H NMR spectrum of the quenched samples revealed a conversion of about 30 % yielding a block with just under ten VDMA-units in both cases.

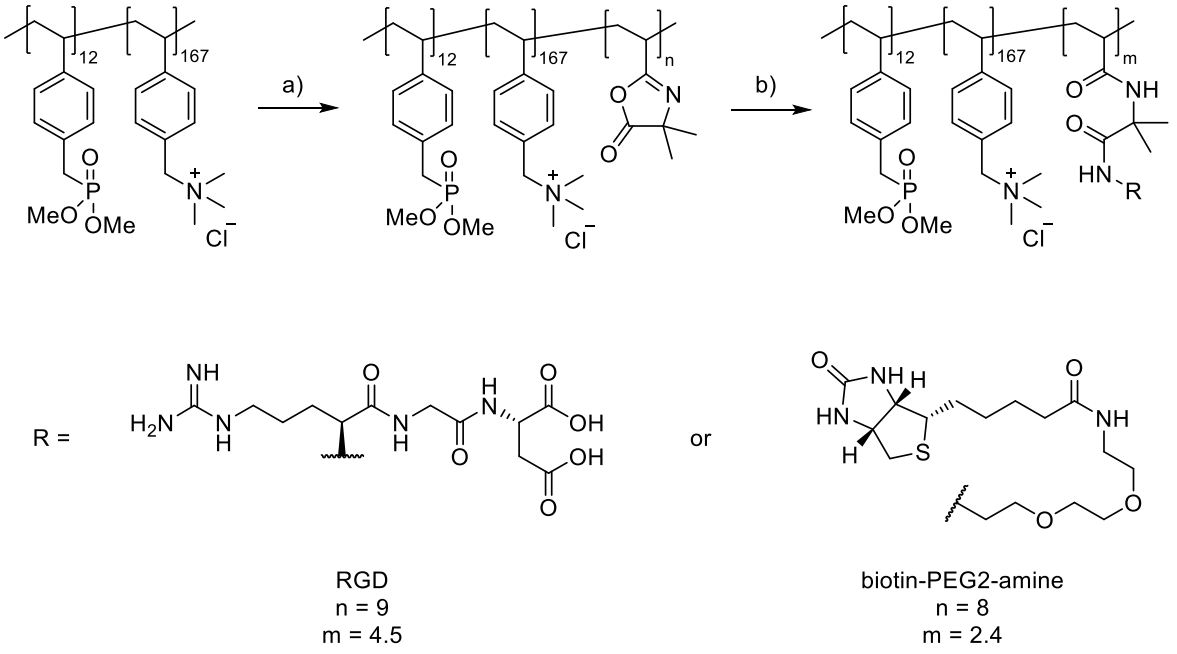

Scheme 4.5: Reaction scheme of block extension of P(DMVBP$_{12}$-b-TMA$_{167}$) with VDMA and subsequent ring-opening with RGD and biotin-PEG2-amine. n denotes the degree of polymerization of VDMA, m the quantity of functionalized units with the respective biomolecule. Reaction conditions: RGD-variant: a) VDMA, AIBN, dry DMSO, 70 °C, 17 h; b) RGD, DBU, rt, 3 d; then quenching of residual VDMA with H$_2$O/HNMe$_2$. Biotin-variant: a) VDMA, AIBN, dry DMSO, 70 °C, 5 h; b) Biotin-PEG2-amine, rt, 17 h; then quenching of residual VDMA with ethanolamine.

After the polymerization was quenched, 0.3 equivalents of biotin-PEG2-amine with respect to the total amount of azlactone-units in the mixture were added to obtain the biotin-functionalized polymer P(DMVBP$_{12}$-b-TMA$_{167}$-b-PBio$_2$). Comparing ^{1}H NMR spectra before and after addition, a new set of vinyl protons was observed (Figure 4.3). Depending on the

integrals used for calculation, 25 % to 33 % of VDMA units underwent the ring-opening reaction, which is in good agreement with the equivalents added and amounts to about 2.4 biotin-units per chain, assuming equal reactivity of free and polymer-bound azlactone. The remaining heterocycles were quenched by addition of excess aminoethanol, after which the polymer was isolated by dialysis and lyophilization. The analysis via SEC confirmed the chain extension as the elution volume peak shifted from 17.60 mL to 17.41 mL corresponding to an increase in average molecular weight from 40,000 g/mol to 41,000 g/mol (PMMA calibration). The dispersity was raised from 1.44 to 1.58, indicating presumably an irregular consumption of polymer-bound azlactone groups by the nucleophile. In the ^{31}P NMR spectrum, a single broad peak at 18.6 ppm was observed which indicated that the phosphonate was quantitatively mono-dealkylized to yield the monoester.

The verification of the desired outcome was limited to indirect methods. Although the purification via dialysis removed the majority of low-molecular impurities, the low mass percentage of biotin in the polymer results in poor signal to noise ratios of potentially meaningful signals in NMR and IR spectra. However, in future works, the presence of biotin could be detected by taking advantage of the protein interactions with the biomolecule, namely with avidin/streptavidin, for example with fluorescence spectroscopy.[152]

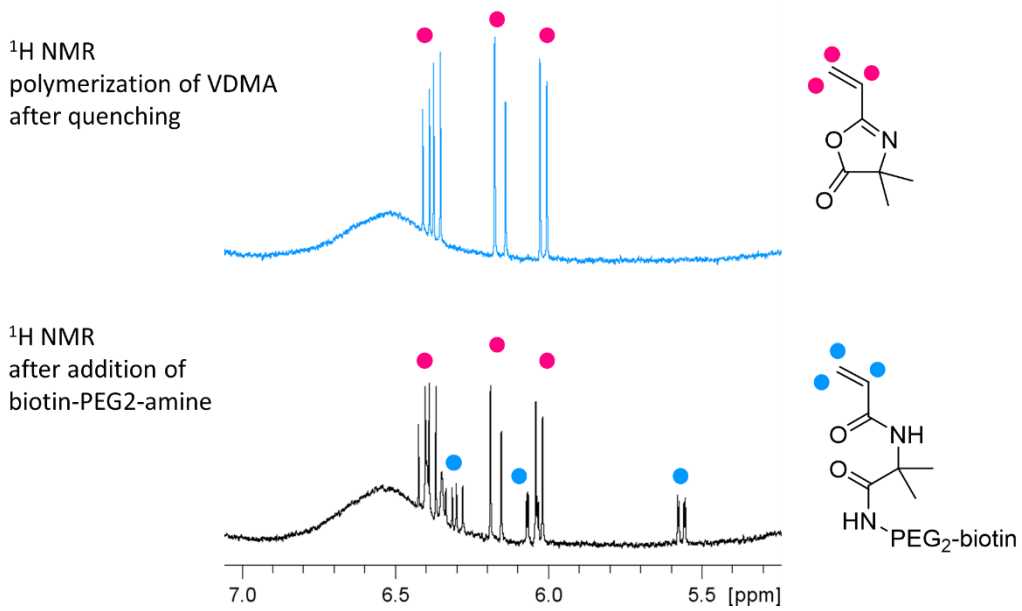

Figure 4.3: Section of ^{1}H NMR spectra in DMSO-d6 of reaction mixture for the synthesis of P(DMVBP$_{12}$-b-TMA$_{167}$-b-PBio$_2$) after block extension with VDMA (top) and after addition of biotin-PEG2-amin (bottom).

To obtain P(DMVBP$_{12}$-b-TMA$_{167}$-b-PRGD$_{4.5}$), P(DMVBP$_{12}$-b-TMA$_{167}$) was chain extended with VDMA (Scheme 4.5). After quenching, 0.5 equivalents of RGD with respect to the total amount of VDMA used and 2.2 equivalents of DBU with respect to RGD were added. Although it was reported that the reaction of azlactone and RGD can be conducted in pure DMSO,[92] it was observed in this work that the solubility of RGD in DMSO is enhanced upon addition of an

aiding base. This ensures that the nucleophilic amine group is not protonated by the two carboxylic acid groups and should facilitate the ring-opening reaction.

In contrast to the functionalization with biotin, the ^{1}H NMR spectrum of the reaction mixture after the addition of RGD/DBU revealed that all azlactone moieties were ring-opened despite using only 0.5 equivalents of RGD. At least three different species had formed, discernible owing to new sets of vinyl protons. While the exact structure of the side products could not be identified, the presence of an excess of DBU presumably accelerated the reaction of VDMA and water, which may be a contaminant since DBU was not dried before use. Moreover, the initially clear solution turned turbid after addition, which indicates that DMSO is not the optimal solvent for this reaction. Dimethylamine in water was added as a nucleophilic agent to quench residual azlactone groups. Subsequently, the reaction mixture was diluted with water and purified by dialysis. Calculating from the conversion of VDMA (30 %) and the equivalents of RGD used, a VDMA-block with $P_n = 9$ was formed, half of which were targeted to be functionalized with RGD. Due to the occurrence of side reactions, the incorporation of RGD is uncertain.

Remarkably, the lyophilized polymer was not soluble in DMSO-*d6* anymore, but in water. The ^{1}H NMR spectrum revealed that several low molecular species were not removed by dialysis. Most notably, peaks in the vinylic range from 5.6 ppm to 6.4 ppm indicate the presence of the side products which presumably stemmed from reactions with free VDMA as discussed above. In SEC analysis, a shift of the elution volume peak from 17.60 mL to 17.43 mL and an increase in dispersity from 1.44 to 1.62 was observed (Figure 4.4) which corresponds to the block extension. In the ^{31}P NMR spectrum, next to the resonance of the dimethyl phosphonate at 29.5 ppm, a second peak at 23.7 ppm was observed, which suggests that the ester was partly dealkylized.

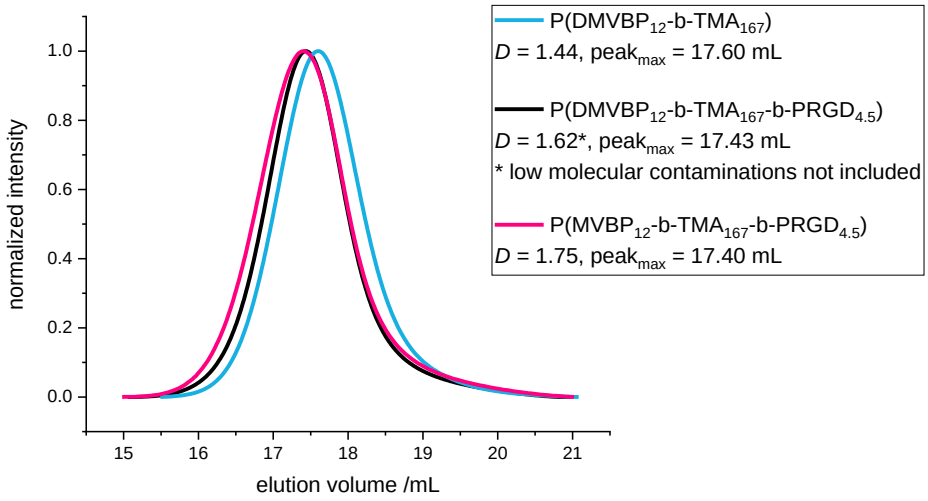

Figure 4.4: SEC traces (HFIP) of polymers for RGD end-functionalized polymer brushes.

By reacting the polymer with excess ethanolamine in water at 50 °C overnight, the conversion to the monoester (MVBP) was completed, which was verified using ^{31}P NMR spectroscopy. The polymer was isolated via dialysis and lyophilization and the analysis via SEC revealed a marginal shift of elution volume from 17.43 mL to 17.40 mL, while the dispersity increased from 1.62 to 1.75. In the ^{1}H NMR spectrum, no resonances in the vinylic range were observed, suggesting that the low molecular side products from the RGD-functionalization were removed. Still, it was not possible to identify the RGD-sequence either due to the poor signal to noise ratio or because it was not linked to the polymer. Similarly, ^{15}N NMR spectroscopy proved inadequate to provide insight into the polymer structure, since there were no detectable resonances from the nitrogen-atoms of the VDMA-derived block. In UV/vis spectroscopy, the aromatic system of the styrene derivates superimpose any bands that could be used to detect the RGD sequence, which shows an absorbance peak at 204 nm.[153] Lastly, investigation with IR spectroscopy and determining the optical rotation before/after block extension and end functionalization did not offer further insight, since neither method uncovered significant differences. All methods suffer from the fact that the targeted structural element makes up less than 5 % by weight of the polymer, which is a necessity by design.

Since this is a general issue when employing small amounts of RGD in a polymer system, other groups have faced similar challenges. In an aforementioned publication (Figure 2.8), Schönherr et al. equipped surface initiated polymer brushes with one terminal RGD-group per chain.[87] They used surface analytics to prove the conjugation of brush and RGD-sequence, showing an increased thickness via ellipsometry and a change in water contact angle. Furthermore, they detected signals in XPS corresponding to N-C and C-NH_3^+ groups. Especially XPS may be suitable for the polymers synthesized in this work if the chemical environments of the different nitrogen species can be resolved. Ellipsometry and contact angle measurements will also be influenced by the grafting density, which in turn is affected by the polymer composition, making the comparison between to polymer brushes made via “grafting to” difficult. Lastly, biocompatibility essays elucidated the difference between unfunctionalized and RGD-coupled polymer brushes, with the latter significantly enhancing cell attachment. In a further exemplary study, Verdoes et al. investigated drug delivery systems, using RGD end-functionalized block copolymers to facilitate cellular accumulation.[154] In order to prove the incorporation of RGD, they cleaved and hydrolyzed the peptide sequence in acidic conditions and derivatized the amino acid with o-phthaldialdehyde. Afterwards, they verified and quantified the presence of each building block with a calibrated HPLC system. This method offers the advantage of not being dependent on surface analytics and would be suitable for the polymers synthesized in this work as well.

Regardless of the difficulties concerning the verification of RGD end groups, the synthesis has potential for optimization. By removing contaminants from the aiding base DBU, most importantly water, the formation of side products may be largely prevented. Since a turbidity of the solution was observed after addition of RGD/DBU, DMSO may not be suitable as solvent for this reaction altogether. Other inert solvents were explored, however, they were discarded since they are not able to dissolve the precursor polymer P(DMVBP$_{12}$-b-TMA$_{167}$), for example DMF or DMAc. By contrast, good solvents like HFIP or water are nucleophilic and therefore no suitable environment for azlactone groups. Lastly, while the presence of free VDMA can be useful to monitor the reaction with nucleophiles as shown in Figure 4.3, the polymer should be liberated from residual monomer after the polymerization once the reaction itself is optimized. For this purpose, a non-nucleophilic solvent for precipitation of the polymer should be explored, leaving polymer-bound azlactone groups intact.

4.3 Conclusions

In order to improve the compatibility of adsorbable antibacterial polymers with human cells, the block composition of the polycationic segment was modified regarding the amphiphilic balance. Hereto, the combination of the hydrophobic monomer Sty and the cationic monomer TMA was explored. The kinetics of the copolymerization using the anchor segment precursor P(DMVBP$_{12}$) as macro-RAFT agent were investigated and revealed that Sty was preferentially incorporated, leading to a slight gradient in monomer sequence. Overall, the reaction exhibited the characteristics of a controlled polymerization and demonstrated that the system is suitable for the intended use. Thus, a series of polymers with varied ratios of Sty to TMA in the second block were synthesized and post modified to liberate the phosphonic acid groups of the anchor block. They can be used in biological evaluation to gain insight into the optimal composition of amphiphilic polymer brushes made by “grafting to”.

With P(DMVBP$_{12}$-b-TMA$_{167}$) as precursor, another strategy to improve biocompatibility was pursued: the diblock copolymer was chain extended with VDMA to introduce a short segment of terminal electrophilic groups that could be modified in a “click”-like manner. Preliminary experiments with a fluorine-containing probe demonstrated that both the block extension and the ring-opening reaction worked as intended. Next, biotin-PEG2-amine was used as nucleophile to obtain a polymer that can be investigated in biochemical assays by taking advantage of specific protein-biotin-interactions. Lastly, an attempt was made to introduce RGD as a cell-adhesion promoter at the polymer terminus. The verification of whether the peptide sequence was incorporated proved difficult due to its low mass fraction in the polymer. More in depth experiments are needed to optimize the reaction and analyze the outcome.

5 Salt-responsive polymer brushes with antibacterial and antifouling properties

Despite the advantages of inherently antibacterial surfaces over approaches that suffer from dissipation of the active compound (e.g. antibiotics), they are not a definite solution to proliferation of bacteria in implantology.[17] One major issue is the loss of function upon buildup of dead bacteria, screening live bacteria from the contact-killing moieties. Inspired by the research on antifouling surfaces, the synergy of antibacterial/polycationic and antiadhesive/polyzwitterionic has gained some attention in recent years.[60,74,155] Responsive systems that allow switching between the two modes seem particularly sustainable and are promising candidates for real future implant systems. As of yet, these approaches suffer from several drawbacks: usually either the synthesis of the involved polymers or the coating process is tedious. For example, “grafting from” is hard to transfer from research level to economic scale, and spin-coating is suitable only for a limited range of sample geometries.[156] Moreover, the chosen trigger is not always fitting for application within the body or compatible with irritated tissue post-surgery.

The antibacterial polymers introduced in the previous chapters are both readily accessible by straightforward synthetic procedures and allow the coating of arbitrary geometries by a simple dip coating and annealing. This concept can be expanded to also include an antifouling moiety, if the difunctional copolymer (antibacterial block + anchor block) is complemented with a polyzwitterionic block. Transferred to the application on a surface, this means that the polymer brush is comprised both of polycationic and polyzwitterionic bristles, whilst the PA-block roots it to the metal interface (Figure 5.1). In order to prevent the charged strands from obstructing each other, the anchor block should constitute the central segment.

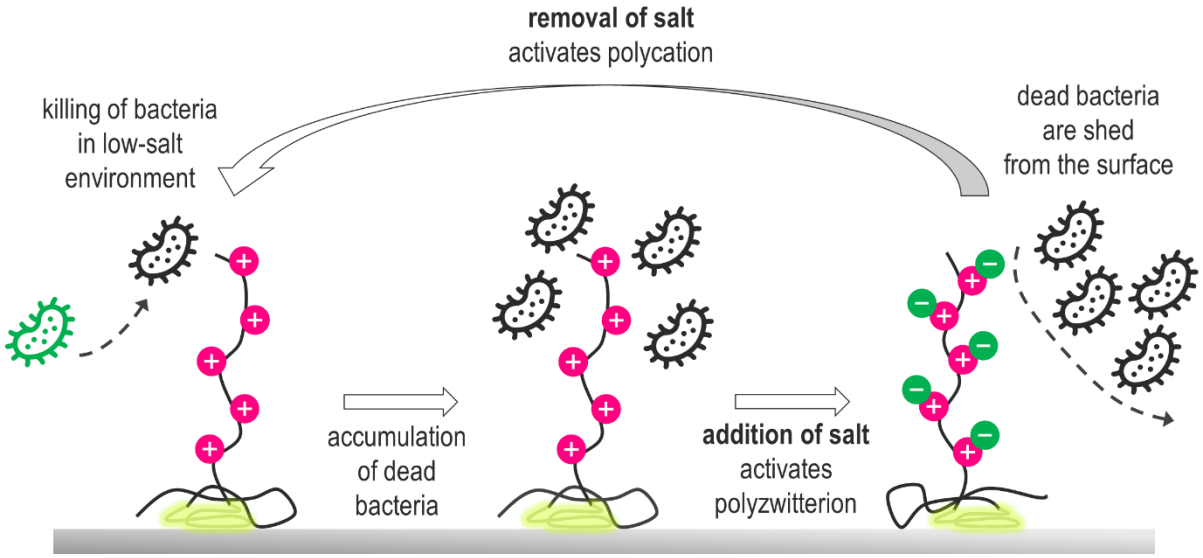

Figure 5.1: Schematic representation of the envisioned kill-shed-mechanism of a salt-responsive triblock copolymer on a titanium surface with a phosphonic-acid-anchor segment (yellow) and cationic/zwitterionic bristles. Live bacteria in green, dead bacteria in black. Note that the size ratio of bacteria and polymer does not correspond to the actual ratio.

Utilizing the (anti)polyelectrolyte effect, the expansion of the respective bristles in an aqueous environment can be controlled by varying the ionic strength: in a low-salt environment, the cationic block stretches far into the solution, while the polyzwitterionic segment is collapsed as it is not soluble under these conditions. Upon addition of salt, the positive charges of the polycation are screened, resulting in a more relaxed conformation. Conversely, the polyzwitterionic moiety now expands and dominates the interface. Since the polymer is firmly attached to the sample, the supernatant solution can be switched without impairing the brush, allowing for numerous transitions between one or the other mode.

Figure 5.1 depicts how this system can be used for killing and shedding bacteria from implant surfaces. In low-salt conditions, bacteria are killed due to the interaction with the extended polycationic segments. As more and more cellular debris accumulates on the surface, a biofilm is formed, and oncoming microorganisms are shielded from the deadly effect. By exposing the implant to a solution of high ionic strength, the polyzwitterionic functionality is activated. The extremely polar strands swell and build an extensive hydration shell in the process which counteracts the close interaction of biomaterial and the surface. After the debris has been washed off, the exchange of the solution with a low-salt environment leads to the collapse of the antifouling moiety, effectively recovering the surface in “killing mode”.

5.1 Synthesis of zwitterionic and cationic copolymers

The previously explored chain transfer agent DMP and monomers, namely 4-vinyl pyridine (VP), DMVBP and TMA, provided the synthetic platform for the responsive triblock copolymer (Scheme 5.1 center). First, P(VP_{64}) was afforded by RAFT polymerization in DMF with 82 % monomer conversion and 53 % yield. After isolation by precipitation in toluene it was chain extended with DMVBP to afford P(VP_{64}-b-$DMVBP_{14}$) with 44 % monomer conversion and 77 % yield. Based on the previous results regarding the optimal anchor block length, a degree of polymerization of 14 was expected to ensure good grafting densities without impairing the overall polymer solubility in water later on. TMA was then used to form the polycationic block by further chain extension via RAFT polymerization. Since TMA and the derived polymer are not soluble in DMF, water was used as cosolvent. In the final polymer brush, the charged strands should have approximately the same length to ensure that depending on which mode is activated, one dominates the interface while the other is collapsed, so the degree of polymerization of the TMA block was matched to the VP block. P(VP_{64}-b-$DMVBP_{14}$-b-TMA_{64}) was afforded with 90 % (crude) yield and 80 % monomer conversion after precipitation in acetone. This did not remove residual monomer completely; however, this was not expected to impair the following reactions and could be easily removed via dialysis afterwards. The polymerization reactions proceeded in a controlled manner as evidenced by monomodal distributions in SEC and dispersities of 1.33 to 1.53 (Figure 5.2).

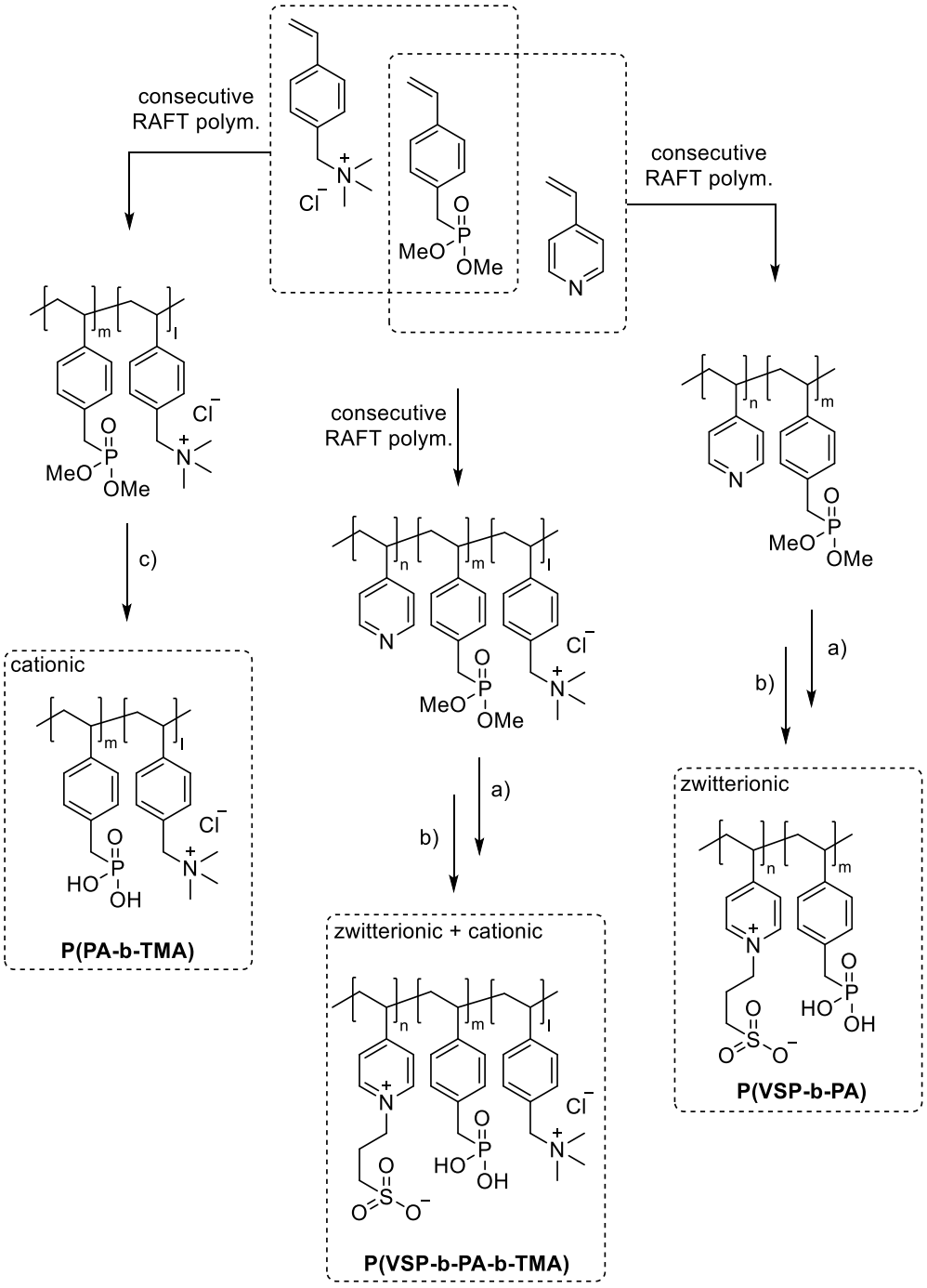

Scheme 5.1: General synthesis of charged di- and triblock copolymers containing PA, VSP and TMA units. Reaction conditions: a)1,3-propane sultone (3 eq. per VP unit), HFIP, 40 °C, 3d; b) 6 M HCl/1 M NaCl, 115 °C, 3-26 h; c) 6 M HCl, 26 h, 115 °C.

In order to introduce zwitterionic groups, pyridine moieties were reacted with 1,3-propane sultone. This cyclic sulfonate ester is frequently used to prepare betaine structures by nucleophilic ring opening which proceeds quantitatively at elevated temperatures.[69,157] Fluorinated alcohols like HFIP and trifluoroethanol are suitable solvents for both polyzwitterions and polycations despite their opposing solubility in water with respect to its ionic strength. Thus, the reaction of the triblock precursor with 1,3-propane sultone was conducted in HFIP at 40 °C and the polymer was isolated by removing roughly half of the solvent in vacuo and dialysis against 1 M NaCl and deionized water. The quantitative

formation of the betaines can be verified in ^{1}H NMR spectra by the shift of the aromatic proton signals adjacent to the pyridine/pyridinium nitrogen atom from 8.0-8.4 ppm to 8.5-9.1 ppm as well as the emergence of broad resonances at 2.5-2.7 ppm, 3.0-3.4 ppm and 4.4-5.0 ppm caused by the sulfopropyl groups. The SEC analysis reveals a shifted monomodal distribution and a slight increase in dispersity to 1.65 (Figure 5.2). The polyzwitterionic character became evident as the polymer was not soluble in water anymore but readily dissolved upon addition of NaCl. Lastly, the methyl phosphonate groups were converted to the respective acid by acidic hydrolysis in 6 M HCl/0.5 M NaCl. After purification by dialysis and lyophilization, the characteristic shift of the phosphorous resonance in the ^{31}P NMR spectrum from 30.8-32.6 ppm to 18.1-22.4 ppm proved the quantitative liberation of the acid. Once again, the elugram confirmed the monomodal molecular weight distribution and revealed a slight decrease in dispersity to 1.50, which was presumably due to removal of lower molecular weight polymer fractions during dialysis. The final polymer requires a NaCl concentration of about 0.5 M to be soluble in water owing to the antipolyelectrolyte properties of its zwitterionic block.

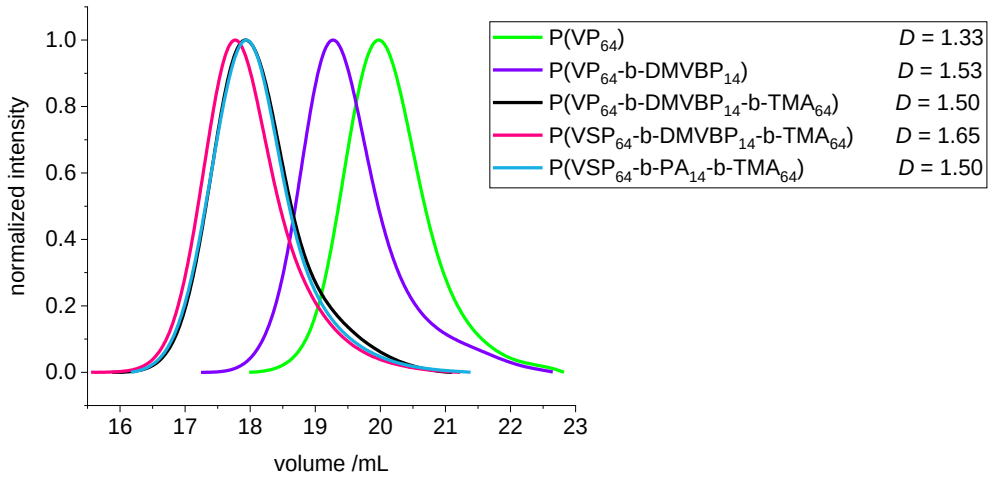

Figure 5.2: SEC (HFIP) traces of polymers involved in the synthesis of P(VSP$_{64}$-b-PA$_{14}$-b-TMA$_{64}$).

To investigate each functionality separately, the respective diblock copolymers containing only the anchor block and either the polycationic or the polyzwitterionic block were synthesized as well (Scheme 5.1). The general procedure was analogous to the triblock copolymer and afforded the targeted polymers whose SEC and NMR data is presented in Table 5.1. All syntheses were conducted on a multi-gram scale, demonstrating the convenient access to these structures.

Table 5.1: Analytic data for charged di- and triblock copolymers.

polymer	M_n(NMR) /gmol^{-1}	M_n(SEC) /gmol^{-1}	*D*
P(VSP$_{63}$-b-PA$_{13}$)	17,300	9,400[a]	1.51[a]
P(PA$_{16}$-b-TMA$_{101}$)	24,500	31,000	1.56
P(VSP$_{64}$-b-PA$_{14}$-b-TMA$_{64}$)	33,000	27,000	1.50

[a] After conversion to phosphonic acid groups, the polymer was not soluble in HFIP anymore, thus data from the polymer before hydrolysis is given.

5.2 Adsorption on titanium oxide particles

The grafting densities on titanium oxide particles were investigated for all three charged polymers by determination of the residual polymer concentration after adsorption via UV/vis spectroscopy (cf. method used in chapter 3.3). Here, the ionic strength of the aqueous solution was adjusted to obtain a good solvent for the respective polymer: 1 M NaCl for P(VSP$_{63}$-b-PA$_{13}$), deionized water for P(PA$_{16}$-b-TMA$_{101}$) and 0.5 M NaCl for P(VSP$_{64}$-b-PA$_{14}$-b-TMA$_{64}$).

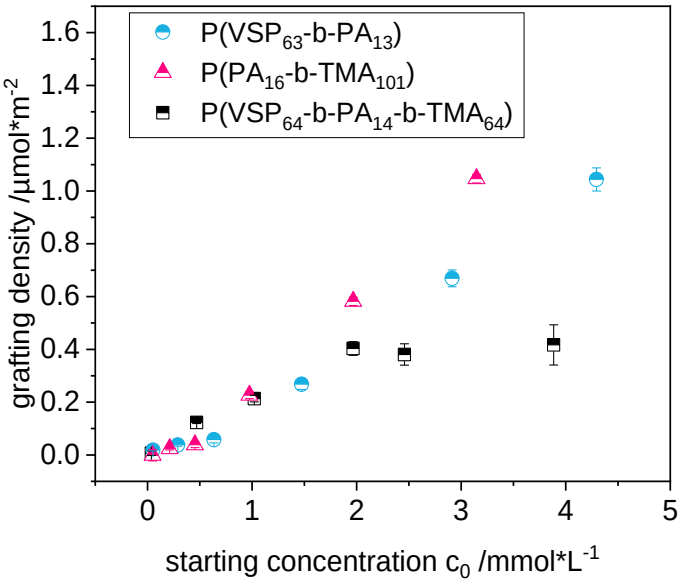

Figure 5.3: Grafting density of charged di- and triblock copolymers on titanium oxide particles at different concentrations of polymers. Solvents: 1 M NaCl for P(VSP$_{63}$-b-PA$_{13}$), deionized water for P(PA$_{16}$-b-TMA$_{101}$), 0.5 M NaCl for P(VSP$_{64}$-b-PA$_{14}$-b-TMA$_{64}$).

In the investigated range, the diblock copolymers showed a nearly linear increase of grafting density with increasing polymer concentration without reaching a saturation plateau. Since the solvent was chosen to accommodate the charged blocks, they assumed a stretched conformation which allowed a dense occupation of the surface. The zwitterionic copolymer P(VSP$_{63}$-b-PA$_{13}$) showed a slightly more efficient adsorption compared to the polycation P(PA$_{16}$-b-TMA$_{101}$) despite having about 3 PA units less which suggested that the interplay between non-adsorbing block, the solvent and/or block order influenced the process. This is

emphasized by the comparison with the previously discussed polymers based on P(VPPr): the best performing polymer with 21 PA units (cf. chapter 3.3, P($VPPr_{65}$-b-PA_{21})) showed a similar adsorption isotherm as the diblock copolymers with only 13 and 16 PA units investigated in this chapter.

Up to a concentration of about 2 mmol/L the adsorption isotherm of triblock copolymer P(VSP_{64}-b-PA_{14}-b-TMA_{64}) exhibited a similar behavior as the zwitterionic/cationic diblock copolymers. Then, the grafting density plateaued at about 0.4 µmol/m² which is a plausible result considering that one equivalent of triblock copolymer effectively formed two bristles, thus taking up more space on the surface than the diblock copolymers. This was exacerbated by the solvent being merely a compromise between the two optimal environments for each strand, namely high ionic strength for the polyzwitterion and low ionic strength for the polycation. Presumably, neither block was expanded as distinctly as it was the case for the diblock copolymers in more optimized conditions. Therefore, the system was likely to be closer to the mushroom regime in comparison, making it hard for oncoming chains to penetrate the already adsorbed polymer bristles. Nevertheless, based on the previous investigations regarding P(VPPr) based polymers and results from literature with similar grafting densities of "grafting to" derived polymer brushes, the surface affinity of the responsive polymer was adequate for the modification of titanium samples.

5.3 Antifouling behavior and switchability of brushes

The formation of polymer brushes from di- and triblock copolymers and their salt-responsive behavior upon adhesion of a model substance for bacterial debris were investigated via SPR spectroscopy (cf. chapter 3.4). The substrate is LaSFN9-glass coated with chromium (ca. 1 nm), gold (ca. 50 nm) and titanium oxide (ca. 4 nm) by atomic layer deposition. The brush is then prepared by grafting the polymer onto the metal layer from solution (30 mg/mL; 1 M NaCl for P(VSP_{63}-b-PA_{13}), deionized water for P(PA_{16}-b-TMA_{101}) and 0.5 M NaCl for P(VSP_{64}-b-PA_{14}-b-TMA_{64}) and annealing at 120 °C. Subsequently, the substrate is cleaned with 1 M NaCl (for zwitterionic polymers), water and ethanol to remove unbound polymer. The measurements were conducted in a flow cell against deionized water.

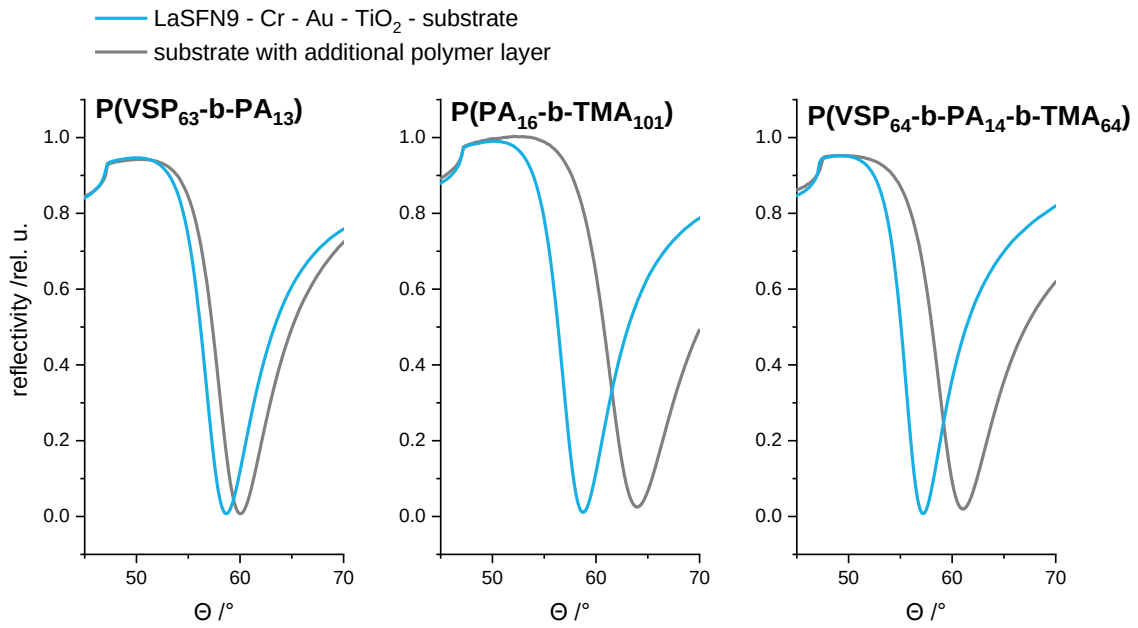

Figure 5.4: Full angle scans of titanium oxide coated substrates before and after coating with charged di- and triblock copolymers against water.

For all polymer coatings, a significant shift of the plasmon minimum was detected which proved the formation of stable adlayers (Figure 5.4). Fitting the total reflection edge and the plasmon minimum yielded average layer thicknesses of 4.4 nm for P(VSP_{63}-b-PA_{13}), 8.0 nm for P(PA_{16}-b-TMA_{101}) and 5.1 nm for P(VSP_{64}-b-PA_{14}-b-TMA_{64}) (Table 5.2, detailed parameter in appendix Table 8.6 to Table 8.7). These values corresponded to how much the plasmon minimum had shifted, however, since the refractive index of the polymers is unknown and must be guessed, the fitting results do not necessarily represent absolute values and may derive significantly from the real thickness. Typical values for polymer refractive indices lay in the range of 1.30 to 1.70.[158]

Remarkably, the zwitterionic diblock copolymer afforded layers with the lowest apparent thickness, although a comparable grafting density was to be expected for the chosen concentration of the grafting solution. Considering the solvent, however, the zwitterionic chains likely collapsed in the absence of ions and formed a flat layer rather than a swollen polymer brush. Opposingly, the strands of the cationic diblock copolymer were extended into the supernatant solution, resulting in a thicker layer. The determined values matched the order of magnitude of comparable polymer brushes made via “grafting to”, indicating that the end tethering had worked as predicted and unbound polymer was removed during the cleaning process.[136]

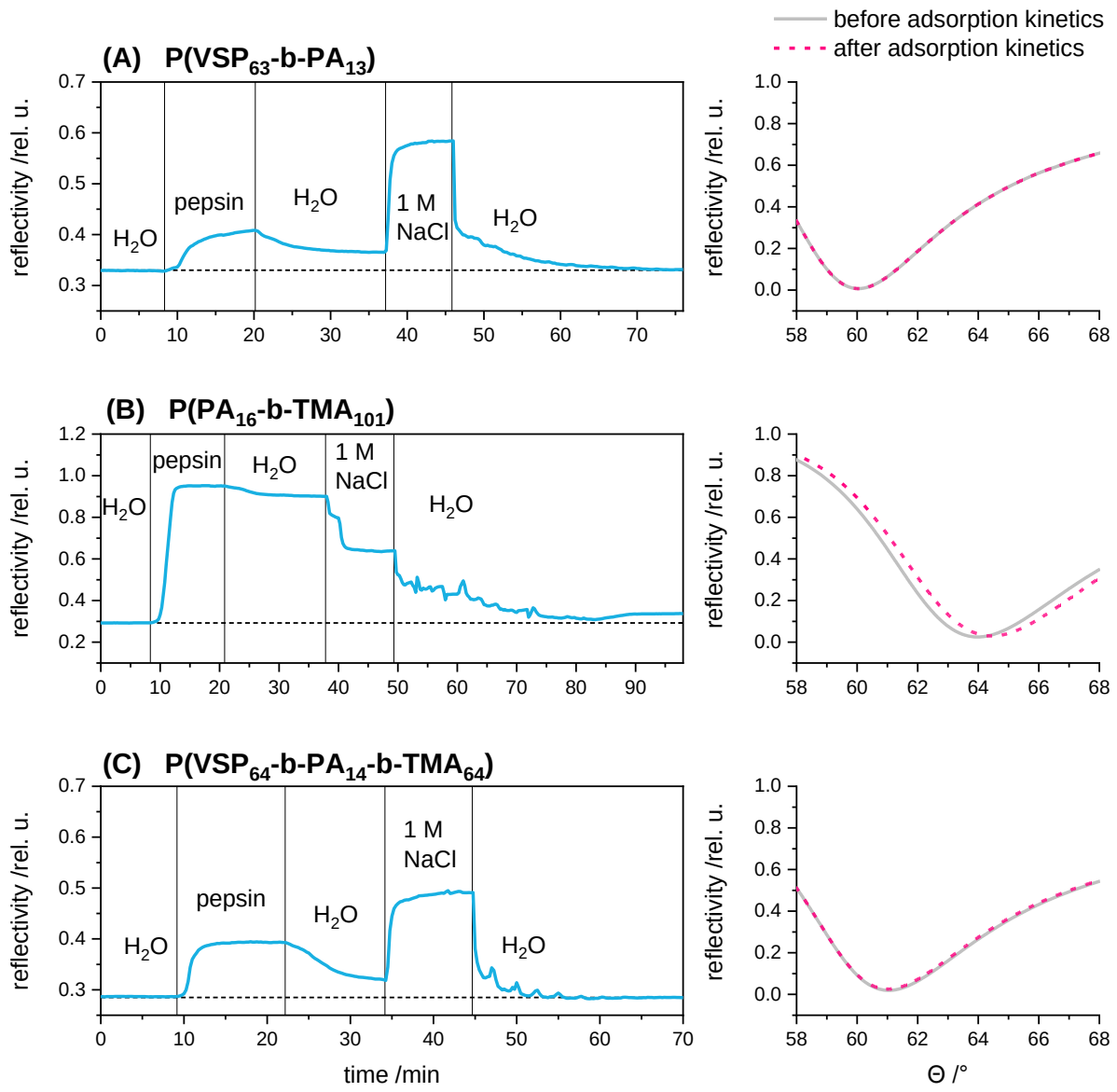

Figure 5.5: Left: measurements of reflectivity against time in SPR kinetic mode using deionized water, 1 mg/mL pepsin in water and 1 M NaCl as solutions in the flow cell with polymer coated substrates at about 1 mL/min. Right: Zoom onto plasmon minimum Θ_{min} of respective full angle scans against water before and after kinetic measurements.

In SPR flow experiments, the antiadhesive properties of the coated substrates can be probed by offering a sticky protein and detecting changes in signal intensity at a fixed angle.[74] An increase in reflectivity corresponds to a shift of the plasmon minimum to higher angles, indicating a thickening or formation of an adlayer. Pepsin, a digesting enzyme, is well-suited as a model substance for strongly adhering bacterial debris as it is negatively charged due to its low isoelectric point and consequently adsorbs onto surfaces equipped with polycations, similar to cell membrane fragments.[159] The three substrates were equilibrated in water at first and then exposed to a solution of pepsin in water (Figure 5.5 left). In all cases, this caused a rise in reflectivity due to the adsorption of pepsin onto the polymer layer which was only partly removed by purging the flow cell with deionized water, which is evident since the reflectivity did not reach the starting level. Even the purely zwitterionic surface modification

did not resist the adherence, which indicates that the presence of ions is necessary for the protective hydration shell to form.

Thus, using a solution containing 1 M NaCl should allow the zwitterionic blocks to swell and release the adsorbed protein in case of (A) P(VSP_{63}-b-PA_{13}). Upon exposure for 10 min, the reflectivity increased owing to the higher refractive index of the salt solution compared to water and presumably the extension of the polymer bristles. When changing the environment to water again, the reflectivity dropped to the starting level. The full angle scans before and after the kinetic experiment are congruent, demonstrating that there was neither residual adsorbed peptide nor detachment of the polymer brush (Figure 5.5A right). In contrast, the purely cationic brush made of P(PA_{16}-b-TMA_{101}) exhibited a decrease in reflectivity in 1 M NaCl. This could only be attributed to shrinking of the adlayer due to a more relaxed conformation of the bristles whose positive charges were screened by the added ions. When the solution was switched to water again, the reflectivity dropped significantly lower than before the washing step with 1 M NaCl. Although the cationic surface typically does not exhibit a salt dependent antiadhesive effect, the salt solution was more effective in removing adsorbed pepsin than deionized water. Presumably, the ions competed with the adsorbed pepsin due to coulomb interactions at the charged polymer chains, superseding it from the surface. Nevertheless, the layer thickness surpassed the starting level after the system is equilibrated (> 90 min). The full angle scans revealed a shift in the plasmon minimum of 0.5° which corresponded to an average pepsin layer thickness of 0.6 nm to 7.2 nm, depending on the refractive index used for fitting (typical values for proteins are between 1.35 to 1.6[160]). Similar results have been observed for cationic surface modifications by Lienkamp et al. and demonstrate the underlying problem in the application of contact-killing implant coatings.[74] Residual biological matter promotes biofilm formation and disables the surface functionality.

The surface modified with the triblock copolymer P(VSP_{64}-b-PA_{14}-b-TMA_{64}) exhibited the same behavior as the purely zwitterionic modification: after the adsorption of pepsin, water was not enough to remove the protein entirely. The activation of the polyzwitterionic strands was evident by the increase of reflectivity upon purging with 1 M NaCl which indicated that these segments were now swollen and expanded. Although the protein was expected to form strong electrostatic interactions with the polycationic segments, the synergy of these segments coiling and the expansion of the heavily hydrated zwitterionic blocks was sufficient to recover the surface completely. This was evident by the starting level being restored as well as the full angle scan which did not derive significantly from before the adsorption experiment. The increase in reflectivity upon exposure to salt solution demonstrated the selective swelling of the zwitterionic bristles, as the purely cationic diblock copolymer exhibited a decrease in reflectivity in the same conditions. Hence, the combined polymer brush offers the advantage of the antifouling properties while still incorporating the potentially bactericidal moieties and

allows triggering the respective properties by adjusting the ionic strength of the aqueous environment.

Table 5.2: Polymer and pepsin layer data before and after kinetic SPR measurements obtained from full angle scans and fitting of total reflection edge and plasmon minimum Θ_{min}. Detailed parameter in appendix Table 8.6 to Table 8.7.

polymer	thickness /nm	Θ_{min}	remaining pepsin layer /nm	Θ'_{min}
P(VSP_{63}-b-PA_{13})	4.4	60.04°	0	60.04°
P(PA_{16}-b-TMA_{101})	8.0	63.96°	0.6-7.2	64.46°
P(VSP_{64}-b-PA_{14}-b-TMA_{64})	5.1	61.04°	0	61.06°

5.4 Physical characterization of coated substrates

The measurements discussed in this chapter were conducted by Michael Greiter at the University of Siegen in the working group of Prof. Schönherr (including sample preparation and coating process, contact angle measurement, ellipsometry, XPS, AFM and SEM imaging).

Glass substrates were coated with titanium (ca. 2.5 nm), gold (ca. 50 nm) and titanium (ca. 2.5 nm) by evaporation and subsequently cleaned in an oxygen plasma to remove organic material adhering to the surface. The substrates were covered with polymer solution (10 mg/mL, 1 M NaCl for P(VSP_{63}-b-PA_{13}) and P(VSP_{64}-b-PA_{14}-b-TMA_{64}), deionized water for P(PA_{16}-b-TMA_{101})) and placed in an oven at 120 °C overnight, evaporating the solvent. Unbound polymer was removed via sonification and rinsing with water. As the surface of P(VSP_{63}-b-PA_{13}) appeared to be inhomogeneous and exhibited a significantly thicker layer compared to the other two samples as measured by ellipsometry (in the dry state), an additional cleaning step in 1 M NaCl was conducted for this sample. Afterwards, the determined value was in the same order of magnitude for all samples (Table 5.3). In contrast to the determined swollen layer thickness observed via SPR spectroscopy (cf. Table 5.2), P(PA_{16}-b-TMA_{101}) yielded the thinnest dry layer with 3.2 nm, followed by the zwitterionic diblock copolymer with 4.1 nm and the triblock copolymer with 5.3 nm. Another “grafting to” system can be considered for comparison: in hydroxyl-terminated random P(Sty-r-MMA) (MMA = methyl methacrylate) copolymers, the layer thickness of the grafted polymer brush was observed to depend on the average molecular weight of the chains.[96,108] Perego et al. found layer thicknesses of 7.1 nm and 9.0 nm for M_n = 11,200 g/mol and 19,500 g/mol when they produced the polymer brushes from melt. In this work, only a concentration of 10 mg/mL was used to coat the substrates with the charged block copolymers, which is the reason for the comparably thinner layers although the average molecular weight exceeds that of the P(Sty-r-MMA) brushes of Perego et al. The results agree with the conclusion drawn from the

adsorption experiments on titanium particles that the concentration is vital for the grafting density which determines the average layer thickness (cf. chapter 5.2).

Table 5.3: Static water contact angles and dry ellipsometric thickness of uncoated and coated titanium oxide samples.

sample	**TiO_2**	**P(VSP_{63}-b-PA_{13})**	**P(PA_{16}-b-TMA_{101})**	**P(VSP_{64}-b-PA_{14}-b-TMA_{64})**
		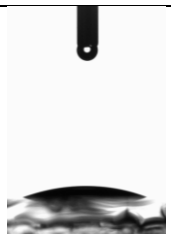		
contact angle	94° ± 1°	21° ± 1°	14° ± 1°	29° ± 2°
thickness /nm	-	4.1 ± 0.3	3.2 ± 0.6	5.3 ± 0.3

Static water contact angle measurements revealed a significantly increased wettability after coating with the charged polymers (Table 5.3). Similar results were reported for brushes based on polymethacrylates carrying tertiary amine groups and mixed cationic/zwitterionic brushes on titanium surfaces.[101,102] P(PA_{16}-b-TMA_{101}) lead to the lowest contact angle with 14°, while the zwitterionic diblock and triblock copolymers afforded values of 21° and 29°, respectively. Huang et al. reported similar findings: using salt-free water, the wettability of zwitterionic surfaces was less pronounced compared to cationic surfaces.[102] When the same measurement was conducted with saturated NaCl solution, the wettability of the zwitterionic surface was greatly improved owing to the antipolyelectrolyte effect.

The elemental surface composition of the coated substrates was characterized by XPS. According to the XPS survey scans, all samples showed O1s, N1s and C1s peaks at 531.0 eV, 400.0 eV and 285.0 eV, respectively (Figure 5.6). As expected, peaks of S2s and S2p at 230.0 eV and 167.0 eV were detected in the samples modified with zwitterionic segments. High resolution spectra confirmed these results. In C1s spectra, two peaks with different chemical environment were determined corresponding to aliphatic carbon atoms in the backbone and alkyl chains C-C at 285.6 eV and aromatic carbon atoms C=C at 283.4 eV (appendix Figure 8.4 to Figure 8.6). The P2p peak at 132.0 eV is evident of the presence of phosphorus atoms in all three samples.

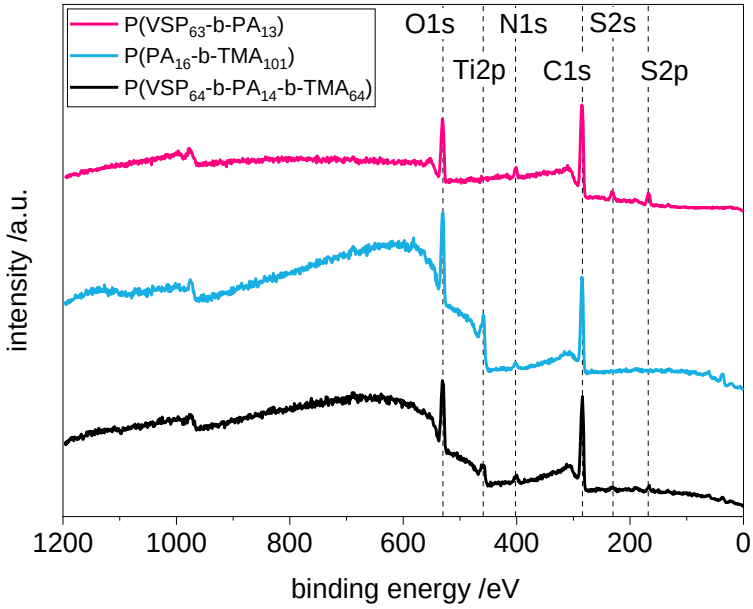

Figure 5.6: XPS survey spectra of titanium oxide surfaces coated with charged di- and triblock copolymers.

The experimental and theoretical atom concentrations were calculated from the XPS data and the structural formulas (Table 5.4). Overall, the respective values were in good agreement, with exception of the contribution of nitrogen. Especially for P(PA_{16}-b-TMA_{101}), the experimentally determined value was significantly lower than expected, whereas the fraction of oxygen was higher. This may be due to degradation under XPS conditions during measurement and contributions of titanium bound oxygen.

Furthermore, the surface topography of all samples was investigated using AFM which showed a clear difference in surface roughness between uncoated TiO_2 and surfaces modified with P(VSP_{64}-b-PA_{14}-b-TMA_{64}) and P(PA_{16}-b-TMA_{101}) (appendix Figure 8.7). The root mean square deviation R_q decreased from 2.3 nm (reference) to 0.4 nm, respectively. The surface coated with P(VSP_{63}-b-PA_{13}) exhibited an R_q value of 2.0 nm, however, the measurement was performed before the second washing-step with NaCl solution, which is why it cannot be compared to the other samples. Lastly, SEM images of a sample equipped with P(VSP_{64}-b-PA_{14}-b-TMA_{64}) at various magnifications revealed a flat and homogeneous surface, verifying a controlled and consistent coating procedure (appendix Figure 8.8).

Table 5.4: Experimental and theoretical elemental contributions derived from XPS spectra and structural formulas of charged di- and triblock copolymers. End groups were neglected in the calculation.

element	P(VSP$_{63}$-b-PA$_{13}$)		P(PA$_{16}$-b-TMA$_{101}$)		P(VSP$_{64}$-b-PA$_{14}$-b-TMA$_{64}$)	
	XPS /%	*theor. /%*	*XPS /%*	*theor. /%*	*XPS /%*	*theor. /%*
C	71.9	67.1	85.1	86.5	79.3	75.3
O	18.4	20.5	10.7	3.9	13.3	13.1
N	3.6	5.7	1.9	8.3	3.6	7.2
P	0.9	1.2	2.2	1.3	1.3	0.8
S	5.2	5.7	0	0	2.5	3.6

5.5 Biological evaluation of polymer coatings

The measurements discussed in this chapter were conducted by Jiwar Al Zawity and Dr. Mareike Müller (Junior research group: Cellular and Applied Microbiology) at University of Siegen in the working group of Prof. Schönherr.

To evaluate the antibacterial effect of polymer coatings with the presented di- and triblock copolymers, an uncoated reference and coated substrates were incubated with Gram-positive (*S. aureus*) and Gram-negative (*E. coli*) bacteria. Afterwards, the cells were stained via a DNA intercalating dye, as DNA is concentrated within bacteria, in order to qualitatively evaluate the surface coverage of bacteria. Substrates were rinsed with PBS, fixed with 2.5 % glutaraldehyde in PBS and analyzed via fluorescence imaging. In Figure 5.7, the results for *S. aureus* with adhering bacteria indicated in green are displayed.

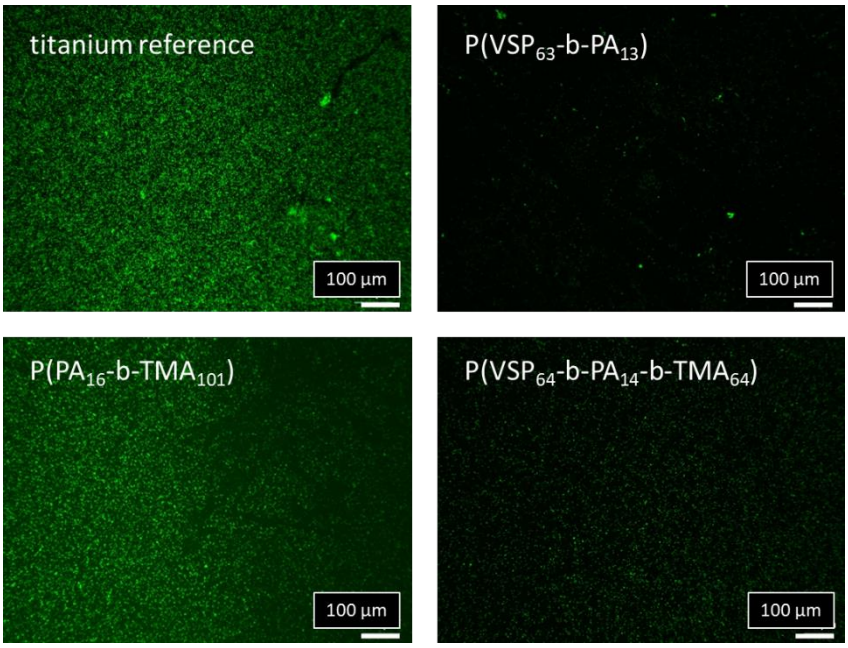

Figure 5.7: Fluorescence microscopic images of adherent bacteria on coated and uncoated substrates after incubation with S. aureus and removal of non-adherent cells. Green fluorescence (staining via the DNA intercalator Syto9) indicate attached bacteria.

Both the reference and the surface with exclusively cationic polymers showed a large number of attached cells, while the zwitterionic surface modifications exhibited a low-fouling profile. These observations are in line with the hypotheses of the strategy depicted in Figure 5.1. It must be noted that the incubation proceeded in a nutrient solution which contains about 0.14 mol/L NaCl among other substances (e.g. yeast extract, Peptone), thus it can be assumed that the zwitterionic chains are swollen to some extent. Since the triblock copolymer also contains positively charged segments, it did not perform as well as P(VSP_{63}-b-PA_{13}), but the presence of the zwitterionic block improved its low-fouling properties compared to P(PA_{16}-b-TMA_{101}). Similar to the results obtained from SPR measurements, this suggests that the separate effects can be utilized in synergy to combine antibacterial with anti- or low-fouling activities.

After incubation with *E. coli*, the surface coverage with bacteria corresponded to the attachment of *S. aureus* (Figure 5.8). The presence of the zwitterionic blocks caused significantly less *E. coli* to adhere to the surface that was detectable after rinsing the not attached bacteria. However, the surface occupation on the titanium substrates coated with P(PA_{16}-b-TMA_{101}) and P(VSP_{64}-b-PA_{14}-b-TMA_{64}) appeared inhomogeneous. Some areas were more densely covered with cells than others which suggests that the polymer coating was not uniform, considering that the reference sample exhibited a homogenous layer of adhering bacteria. Consequently, the antifouling effect of P(VSP_{64}-b-PA_{14}-b-TMA_{64}) could presumably be even more pronounced after optimization of the coating process. The purely cationic surface modification exhibited an inhomogeneous occupation with bacteria that was in parts even more densely covered than the uncoated reference.

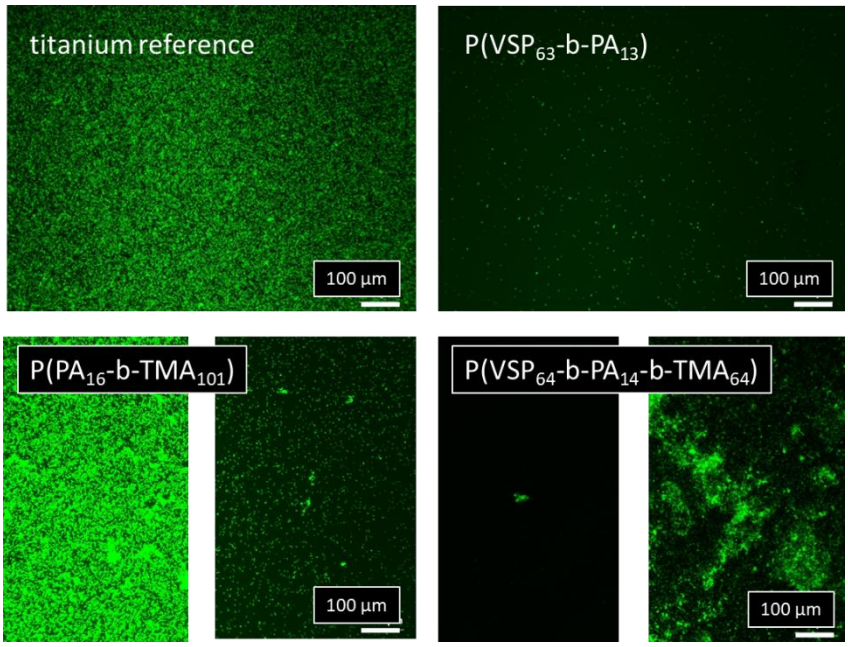

Figure 5.8: Stained cells on coated and uncoated substrates after incubation with E. coli and washing with water in fluorescence imaging. Fluorescence microscopic images of adherent bacteria on coated and uncoated substrates after incubation with E. coli and removal of non-adherent cells. Green fluorescence (staining via the DNA intercalator Syto9) indicate presence of DNA (concentrated within bacteria).

All polymers lead to a reduction of viable bacteria of *S. aureus* compared to the reference sample (Figure 5.9A). Although zwitterionic surfaces are not known for their antibacterial properties, a minimal reduction of CFUs was observed for P(VSP_{63}-b-PA_{13}) as well. The polymers containing polycationic segments lead to a reduction in viable bacteria of just over 70 % which agrees with the notion that these structures are contact-active. The presence of zwitterionic groups in case of the triblock copolymer did not interfere with the antibacterial properties of the surface, on the contrary, it exceeded the performance of the purely cationic modification marginally. The observed effects were comparably small but confirmed the expectations regarding the presence of polycationic chains to affect bacterial colonization. The design of the bacterial assay is particularly important to consider when comparing the results to published studies on antibacterial surfaces. Small deviations in procedure have a severe impact on the outcome of the bacterial assay.[161] The volume and concentration of bacterial suspensions are key parameters, since they affect how many bacteria are in contact with the surface in a given timeframe.

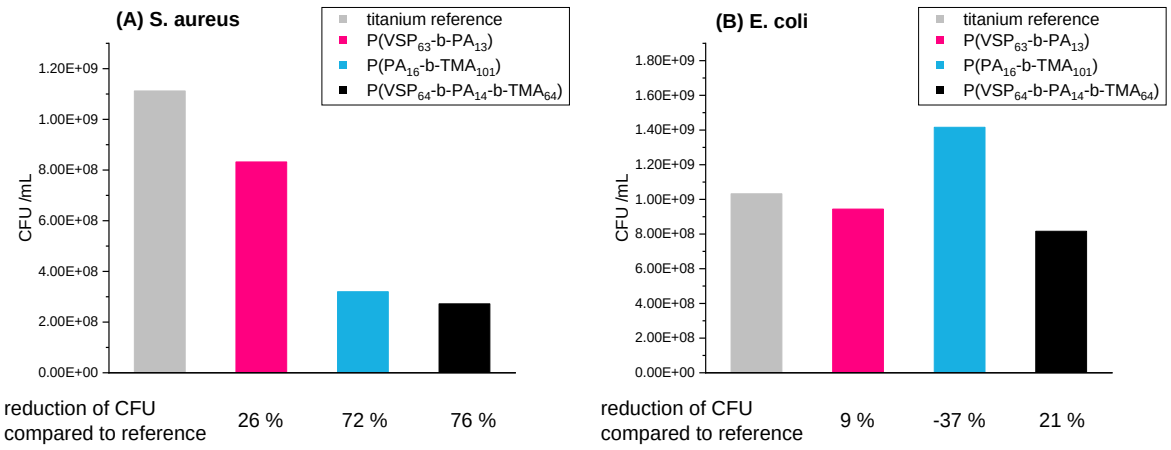

Figure 5.9: Colony forming units (CFU) in supernatants after incubation of titanium substrates with and without polymer coating with bacteria: A) S. aureus (Gram-positive) and B) E. coli (Gram-negative).

Against *E. coli* (Figure 5.9B), the polymer modifications containing zwitterionic segments showed a slight reduction in CFUs after a 24 h cultivation, but less so in comparison to *S. aureus*. Since Gram-negative bacteria possess an inner and an outer membrane, they are generally harder to disrupt by antibacterial polymers.[162] Similar to the results obtained for P(VPPr$_{65}$-b-PA$_{16}$) in chapter 3.6, which was also tested against *E. coli* and increased the number of viable bacteria in the supernatant, P(PA$_{16}$-b-TMA$_{101}$) resulted in an increase in CFUs by 37 % compared to the reference. Although the triblock copolymer also contains a polycationic block, it showed the most pronounced reduction in CFUs with 21 % compared to the reference sample, which suggests that there is a synergy of zwitterionic and cationic block which is necessary to impair bacterial colonization. The effect of P(VSP$_{63}$-b-PA$_{13}$) was negligibly small.

Lienkamp et al. reported highly efficient antibacterial coatings which showed up to a 6 log reduction against *S. aureus*.[74] Besides the effect of different molecular structures in the referenced work, the comparably worse performance of the system presented here is presumably a drawback from the “grafting to” approach, as the coatings of Lienkamp et al. are composed of highly crosslinked polymer networks prepared by spin-coating, resulting in a much denser surface occupation. However, due to the different design of the bacterial assay, the comparability is limited: Lienkamp et al. used a much smaller volume of bacterial suspension (100 µL vs. 3 mL in this work) at a higher concentration. In order to give a definite evaluation among published systems, the conditions of the respective bacterial assays have to be reproduced.

5.6 Conclusions

Three biologically active polymers with anchor segments were synthesized: two diblock copolymers, comprising a polyzwitterionic/antifouling and a polycationic/antibacterial block, respectively. The third polymer combined both of these functional segments with the anchor

block in the center. It was demonstrated that the polymers were well-accessible via RAFT polymerization with good end group retention and narrow dispersities as confirmed by SEC monitoring. Evaluation with NMR spectroscopy revealed that the subsequent post modifications proceeded quantitatively to afford the targeted polymer structures. All products were synthesized in a multigram scale.

Titanium substrates were coated with the charged polymers to afford functional polymer brushes. The antifouling properties of surfaces with zwitterionic moieties in presence of salty water could be observed in situ via SPR spectroscopy. Most importantly, the irreversible adherence of a model compound for bacterial debris (pepsin) could still be prevented in case of the triblock copolymer, although it comprised a polycationic segment that attracts the adsorption of negatively charged substances. The results verified the concept of salt-responsiveness, i.e. the utilization of the (anti)polyelectrolyte effect to switch between blocks.

Physical characterization of coated titanium substrates with XPS, ellipsometry, contact angle measurements, SEM and AFM confirmed the formation of thin and uniform layers of the adsorbable polymers. In biological assays, the antibacterial and antifouling properties of coated substrates were probed: both against *S. aureus* and *E. coli*, the synergy of polycationic and polyzwitterionic segment in the triblock copolymer proved most effective and reduced the number of CFUs by 76 % and 21 %, respectively, compared to a titanium reference. Staining the adherent cells after removal of not attached bacteria uncovered the low-fouling properties in surfaces equipped with zwitterionic segments (P(VSP_{63}-b-PA_{13}) and P(VSP_{64}-b-PA_{14}-b-TMA_{64})), as they significantly impaired surface colonization of bacteria compared to the reference and the surface modified with polycationic chains. Experiments which give further insight into the recyclability of the surfaces have not yet been performed but are a next step in assessing the sustainability of this approach.

By comparing the charged diblock copolymers to the triblock copolymer with several experimental techniques, the concept of a salt-responsive synergy of antibacterial and antifouling was verified. The required polymer brush was formed by convenient “grafting to” of well-accessible polymers, whose synthesis was established in this work, and offers new opportunities in the design of sustainable and durable dental implants. The biological evaluation revealed deficiencies in antibacterial activity of the polymer coatings, especially against Gram-negative bacteria. This was presumably partly due to the comparably low grafting densities resulting from the “grafting to” approach. Optimizing the coating by increasing the concentration of polymer in the grafting solution, for example, may increase the antibacterial performance. Further, in future antimicrobial tests the design of the bacterial assay should be tailored to address more specifically the contact-killing effects, for example according to JIS Z 2801.[161] Beyond that, the fundamental design of the responsive triblock copolymer (cationic block – anchor block – zwitterionic block) can also be realized using

different structures with regards to backbone and functional groups. RAFT polymerization is compatible with a wide variety of cationic monomers/precursors beside styrene derivates, for example acrylates or acrylamides,[41,45] which may exceed the antibacterial properties of P(TMA). Since the synergy of zwitterionic and cationic segment appeared to play a role in reduction of CFUs, different combinations of blocks can be assumed to make a difference as well.

The results of this work demonstrated the advantages of a synergistic system compared to purely antibacterial or antifouling coatings. Based on the developed triblock structure, conveniently applicable polymers will aid in the design of next-generation implant systems.

6 Experimentals

6.1 Materials

chemical	supplier	purity/remarks
1,3-Propane sultone	Merck	98 %
1-Bromopropane	Acros Organics	99 %
2-(Dodecylthiocarbonothioylthio)-2-methylpropionic acid	Merck	98 %
2-Methylalanine	Merck	98 %
4-Fluorobenzylamine	Merck	97 %
4-Vinyl pyridine	Merck	distilled
4-Vinylbenzyl chloride	Merck	distilled
Acetone	technical	-
Acryloyl chloride	Sigma Aldrich	97 %
Aeroxide P25 (titanium oxide particles)	Merck	see product data sheet
AIBN	Merck	recrystallized from EtOH
BHT	Fluka	99 %
Biotin-PEG2-Amine	TCI	95+ %
D_2O	Deutero	99.9 %
Diethyl ether	technical	-
Diethyl phosphite	Merck	98 %
Dimethylamin in H_2O	Alfa Aesar	40 %
DMF	thermo scientific	99.5 %, extra dry
DMSO-*d6*	Deutero	99.8 %
Ethanol	Grüssing	99.5 %
Ethanolamine	Alfa Aesar	98+ %
Ethyl acetate	technical	-
Ethyl chloroformate	Merck	97 %
H_2O		deionized
Hexafluoroisopropanol (HFIP)	Carbolution	99 %
Isohexane	technical	-

Isopropanol	technical	-
Methanol	Carl Roth	HPLC grade
n-Hexane	technical	-
Nitro methane	thermo scientific	98+ %
Pepsin from porcine gastric mucosa	Sigma Aldrich	≥250 units/mg solid
RGD	abcr	97+ %
sodium hydride	Merck	60 % (in mineral oil)
Styrene	Merck	distilled
THF	Grüssing	99.5 %
Toluene	technical	-
Triethyl phosphite	Acros Organics	98 %
Triethylamine	Merck	99.5 %
Trimethyl phosphite	Merck	97 %
Trimethylamine	Fluka	4.2 M in EtOH
Trimethylsilylbromide	Acros Organics	98 % AcroSeal

6.2 Instrumentation and methods

6.2.1 Conducted at Paderborn University

6.2.1.1 NMR spectroscopy

NMR spectra were recorded on a Bruker Avance 500 and a Bruker Ascent 700 and processed using Bruker TopSpin. The chemical shifts (δ) are listed in ppm and coupling constants (J) are listed in Hz, respectively.

6.2.1.2 Calculation of molecular weight

The theoretical molecular weight of the polymers synthesized in this work were calculated using equation 4 and assuming $D = 1$. The monomer conversion was determined from ^{1}H NMR samples of the quenched reaction mixture by comparing integrals of monomer and polymer signals.

6.2.1.3 Dialysis and lyophilization

Dialysis was performed with Spectra Pore 6 dialysis membranes (MWCO = 1 kD) against water or as specified in the procedure. An Alpha 2-4 LDplus freeze dryer by Christ was used to remove water afterwards.

6.2.1.4 IR spectroscopy

Attenuated total reflection infrared (IR) spectra were recorded on the Bruker “Vertex 70” spectrometer and processed using ACD/spectrus.

6.2.1.5 Mass spectrometry (MS)

The samples were analyzed by means of electrospray ionization mass spectrometry (ESI-MS) using a “Synapt-G2 HDMS” mass spectrometer from “Waters” with a time-of-flight analyzer.

6.2.1.6 UV/vis spectroscopy and adsorption isotherms

UV/vis spectra were recorded on an Analytik Jena Specord 50 PLUS UV/vis spectrophotometer using Aspect UV software.

To obtain adsorption isotherms, UV/vis-spectra of solutions in methanol (0.01 mg/mol to 0.2 mg/mol) were recorded for calibration for each polymer. Adsorption experiments were conducted by adding the respective amount of polymer and Aeroxide® P25 (5 mg) to methanol (1 mL). After treating the samples for 10 min in an ultrasonic bath, they were stirred for 2-4 h. The dispersions were filtered through syringe filters. The resulting solutions were diluted with methanol until the absorption was in the calibrated range and their UV/vis-spectra recorded to determine the concentration of residual polymer.

6.2.1.7 Size exclusion chromatography (SEC)

HFIP + 0.05 M CF_3COOK as eluent was used in a system with two consecutive columns (PSS-PFG, 10^3 Å and 10^2 Å) and a Merck L-6200 pump operating at 1 mL/min. A Shodex RI 101 detector was employed to obtain the molar masses and dispersities according to a PMMA standard.

A second system with THF as eluent and two consecutive columns (PPS-SDV 10^5 Å and 10^3 Å) and a Merck L-6200 pump operating at 1 mL/min with a Knauer RI detector was employed. The system was calibrated using polystyrene standards.

6.2.1.8 SPR sample preparation and measurement

Surface plasmon resonance (SPR) measurements were performed using a He-Ne laser with a wavelength of 623.8 nm in Kretschmann configuration. A RES-TEC RT2005 spectrometer from Res-Tec – Resonant Technologies GmbH was used with a LaSFN9 prism. LaSFN9 glass wafers were coated via ALD with chromium (ca. 1 nm), gold (ca. 50 nm) and titanium oxide (ca. 4 nm), respectively. For the grafting process, the wafer was overlayed with a solution of polymer overnight. Afterwards, the remaining liquid was removed with a pipette and the sample was dried in a compressed nitrogen flow. It was annealed in an oven at 120 °C for 24 h and thoroughly washed with methanol and absolute ethanol. For kinetic measurements, the angle was set to the flank left to the plasmon minimum at about 30% reflectivity.

6.2.2 Conducted at IPF Dresden and TU Dresden

Physicochemical and biological characterization of polymers on surfaces in chapter 3 (Preparation of antibacterial polymer brushes on titanium via “grafting to”) conducted by Dr. Frank Simon (Leibniz-Institut für Polymerforschung Dresden) and Dr. Cornelia Wolf-Brandstetter (TU Dresden).

6.2.2.1 Contact angle measurements

Dynamic contact angle measurements (Figure 3.10Figure 3.10) were conducted with an OCA-30 (DataPhysics, Germany) using ultrapure water with samples stored at air no longer than 1 d. The images of advancing and receding drops were recorded with the internal camera and subsequently analysed with the software provided by the manufacturer. The initial drop size was 8 µL and pictures and dosing speed during measurements was set to 0.1 µL/s. Receding angles could not be determined for all surfaces but were rather comparable with values close to or below 10°.

6.2.2.2 Streaming potential measurements

Measurements of zeta potential were performed by means of a commercial electrokinetic analyzer (EKA, Anton Paar GmbH, Austria) equipped with a gap cell. For each experiment a set of two discs mounted via double sided tape onto samples holders resulting in a parallel orientation and the channel was adjusted to 150 µm. The electrolyte consisted of 0.001 M KOH, that was automatically titrated with 0.1 M HCl and 0.1 M KOH in a pH range of 3.0 - 9.0. Pressure profiles were recorded in two directions from 0 to 250 mbar and four measurement points per titration step were analysed. The zeta potential values were calculated from

determined streaming potential according to the Fairbrother-Mastin method by means of software supplied by the manufacturer.

6.2.2.3 Analysis of attachment and biofilm formation under starving conditions

The bacteria adhesion experiment was conducted as described in Kaiser et al. in more detail.[143] In brief, coated titanium samples and respective uncoated reference samples, all disinfected with UV irradiation for 30 min, were seeded by placing 100 µL of a bacteria suspension of E. coli SM2997 containing 10^8 colony forming units (CFU)/mL onto the surfaces for 1 h at 30 °C. After this the bacteria suspension was removed and immediately rinsed 3 times with 100 µL phosphate buffered saline (PBS). Cultivation of samples with remaining attached bacteria was continued under dynamic conditions for 17 h at 30 °C hanging in reverse position in 24 well plates filled with 1.2 mL biofilm (BF) medium per well (see receipt for this medium in Kaiser et al.[143]). The fraction of bacteria being only weakly attached was removed by 3 washing steps with 1.2 mL PBS under shaking for 5 min. Subsequently, the attached bacteria were completely removed by 3 consecutive steps of vortexing, ultrasonic bath and repeated vortexing (30 s each) with the samples placed in 50 ml Falcon tubes filled with 1 mL of LB medium. The number of viable bacteria was determined by means of a proliferation assay described in detail elsewhere.[143]

6.2.2.4 Biocompatibility assessment

Titanium samples coated with antimicrobial polymers as described above were disinfected by 30 min UV irradiation. Afterwards they were transferred to 48 well plates (Nunclon Delta, NuncTM) and cell seeding was performed by addition of 1 mL cell suspension containing 5.000 primary human gingival fibroblasts. Cells were used in 7th passage and cultivated in Dulbecco's Modified Eagle Medium (DMEM) supplemented with 10 % fetal bovine serum, 2 mM glutamate, 100 U penicillin and 100 µg/mL streptomycin.

After 24 h of cultivation the samples were washed with PBS, fixed with 3.7 % formaldehyde solution for 20 min at 4 °C. Prior to staining cells were permeabilized with 0.2 % Triton X-100 in PBS for 2 min and then incubated for 1 h with 2 µg/mL of 4',6-Diamidino-2-phenyl-indol-dihydrochlorid, 2-(4-Amidinophenyl)-6-indolcarbamidin-dihydrochlorid (DAPI) and AlexaFluor™ 546 Phalloidin (InvitrogenTM), diluted 1:40 in PBS. Samples were analysed with a cLSM 510 meta (Zeiss, Germany) equipped with a CCD camera.

6.2.2.5 Statistical analysis

Bacterial experiments were conducted in duplicate, with each individual experiment performed with n = 4. All results are shown as mean ± standard error. Statistical analysis was

performed using one-way Anova, with Levene's test for equal variances and Tukey's post hoc test with respective correction for multiple comparisons of means. Significant differences were assumed at $p < 0.05$. Significant differences are assigned in the graphs by use of asterisks with * for $p < 0.05$, ** for $p < 0.01$ and *** for $p < 0.001$.

6.2.2.6 Live/dead staining

Staining of the samples was performed with the LIVE/DEAD kit (Invitrogen) according to the manufacturer's instructions after 17 h of biofilm formation as described above, followed by the three rinsing steps with PBS. Staining of individual samples was conducted immediately prior to fluorescence microscopy. Pictures were taken with a cLSM 510 meta (Zeiss, Jena, Germany).

6.2.2.7 X-ray photoelectron spectroscopy (XPS)

All XPS studies were carried out by means of an Axis Ultra photoelectron spectrometer (Kratos Analytical, Manchester, UK). The spectrometer was equipped with a monochromatic Al Kα ($h \cdot \nu$ = 1486.6 eV) X-ray source of 300 W at 15 kV. The kinetic energy of photoelectrons was determined with hemispheric analyser set to pass energy of E_{pass} = 160 eV for wide-scan spectra and E_{pass} = 20 eV for high-resolution spectra. During all measurements, electrostatic charging of the sample was avoided by means of a low-energy electron source working in combination with a magnetic immersion lens. Later, all recorded peaks were shifted by the same value that was necessary to set the C 1s peak to 285.00 eV. Quantitative elemental compositions were determined from peak areas using experimentally determined sensitivity factors and the spectrometer transmission function. Spectrum background was subtracted according to Shirley.[163] The high-resolution spectra were deconvoluted by means of the Kratos spectra deconvolution software. Free parameters of component peaks were their binding energy (BE), height, full width at half maximum and the Gaussian-Lorentzian ratio.

6.2.3 Conducted at the University of Siegen

Characterization of polymers on surfaces in chapter 5 (Salt-responsive polymer brushes with antibacterial and antifouling properties) conducted by Michael Greiter (physical characterization), Jiwar Al Zawity and Dr. Mareike Müller (bacterial assays) at the University of Siegen in the group of Prof. Dr. Schönherr.

6.2.3.1 Atomic Force Microscopy (AFM)

The procedure is according to the published method by Schönherr et al.[87] Height images were acquired under ambient conditions with an MFP-3D-Bio AFM (Asylum Research, Santa Barbara, CA) using rectangular silicon cantilevers (OMCL AC 160TS, Olympus, Japan) with a nominal resonance frequency of 300 ± 100 kHz, a nominal tip radius of 7 nm, and a nominal spring constant of 26 N/m in intermittent contact mode. The rms roughness data were evaluated excluding isolated elevated particles.

6.2.3.2 Contact angle measurements

The procedure is according to the published method by Schönherr et al.[164] Static water contact angle measurements (Table 5.3) were conducted on an OCA-15 model instrument (Dataphysics, Filderstadt, Germany) by applying a 2 µL drop of Milli-Q water to the surfaces. At least three measurements were taken at room temperature of each surface.

6.2.3.3 Ellipsometry

The procedure is according to the published method by Schönherr et al.[164] The film thickness of the surfaces was determined at three different angles (65°, 70° and 75°) using an alpha-SE ellipsometer (J. A. Woollam Co., Inc., Lincoln, USA) device with wavelengths between 380 nm and 900 nm. A Cauchy model was used to determine thickness. The first layer was determined as background and the second layer as polymer. Independent measurements for each surface were taken in at least three different regions. The arithmetic mean of the data obtained in the measurements are stated together with the standard deviation (n = 3).

6.2.3.4 Tests with Gram-positive and Gram-negative bacteria

LB (Lysogeny broth) was prepared by dissolving 7 g/l sodium chloride (Th Geyer), 5 g/l yeast extract (Carl Roth) and 10 g/l tryptone/peptone (granulated, Carl Roth) in distilled water.

Dulbecco's phosphate buffered saline (PBS, 10 x, 95 mM (PO_4) DPBS, without calcium or magnesium; Lonza Walkersville, MD USA) was diluted 1:9 in Milli-Q water (Millipore Elix® Advantage 3, Millipak® Filter). 1 x PBS and media were autoclaved for 15 min at 121°C (1.2 bar).

Glycerol stocks of *Staphylococcus aureus* (DSM No. 2569) and *Escherichia coli* NCTC 10418 stored at -80 °C were streaked with a sterile loop onto LB agar (Luria/Miller, Carl Roth) and incubated at 37 °C. Overnight cultures were prepared by inoculating 3 mL of LB with a single bacterial colony and incubated in a shaker at 180 rpm and 37 °C (incubator MaxQ6000, Fisher Scientific, Hampton, NH, USA) for 17 h +/- 2 h. Overnight cultures were adjusted in a cuvette

photometer to an optical density (OD_{600nm}) of 0.5 via addition of LB and then 100-fold diluted in LB. 3 mL of each diluted bacterial suspension corresponding to $2x10^7$ CFU (colony forming units)/mL was added into a 6-well plate (Sarstedt). Each well contained a glass-Au-Ti-Au substrate coated or not coated with the tested polymer, that had been previously submerged in 70 % EtOH for sterilization. Plates were incubated for 24 hours in a humid chamber at 37 °C without shaking. On the next day the supernatants (floating bacteria) and substrates were washed 3 times with 3 mL LB medium. Washing solutions were pooled with the supernatant to determine the CFU/mL (concentration of living floating bacteria). For fluorescence microscopical analysis substrates were washed twice with 1 x PBS. Next, the cells were fixed in a 2.5 % Glutaraldehyde in PBS for 2 hours at RT.

To stain the cells, Syto9 (Working solution: 5 mM, Thermo fisher scientific), that stains bacterial DNA, was diluted 500-fold in H_2O and 100 µl of the working solution (10 µM) was pipetted onto parafilm for each condition/substrate and the substrates side with the bacteria was placed onto the droplet and incubated at RT for 30 minutes. Afterwards, the substrates were washed three times with water. Attached bacteria were analyzed via Zeiss Axio Inverted microscope (Carl Zeiss, Germany), using the filter set for fluorescence imaging (Ex: 450-490 nm, Em>515 nm) and bright field.

6.2.3.5 Scanning electron microscopy (SEM)

Scanning electron microscopy (SEM) was performed with a CamScan 24 (Cambridge Scanning Ltd., Bedford, USA) with an acceleration voltage of 25 kV. To avoid imaging artifacts related to surface charging, samples were sputter-coated with a thin film of gold (≈ 30 nm) with a S150B sputter-coater (Edwards, Crawley, United Kingdom) prior to imaging.

6.2.3.6 X-ray photoelectron spectroscopy (XPS)

The procedure is according to the published method by Schönherr et al.[164] To determine the elemental composition and corresponding concentrations of the surfaces, an ESCA spectrometer (S-probe ESCA SSX-100S Surface Science Instruments, USA) with Al Kα X-ray radiation of 200 W was used. Analysis of the data obtained was made using Casa XPS processing software (version 2.3.16 PR 1.6). General spectra of all elements with energy resolution 1.0 eV were defined in the range of 0–1200 eV. Atomic concentrations on the surfaces were determined from the peak areas and sensitivity factors. The atomic concentrations on the sample surface (<8 nm analysis depth) were calculated in atom-%. For high resolution scans, the energy resolution was reduced to 0.1 eV and the spot size was reduced to 300 μm^2. The fitting of the spectra with Casa XPS software was done by adjusting the aliphatic carbon C1s signal to 285.0 eV.

6.3 Syntheses

Syntheses of polymers and respective post modifications in this work were conducted several times with the same structure but different degrees of polymerization due to variation of the ratio of monomer to CTA and/or different monomer conversions. The descriptions below are representative examples for the synthetic procedures.

6.3.1 Diethyl 4-vinylbenzyl phosphonate (DEVBP)

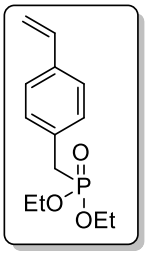

Michaelis-Becker variant: To a solution of diethyl phosphite (14 mL, 94.6 mmol) in toluene (35 mL) sodium hydride (60 % suspension, 4.12 g, 103.2 mmol) was added over 2 h at 0 °C. After stirring overnight at room temperature, 4-vinylbenzyl chloride (9.88 g, 64.7 mmol) was added over 10 min. The mixture was heated to 80 °C for 27 h and filtered after cooling. The solid residue was washed with toluene (50 mL) and the collected organic phase was washed with sat. $NaHCO_3$ (2x30 mL) and brine (2x30 mL). The aqueous phases were reextracted with toluene (30 mL) and the combined organic phases were dried by filtration with a hydrophobic filter. Toluene was removed in vacuo (rotary evaporator, then $5.0x10^{-2}$ at 50 °C). The raw product was purified by column chromatography (*n*-hexane/ethyl acetate 1:1 [R_f = 0.18], then ethyl acetate) to afford DEVBP as colorless oil (7.814 g, 30.7 mmol, 47 %).

Michaelis-Arbuzov variant: 4-vinylbenzyl chloride (14 mL, 84.7 mmol) was reacted with triethyl phosphite (60 mL, 372.6 mmol) with traces of BHT as radical scavenger at 90 °C under argon atmosphere for 18 h. Excess phosphite was removed in vacuo and the raw product was purified by column chromatography (*n*-hexane/ethyl acetate 1:1 [R_f = 0.18], then ethyl acetate) to afford DEVBP as colorless oil (8.896 g, 35.0 mmol, 41 %).

^{1}H NMR ($CDCl_3$, 500 MHz) δ (ppm): 1.24 (t, $^3J_{HH}$=7.1 Hz, 6H, P-O-CH_2-C**H**$_3$), 3.14 (d, $^2J_{PH}$=21.5 Hz, 2H, P-C**H**$_2$), 3.96-4.07 (m, 4H, P-O-C**H**$_2$), 5.22 (dt, $^2J_{HH}$=0.8 Hz, $^3J_{HH}$=10.9 Hz, 1H, CH=C**H**$_{trans}$), 5.72 (dt, $^2J_{HH}$=1.0 Hz, $^3J_{HH}$=17.6 Hz, 1H, CH=C**H**$_{cis}$), 6.69 (dd, $^3J_{HH}$=10.9 Hz, $^3J_{HH}$=17.6 Hz, 1H, Ar-C**H**), 7.23-2-37 (m, 4H, Ar-**H**)

^{13}C NMR ($CDCl_3$, 126 MHz) δ (ppm): 16.7 (**C**H_3), 34.0 (Ar-**C**H_2, $^2J_{CP}$=138 Hz), 62.5 (O-**C**H_2), 126.8 (**C**$_{Ar}$-H), 130.3 (**C**$_{Ar}$-H), 131.6 (**C**$_{Ar}$), 136.7 (**C**$_{Ar}$) 136.8 (CH_2-**C**H-Ar)

^{31}P NMR ($CDCl_3$-*d6*, 202 MHz) δ (ppm): 26.27 (s, P)

ESI-ToF-MS: calculated: 277.0970 g/mol $[M+Na]^+$, found: 277.0945 g/mol

6.3.2 Dimethyl 4-vinylbenzyl phosphonate (DMVBP)

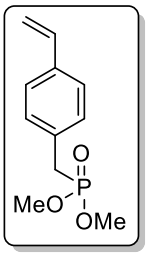

4-vinylbenzyl chloride (15 mL, 90.8 mmol) was reacted with trimethyl phosphite (45 mL, 345.0 mmol) with traces of BHT as radical scavenger at 110 °C under argon atmosphere for 19.5 h. Excess phosphite was removed in vacuo and the raw product was isolated via column chromatography (*n*-hexane/ethyl acetate 1:1, then ethyl acetate/acetone 1:1 [R_f = 0.47]), which yielded DMVBP as a colorless oil (6.19 g, 27.4 mmol, 30 %).

^{1}H NMR (DMSO-*d6*, 700 MHz) δ (ppm): 3.26 (d, $^2J_{PH}$=21.7 Hz, 2H, P-C**H**$_2$), 3.60 (d, $^3J_{PH}$=10.8 Hz, 6H, O-C**H**$_3$), 5.24 (dt, $^2J_{HH}$=1.0 Hz, $^3J_{HH}$=10.9 Hz, 1H, CH=C**H**$_{trans}$), 5.80 (dt, $^2J_{HH}$=1.0 Hz, $^3J_{HH}$=17.6 Hz, 1H, CH=C**H**$_{cis}$), 6.71 (dd, $^3J_{HH}$=10.9 Hz, $^3J_{HH}$=17.7 Hz, 1H, Ar-C**H**), 7.24-7.43 (m, 4H, Ar-**H**)

^{13}C NMR (DMSO-*d6*, 176 MHz) δ (ppm): 31.4 (Ar-**C**H$_2$), 52.8 (O-**C**H$_3$), 114.4(CH-**C**H$_2$), 126.6 (**C$_{Ar}$**), 130.4 (**C$_{Ar}$**), 132.5 (CH$_2$-**C$_{Ar}$**), 136.2 (CH-**C$_{Ar}$**), 136.8 (CH$_2$-**C**H)

^{31}P NMR (DMSO-*d6*, 202 MHz) δ (ppm): 28.95 (s, P)

ESI-ToF-MS: calculated: 249.0657 g/mol $[M+H]^+$, found: 249.0651 g/mol

6.3.3 4-vinylbenzyltrimethyl ammonium chloride (TMA)

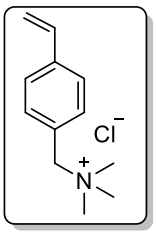

4-vinylbenzyl chloride (12 mL, 85.2 mmol) was dissolved in ethanol (20 mL) and cooled to 0 °C. Within 20 min, trimethylamine in ethanol (4.2 M, 24.3 mL, 10 mmol) was added. The reaction was allowed to come to room temperature and stirred for 19 h. Ethanol and residual trimethylamine were removed in vacuo. The raw product was recrystallized from acetonitrile to yield TMA (10.27 g, 45.5 mmol, 57 %) as colorless crystals.

^{1}H NMR (DMSO-*d6*, 700 MHz) δ (ppm): 3.05 (s, 9H, C**H**$_3$), 4.54 (s, 2H, Ar-C**H**$_2$), 5.36 (dd, 1H, $^2J_{HH}$=0.8 Hz, $^3J_{HH}$=10.7 Hz, CH=C**H$_{trans}$**), 5.96 (dd, 1H, $^2J_{HH}$ =0.8 Hz, $^3J_{HH}$ =17.7 Hz, CH=C**H$_{cis}$**), 6.80 (dd, 1H, ^{3}JHH =10.9 Hz, $^3J_{HH}$=17.7 Hz, C**H**), 7.51 (dd, 2H, Ar-**H**), 7.61 (dd, 2H, Ar-**H**)

^{13}C NMR (176 MHz, DMSO-*d*6) δ (ppm): 52.1 (**C**H$_3$), 67.7 (Ar-**C**H$_2$), 116.2 (CH-**C**H$_2$), 126.5 (**C**$_{Ar}$-H), 127.8 (**C**$_{Ar}$), 133.1 (**C**$_{Ar}$-H), 135.8 (Ar-**C**H), 138.9 (**C**$_{Ar}$)

ESI-ToF-MS: calculated: 176.1434 g/mol $[M\text{-}Cl^-]^+$, found: 176.1424 g/mol

T_m = 260 °C (decomposition)

6.3.4 *N*-acryloyl-2-methylalanine

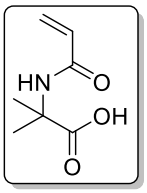

2-Methylalanine (30.04 g, 291.1 mmol) and traces of BHT were dissolved in a solution of sodium hydroxide (26.55 g, 0.66 mol) in water (66 mL) at 0 °C. Acryloyl chloride (27 mL, 268.7 mmol) was added over 15 min and the mixture was stirred at room temperature for 2 h. The precipitated raw product was collected by filtration, washed with water and recrystallized from water/ethanol (1:1). Drying in vacuo afforded the product as colorless crystals (17.1974 g, 109.4 mmol, 41 %).

^{1}H NMR (DMSO-*d6*, 700 MHz) δ (ppm): 1.36 (s, 6H, C**H**$_3$), 5.57 (dd, $^{3}J_{HH}$ =2.2 Hz, $^{2}J_{HH}$ =10.2 Hz, 1H, CH=C**H**$_{trans}$), 6.05 (dd, $^{3}J_{HH}$ =2.1 Hz, $^{2}J_{HH}$ =17.1 Hz, 1H, CH=C**H**$_{cis}$), 6.26 (dd, $^{3}J_{HH}$ =17.1 Hz, $^{3}J_{HH}$ =10.2 Hz, 1H, C**H**), 8.25 (s, 1H, N**H**), 12.19 (s, 1H, C-O**H**)

^{13}C NMR (DMSO-*d6*, 176 MHz) δ (ppm): 25.6 (**C**H$_3$), 55.5 (**C**-CH$_3$), 125.9 (**C**H$_2$), 132.3 (**C**H), 164.5 (**C**(O)NH), 176.0 (**C**(O)OH)

ESI-ToF-MS: calculated: 158.0817 g/mol $[M]^+$, found: 158.0807 g/mol

6.3.5 2-Vinyl-4,4-dimethylazlactone (VDMA)

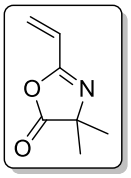

N-acryloyl-2-methylalanine (17.01 g, 108.2 mmol) was suspended in acetone (250 mL) and dissolved after addition of triethylamine (23 mL, 311.4 mmol). The solution was cooled to 0 °C and ethyl chloroformate (10.5 mL, 84.9 mmol) was added over 15 min. After stirring for 2 h at room temperature, the precipitate was filtered off and the solvent was removed in vacuo. Addition of isohexane (250 mL) resulted in the formation of colorless precipitate, which was filtered off. The solvent was removed in vacuo (pressure not less than 100 mbar at 30 °C). The procedure was repeated four times, after which traces of BHT were added and the raw product was dried for 15 min at 50 mbar and 30 °C. It was purified by vacuum distillation (1.2-2.0 mbar, 25 °C head temperature) over benzoic acid (400 mg, 3,2 mmol) to afford the product as a colorless liquid (8.4425 g, 60.7 mmol, 71 %).

^{1}H NMR (DMSO-*d6*, 500 MHz) δ (ppm): 1.42 (s, 6H, C**H**$_3$), 5.90 (dd, $^{3}J_{HH}$=10.2Hz, $^{2}J_{HH}$=1.7, 1H, CH=C**H**$_{trans}$), 6.19 (dd, $^{3}J_{HH}$=17.6 Hz, $^{2}J_{HH}$=1.7, 1H, CH=C**H**$_{cis}$), 6.26 (dd, $^{3}J_{HH}$=17.6 Hz, $^{3}J_{HH}$ =10.3 Hz, 1H, C**H**), 7.26 (s, 1H, N**H**)

^{13}C NMR (DMSO-*d6*, 176 MHz) δ (ppm): 24.1 (**C**H$_3$), 65.4 (**C**-CH$_3$), 123.9 (**C**H), 129.1 (**C**H$_2$), 158.0 (N-**C**-CH), 180.6 (**C**=O)

ESI-ToF-MS: calculated: 140.0716 g/mol $[M+H]^+$, found: 140.0712 g/mol

IR (ATR, ṽ, cm^{1}, selected bands): 1599 (m, C=C), 1668 (s, C=N), 1821 (s, C=O), 2935 (w, C-H), 2981 (w, C-H), 3380 (w, C-H)

6.3.6 P(DEVBP$_{17}$)

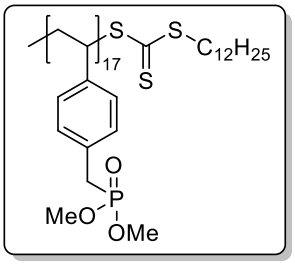

DEVBP (1,059 mg, 4.17 mmol), DMP (70.9, 0.19 mmol) and AIBN (11.1 mg, 0.07 mmol) were dissolved in DMF (4 mL) in a Schlenk tube. The solution was purged with argon for 30 min and placed in a preheated oil bath at 70 °C for 22 h. The reaction was quenched by exposure to air and freezing in liquid nitrogen. For the determination of monomer conversion, a sample was taken and examined by ^{1}H NMR spectroscopy. The polymer was isolated by precipitation from diethyl ether (120 mL) and dried in vacuo to give the product as a yellow oil (84 % conversion, 905 mg, 93 % yield).

^{1}H NMR ($CDCl_3$, 500 MHz) δ (ppm): 0.83-0.90 (br, $C_{11}H_{22}$-C**H**$_3$), 1.08-2.22 (br, C**H**$_2$-C**H** and C_{10}**H**$_{20}$-CH_3 and O-CH_2-C**H**$_3$), 2.97-3.30 (br, Ar-C**H**$_2$-P), 3.81-4.20 (br, O-C**H**$_2$-CH_3), 6.18-7.22 (br, Ar-**H**)

$M_{n(theo., NMR)}$ = 4,700 g/mol

SEC (THF, calibration with polystyrene): M_n = 2,500 g/mol, *D* = 1.13

6.3.7 P(DMVBP$_{12}$)

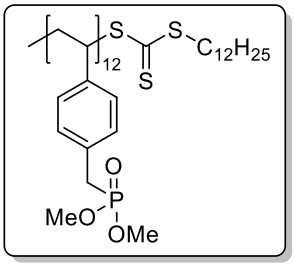

DMVBP (4.1567 mg, 18.38 mmol), DMP (203.1, 0.56 mmol) and AIBN (18.1 mg, 0.11 mmol) were dissolved in DMF (21 mL) in a Schlenk tube under argon atmosphere. The solution was purged with argon for 30 min and placed in a preheated oil bath at 70 °C for 19 h. The reaction was quenched by exposure to air and freezing in liquid nitrogen. For the determination of monomer conversion, a sample was taken and examined by ^{1}H NMR spectroscopy. The polymer was isolated by precipitation from cold diethyl ether (300 mL, -50 °C), dissolved in DMF (12 mL) and precipitated again by the same procedure. The polymer was dissolved in ethanol, moved into a flask and dried in vacuo to give the product as a yellow solid (40 % conversion, 1.6193 g, 37 % yield).

^{1}H NMR (DMSO-*d6*, 500 MHz) δ (ppm): 0.82-0.87 (br, $C_{11}H_{22}$-C**H**$_3$), 1.12-2.28 (br, C**H**$_2$-C**H** and C_{10}**H**$_{20}$-CH_3), 3.03-3.35 (br, Ar-C**H**$_2$-P), 3.35-3.71 (br, O-C**H**$_3$), 4.50-4.89 (br, S-C**H**$_2$), 6.06-7.24 (br, Ar-**H**)

^{31}P NMR (DMSO-*d6*, 202 MHz) δ(ppm): 28.7-29.7 (br, P)

$M_{n(theo., NMR)}$ = 3,100 g/mol

SEC (HFIP + 0.05 M CF_3COOK, calibration with PMMA): M_n = 1,800 g/mol, *D* = 1.19

6.3.8 P(VP_{64})

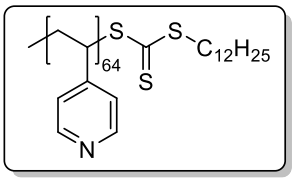

4-Vinyl pyridine (VP) (3.131 g, 29.8 mmol), DMP (130.1 mg, 0.36 mmol) and AIBN (8.8 mg, 54 µmol) were dissolved in dry DMF (10 mL) in a Schlenk tube with a rubber septum and a stirring bar. The solution was purged with argon for 30 min and placed in a preheated oil bath at 70 °C afterwards. After stirring for 19 h, the reaction was quenched by freezing the mixture with liquid nitrogen and exposure to air. For the determination of monomer conversion, a sample was taken and examined by ^{1}H NMR spectroscopy. The polymer was precipitated from toluene (250 mL), collected by filtration and dried in vacuo, yielding P(VP_{64}) (82 % monomer conversion, 1724 mg, 53 % yield) as red solid.

^{1}H NMR (DMSO-*d6*, 500 MHz) δ (ppm): 0.80-0.85 (br, $C_{11}H_{22}$-C**H**$_3$), 1.17-1.24 (br, C_{10}**H**$_{20}$), 1.28-2.25 (br, C**H**$_2$-C**H**), 6.35-6.96 (br, C_{Ar}-C**H**), 7.99-8.51 (br, N-C**H**)

$M_{n(theo., NMR)}$ = 7,100 g/mol

SEC (HFIP + 0.05 M CF_3COOK, calibration with PMMA): M_n = 5,100 g/mol, *Đ* = 1.33

6.3.9 P(VP_{64}-b-$DMVBP_{14}$)

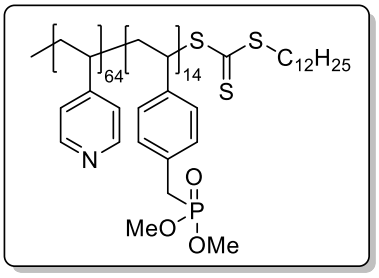

P(VP_{64}) (1420.3 mg, 0.19 mmol), DMVBP (1500.2 mg, 6.63 mmol) and AIBN (7.7 mg, 47 µmol) were dissolved in dry DMF (20 mL) in a Schlenk tube with a rubber septum and a stirring bar. The solution was purged with argon for 30 min and placed in a preheated oil bath at 70 °C afterwards. After stirring for 21 h, the reaction was quenched by freezing the mixture with liquid nitrogen and exposure to air. For the determination of monomer conversion, a sample was taken and examined by ^{1}H NMR spectroscopy. The polymer was precipitated from cold diethyl ether (250 mL), dissolved in methanol and isolated by removing the solvent in vacuo. P(VP_{64}-b-$DMVBP_{14}$) (44 % monomer conversion, 2.24 g, 77 % yield) was obtained as a light-yellow solid.

^{1}H NMR (DMSO-*d6*, 500 MHz) δ (ppm): 0.82-0.87 (br, $C_{11}H_{22}$-C**H**$_3$), 1.18-1.27 (br, C_{10}**H**$_{20}$), 1.28-2.25 (br, C**H**$_2$-C**H**), 3.05-3.27 (br, P-C**H**$_2$), 3.43-3.63 (br, P-OC**H**$_3$), 6.26-7.15 (br, PC**H**$_2$-C_{Ar}**H**-C_{Ar}**H** and NC$_{Ar}$H-C_{Ar}**H**), 8.01-8.45 (br, N-C_{Ar}**H**)

^{31}P NMR (DMSO-*d6*, 202 MHz) δ(ppm): 29.0-29.5 (br, P)

$M_{n(theo., NMR)}$ = 10,200 g/mol

SEC (HFIP + 0.05 M CF_3COOK, calibration with PMMA): M_n = 7,900 g/mol, *Đ* = 1.53

6.3.10 P(VPPr$_{65}$-b-DMVBP$_6$)

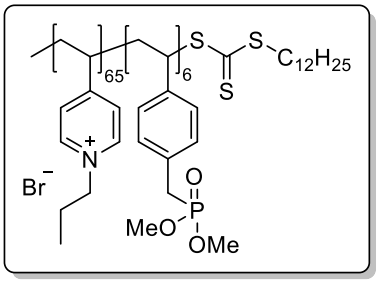

P(VP$_{65}$-b-DMVBP$_6$) (282.5 mg, 0.03 mmol) was reacted with 1-bromopropane (590 µL, 0.64 mol) in nitromethane (6 mL) at 60 °C for 24 h. Due to precipitation from the reaction mixture, nitromethane (4 mL) was added and the slightly turbid solution was stirred at 70 °C for 6 h. The polymer was precipitated from diethyl ether (200 mL), collected by filtration and dried in vacuo, which afforded P(VPPr$_{65}$-b-DMVBP$_6$) (483.3 mg, 88 %, 0.03 mmol) as green solid.

^{1}H NMR (DMSO-*d6*, 500 MHz) δ (ppm): 0.69-1.08 (br, NCH$_2$CH$_2$-C**H**$_3$ and C$_{11}$H$_{22}$-C**H**$_3$), 1.16-1.26 (br, C$_{10}$**H**$_{20}$), 1.30-2.44 (br, NCH$_2$-C**H**$_2$ and C**H**$_2$-C**H**), 3.18-3.26 (br, P-C**H**$_2$), 3.44-3.65 (br, O-C**H**$_3$), 4.15-5.00 (br, N-C**H**$_2$), 6.26-7.21 (br, P-CH$_2$-Ar-**H**), 7.69-9.42 (br, Pyr-**H**)

^{31}P NMR (DMSO-*d6*, 202 MHz) δ (ppm): 28.6-29.7 (br, P)

$M_{n(theo., NMR)}$ = 16,500 g/mol

SEC (HFIP + 0.05 M CF_3COOK, calibration with PMMA): M_n = 17,100 g/mol, *D* = 1.31

6.3.11 P(VPPr$_{65}$-b-PA$_6$)

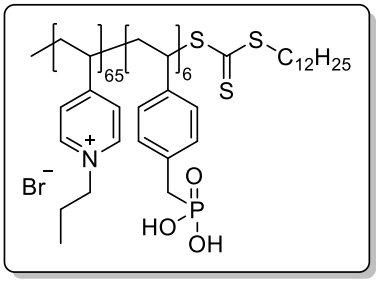

P(VPPr$_{65}$-b-DMVBP$_6$) (463,3 mg, 0.03 mmol) was dissolved in dry DMF (11 mL) under argon atmosphere. The solution was cooled with an ice bath and TMS-Br (0.3 mL, 2.3 mmol) was added with a syringe. The mixture was stirred over night at 40 °C and volatiles were removed in vacuo afterwards. Methanol (15 mL) was added to the residue and stirred for 2 d. After dialysis and lyophilization of the reaction mixture, P(VPPr$_{65}$-b-PA$_6$) (296.9 mg, 64 %, 0,02 mmol) was afforded as a brown solid.

^{1}H-NMR (DMSO-*d6*, 500 MHz) δ (ppm): 0.66-1.11 (br, NCH$_2$CH$_2$-C**H**$_3$ and C$_{11}$H$_{22}$-C**H**$_3$), 1.19-1.28 (br, C$_{10}$**H**$_{20}$), 1.32-3.14 (br, NCH$_2$-C**H**$_2$ and C**H**$_2$-C**H**), 3.18-3.26 (br, P-C**H**$_2$), 4.35-4.88 (br, N-C**H**$_2$), 6.42-7.24 (br, P-CH$_2$-Ar-**H**), 7.57-9.43 (br, Pyr-**H**)

^{31}P-NMR (DMSO-*d6*, 202 MHz) δ (ppm): 21.4-23.8 (br, P)

Traces of conc. HCl were added to the NMR sample of P(VPPr$_{65}$-b-PA$_6$) to make PA resonances visible.

$M_{n(theo., NMR)}$ = 16,400 g/mol

SEC (HFIP + 0.05 M CF_3COOK, calibration with PMMA): M_n = 15,400 g/mol, *D* = 1.52

6.3.12 P(DMVBP$_{12}$-b-TMA$_{171}$)

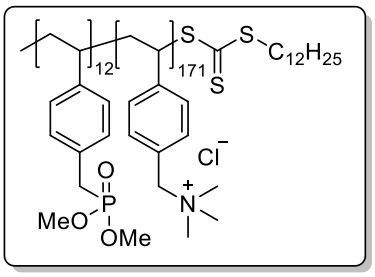

P(DMVBP$_{12}$) (87.9, 0.02 mmol), TMA (1198.6 mg, 5.66 mmol) and AIBN (0.9 mg, 5 µmol) were dissolved in DMF (5 mL) and water (5 mL) in a Schlenk tube with a rubber Septum and a stirring bar. The solution was purged with argon for 20 min and placed in a preheated oil bath at 70 °C afterwards. After stirring for 23 h, the reaction was quenched by freezing the mixture with liquid nitrogen and exposure to air. For the determination of monomer conversion, a sample was taken and examined by ^{1}H NMR spectroscopy. The polymer was isolated by dialysis and lyophilization as a colorless solid (94 % conversion, 732.4 mg, 57 % yield).

Polymers of the general structure P(DMVBP-b-TMA) can also be isolated by precipitation from isopropanol.

^{1}H NMR (D_2O, 500 MHz) δ (ppm): 0.63-0.87 (br, $C_{11}H_{22}$-C**H**$_3$), 1.05-2.30 (br, C**H**$_2$-C**H** and C_{10}**H**$_{20}$), 2.74-3.24 (br, N-C**H**$_3$), 3.51-3.85 (br, P-OC**H**$_3$), 4.16-4.66 (br, N-C**H**$_2$-Ar and P-C**H**$_2$-Ar), 6.34-7.61 (br, P-CH_2-Ar**H** and N-CH_2Ar**H**)

^{31}P NMR (DMSO-*d6*, 202 MHz) δ (ppm): 31.3-32.2 (br, P)

$M_{n(theo., NMR)}$ = 30,000 g/mol

SEC (HFIP + 0.05 M CF_3COOK, calibration with PMMA): M_n = 40,000 g/mol, *D* = 1.44

6.3.13 P(VBPA$_{16}$-b-TMA$_{101}$)

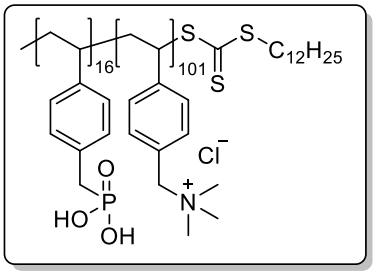

P(DMVBP$_{16}$-b-TMA$_{101}$) (7 g, 0.28 mmol) were dissolved in water (15 mL) and conc. HCl (15 mL). The mixture was heated to reflux for 3 h, whereby the solution became increasingly turbid. Afterwards, the polymer was isolated via dialysis and lyophilization. The ^{31}H NMR spectrum revealed that the conversion to phosphonic acid was not completed, thus the procedure was repeated in water (40 mL) and conc. HCl (40 mL) at 115 °C bath temperature for 23 h, which led to quantitative conversion of the ester. The polymer was purified by dialysis and lyophilization to obtain a colorless solid (4.4698 g, 0.18 mmol, 64 %).

^{1}H NMR (D_2O, 500 MHz) δ (ppm): 0.93-0.98 (br, $C_{11}H_{22}$-C**H**$_3$), 1.21-2.30 (br, C**H**$_2$-C**H** and C_{10}**H**$_{20}$), 2.70-3.27 (br, N-C**H**$_3$), 4.23-4.64 (br, N-C**H**$_2$-Ar and P-C**H**$_2$-Ar), 6.42-7.49 (br, P-CH_2-Ar**H** and N-CH_2Ar**H**)

^{31}P NMR (DMSO-*d6*, 202 MHz) δ (ppm): 18.3-21.4 (br, P)

$M_{n(theo., NMR)}$ = 24,500 g/mol

SEC (HFIP + 0.05 M CF_3COOK, calibration with PMMA): M_n = 31,000 g/mol, *D* = 1.56

6.3.14 P(DMVBP$_{12}$-b-TMA$_{89}$-b-Sty$_{23}$)

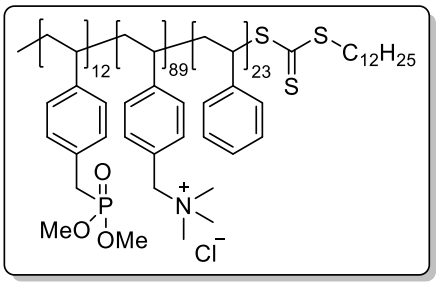

P(DMVBP$_{12}$-b-TMA$_{89}$) (486.0 mg, 0.02 mmol), Sty (218.7 mg, 2.10 mmol) and AIBN (0.9 mg, 5 µmol) were dissolved in DMF (4.5 mL) and water (3 mL) in a Schlenk tube with a rubber Septum and a stirring bar. The solution was purged with argon for 30 min and placed in a preheated oil bath at 70 °C afterwards. After stirring for 20 h, the reaction was quenched by freezing the mixture with liquid nitrogen and exposure to air. The polymer was isolated by dialysis and lyophilization as a light-yellow solid (conversion not determinable, 390.2 mg, 0,016 mmol, 72 % yield).

The degree of polymerization of Sty was determined from the ^{1}H NMR spectrum of P(DMVBP$_{12}$-b-TMA$_{89}$-b-Sty$_{23}$) by comparing signals from TMA with the aromatic signals.

^{1}H NMR (D_2O, 500 MHz) δ (ppm): 1.07-2.26 (br, C**H**$_2$-C**H** and C_{10}**H**$_{20}$), 2.65-3.20 (br, N-C**H**$_3$), 3.50-3.75 (br, P-OC**H**$_3$), 4.15-4.56 (br, N-C**H**$_2$-Ar and P-C**H**$_2$-Ar), 6.20-7.59 (br, Ar**H**$_{Sty}$, P-CH$_2$-Ar**H** and N-CH$_2$Ar**H**)

^{31}P NMR (DMSO-*d6*, 202 MHz) δ (ppm): 31.2-32.4 (br, P)

$M_{n(theo., NMR)}$ = 24,300 g/mol

SEC (HFIP + 0.05 M CF_3COOK, calibration with PMMA): M_n = 30,000 g/mol, *D* = 1.45

6.3.15 P(VBPA$_{12}$-b-TMA$_{89}$-b-Sty$_{23}$)

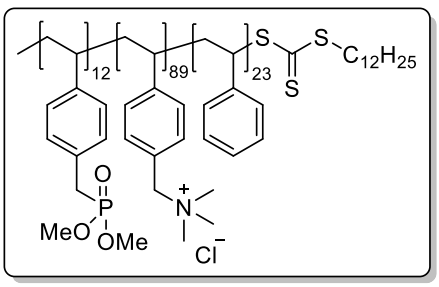

P(DMVBP$_{12}$-b-TMA$_{89}$-b-Sty$_{23}$) (360.0 mg, 0.018 mmol) was dissolved in water (1.5 mL), 1,4-dioxane (3 mL) and conc. HCl (1.5 mL). The solution was heated to reflux for 18 h and isolated by dialysis and lyophilization. The product was obtained as a colorless solid (348.9 mg, 0.015 mmol, 81 %).

^{1}H NMR (D_2O, 500 MHz) δ (ppm): 0.85-2.25 (br, C**H**$_2$-C**H** and C_{10}**H**$_{20}$), 2.55-3.39 (br, N-C**H**$_3$), 4.06-4.64 (br, N-C**H**$_2$-Ar and P-C**H**$_2$-Ar), 6.27-7.70 (br, P-CH$_2$-Ar**H** and N-CH$_2$Ar**H**)

^{31}P NMR (DMSO-*d6*, 202 MHz) δ (ppm): 18.4-20.4 (br, P)

$M_{n(theo., NMR)}$ = 24,000 g/mol

SEC (HFIP + 0.05 M CF_3COOK, calibration with PMMA): M_n = 40,000 g/mol, *D* = 1.65

6.3.16 P(DMVBP$_{12}$-b-Sty$_{89}$-co-TMA$_{74}$)

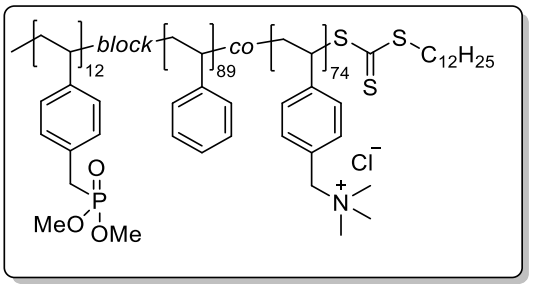

P(DMVBP$_{12}$) (103.3 mg, 0.03 mmol), TMA (707.4 mg, 3.34 mmol), Sty (349.4 mg, 3.35 mmol) and AIBN (1.1 mg, 7 µmol) were dissolved in DMF (6 mL) and water (4 mL) in a Schlenk tube with a rubber Septum and a stirring bar. The solution was purged with argon for 30 min and placed in a preheated oil bath at 70 °C afterwards. After stirring for 24 h, the reaction was quenched by freezing the mixture with liquid nitrogen and exposure to air. The polymer was isolated by dialysis and lyophilization as a light-yellow solid (TMA conversion 81 %, 722.3 mg, 62 % yield).

The degree of polymerization of Sty was determined from the ^{1}H NMR spectrum of P(VBPA$_{12}$-b-TMA$_{89}$-b-Sty$_{23}$) (chapter 6.3.17) by comparing signals from TMA with the aromatic signals.

^{1}H NMR (D_2O, 500 MHz) δ (ppm): 0.60-2.26 (br, C**H**$_2$-C**H** and C_{10}**H**$_{20}$), 2.59-3.22 (br, N-C**H**$_3$), 3.47-3.83 (br, P-OC**H**$_3$), 4.04-4.67 (br, N-C**H**$_2$-Ar and P-C**H**$_2$-Ar), 5.98-7.83 (br, Ar**H**$_{Sty}$, P-CH$_2$-Ar**H** and N-CH$_2$Ar**H**)

^{31}P NMR (D_2O, 202 MHz) δ (ppm): 30.6-32.4 (br, P)

$M_{n(theo., NMR)}$ = 27,000 g/mol

SEC (HFIP + 0.05 M CF_3COOK, calibration with PMMA): M_n = 26,000 g/mol, *D* = 1.34

6.3.17 P(VBPA$_{12}$-b-Sty$_{89}$-co-TMA$_{74}$)

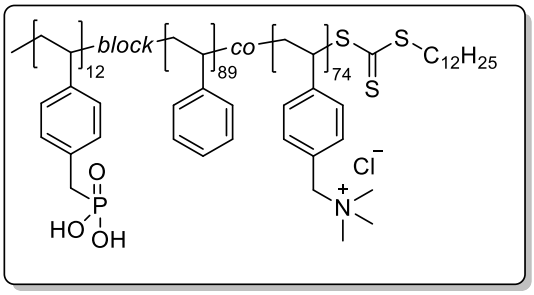

P(DMVBP$_{12}$-b-Sty$_{89}$-co-TMA$_{74}$) (700.0 mg, 0.03 mmol) was dissolved in water (2.5 mL) and conc. HCl (2.5 mL) and heated to reflux for 23 h. The polymer was isolated by dialysis and lyophilization to obtain the product as a light-yellow solid (631.5 mg, 0.023 mmol, 78 %).

^{1}H NMR (D_2O, 500 MHz) δ (ppm): 0.92-0.99 (br, $C_{11}H_{22}$-C**H**$_3$), 1.04-2.35 (br, C**H**$_2$-C**H** and C_{10}**H**$_{20}$), 2.61-3.24 (br, N-C**H**$_3$), 4.14-4.64 (br, N-C**H**$_2$-Ar and P-C**H**$_2$-Ar), 6.20-7.73 (br, Ar**H**$_{Sty}$, P-CH$_2$-Ar**H** and N-CH$_2$Ar**H**)

^{31}P NMR (D_2O, 202 MHz) δ (ppm): 18.4-20.9 (br, P)

$M_{n(theo., NMR)}$ = 27,000 g/mol

SEC (HFIP + 0.05 M CF_3COOK, calibration with PMMA): M_n = 32,000 g/mol, *D* = 1.55

6.3.18 P(DMVBP$_{12}$-b-Sty$_{39}$-co-TMA$_{64}$-b-4FBA$_{19}$)

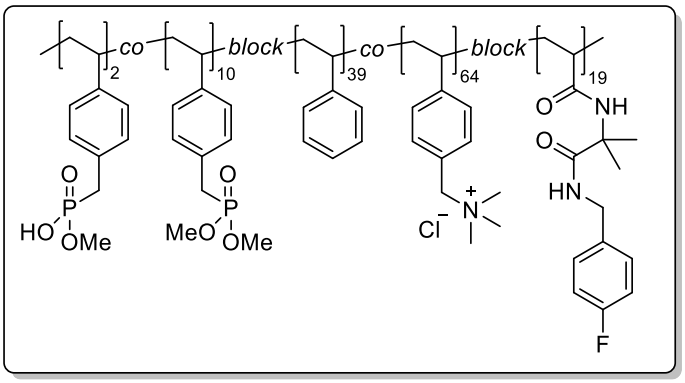

(DMVBP$_{12}$-b-Sty$_{39}$-co-TMA$_{64}$) (89.7 mg, 4.3 µmol), VDMA (32.0 mg, 0,23 mmol) and AIBN (0.1 mg, 0.6 µmol) were dissolved in dry DMSO (2 mL) in a Schlenk tube with a rubber septum and a stirring bar. The solution was purged with argon for 30 min and placed in a preheated oil bath at 70 °C afterwards. After stirring for 5 h, the reaction was quenched by freezing the mixture with liquid nitrogen and short exposure to air. For the determination of monomer conversion, a sample was taken and examined by ^{1}H NMR spectroscopy (38 % VDMA conversion). Then, 4-fluorobenzylamine (27 µL, 0.24 µmol) was added and the solution was stirred overnight. The product (94 mg, 3.6 µmol, 84 %) was isolated as a colorless solid by dialysis and lyophilization.

^{1}H NMR (DMSO-*d6*, 700 MHz) δ (ppm): 0.80-0.89 (br, $C_{11}H_{22}$-C**H**$_3$), 0.92-2.30 (br, C**H**$_2$-C**H** and C_{10}**H**$_{20}$), 2.76-3.30 (br, N-C**H**$_3$), 3.45-3.66 (br, P-OC**H**$_3$), 3.91-4.42 (br, NH-C**H**$_2$), 4.41-5.18 (br, N-C**H**$_2$-Ar and P-C**H**$_2$-Ar), 6.07-7.58 (br, Ar**H**$_{Sty}$, P-CH$_2$-Ar**H** and N-CH$_2$Ar**H**), 7.89-8.59 (br, N**H**)

^{19}F NMR (DMSO-*d6,* 659 MHz) δ (ppm): -117.6-(-115.9) (br, F)

^{31}P NMR (DMSO-*d6*, 202 MHz) δ (ppm): 24.4-25.0 (br, P(OH)(OCH$_3$)), 28.8-29.5 (br, P-(OCH$_3$)$_2$)

$M_{n(theo., NMR)}$ = 26,000 g/mol

SEC (HFIP + 0.05 M CF_3COOK, calibration with PMMA): M_n = 21,000 g/mol, *Đ* = 1.74

IR (ATR, ṽ, cm^{1}, selected bands): 1489 (s, C-H) 1645 (vs, C=C), 2924 (m, C-H), 3026 (w, C-H$_{Ar}$)

6.3.19 P(MVBP$_{12}$-b-TMA$_{167}$-b-Biotin$_2$)

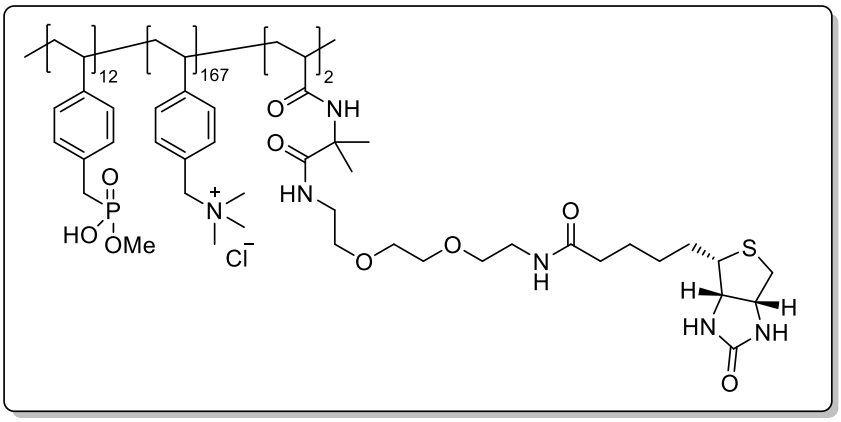

P(DMVBP$_{12}$-b-TMA$_{167}$) (500.6 mg, 12.8 µmol), VDMA (57 mg, 0.41 mmol) and AIBN (1.0 mg, 6 µmol) were dissolved in dry DMSO (9.8 mL) in a Schlenk tube with a rubber septum and a stirring bar. The solution was purged with argon for 20 min and placed in a preheated oil bath at 70 °C afterwards. After stirring for 5 h, the reaction was quenched by freezing the mixture with liquid nitrogen and short exposure to air. For the determination of monomer conversion, a sample was taken and examined by ^{1}H NMR spectroscopy (32 % VDMA conversion). Then, biotin-PEG2-amine (46 mg, 0.12 mmol, 0.3 equivalents with respect to VDMA) was added and the solution was stirred for 17 h. A ^{1}H NMR sample was taken and ethanolamine (410 µL, 6.6 mmol) was added to quench residual azlactone groups. After stirring for 7 h and storage in the fridge for 3 d, the polymer was isolated by dialysis and lyophilization and obtained as colorless solid (444.5 mg, 10.8 µmol, 85 %).

^{1}H NMR (DMSO-*d6*, 500 MHz) δ (ppm): 0.86-2.26 (br, C**H**$_2$-C**H**), 2.67-3.19 (br, N-C**H**$_3$), 3.47-3.69 (br, P-OC**H**$_3$), 4.13-4.79 (br, N-C**H**$_2$-Ar and P-C**H**$_2$-Ar), 6.11-7.56 (br, P-CH$_2$-Ar**H** and N-CH$_2$-Ar**H**)

^{31}P NMR (DMSO-*d6*, 202 MHz) δ (ppm): 18.0-19.0 (br, P)

$M_{n(theo., NMR)}$ = 41,000 g/mol

SEC (HFIP + 0.05 M CF_3COOK, calibration with PMMA): M_n = 41,000 g/mol, $Đ$ = 1.58

IR (ATR, ṽ, cm^1, selected bands): 1385 (m, C-H) 1427 (m, C-H) 1485 (s, C-H) 1645 (s, C=C) 2923 (w, C-H) 3022 (w, C-H$_{Ar}$)

6.3.20 P(DMVBP$_{12}$-b-TMA$_{167}$-b-RGD$_5$)

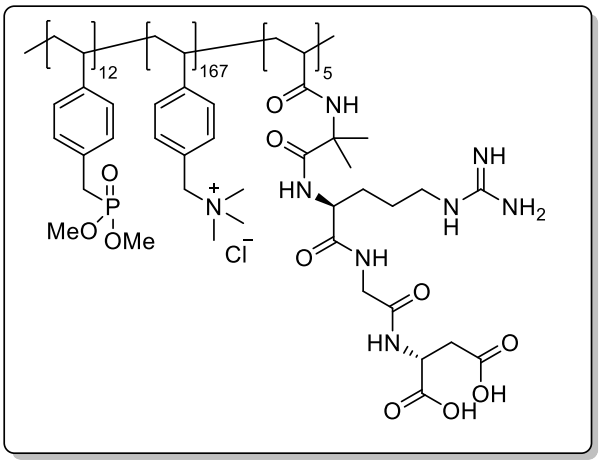

P(DMVBP$_{12}$-b-TMA$_{167}$) (250.0 mg, 6.4 µmol), VDMA (57 mg, 0,22 mmol) and AIBN (0.3 mg, 2 µmol) were dissolved in dry DMSO (4.3 mL) in a Schlenk tube with a rubber septum and a stirring bar. The solution was purged with argon for 20 min and placed in a preheated oil bath at 70 °C afterwards. After stirring for 17 h, the reaction was quenched by freezing the mixture with liquid nitrogen and short exposure to air. For the determination of monomer conversion, a sample was taken and examined by ^{1}H NMR spectroscopy (30 % VDMA conversion). Then, RGD (37.8 mg, 0.11 mmol) and DBU (36 µL, 0.23 mmol) were added. The turbid solution was stirred for 20 h. Dimethylamine (40 % in water, 40 µL) was added. After 6 h, water (3 mL) was added and the polymer was isolated by dialysis and lyophilization. A colorless solid (229.9 mg) was afforded.

^{1}H NMR (D_2O, 500 MHz) δ (ppm): 1.14-2.29 (br, C**H**$_2$-C**H**), 2.74-3.19 (br, N-C**H**$_3$), 4.14-4.54 (br, N-C**H**$_2$-Ar and P-C**H**$_2$-Ar), 6.39-7.43 (br, P-CH$_2$-Ar**H** and N-CH$_2$Ar**H**)

^{31}P NMR (DMSO-*d6*, 202 MHz) δ (ppm): 22.3-24.7 (br, P(OH)(OCH$_3$)), 28.9-29.9 (br, P-(OCH$_3$)$_2$)

$M_{n(theo., NMR)}$ = 41,000 g/mol

SEC (HFIP + 0.05 M CF_3COOK, calibration with PMMA): M_n = 38,000 g/mol, *D* = 1.62

6.3.21 P(MVBP$_{12}$-b-TMA$_{167}$-b-RGD$_5$)

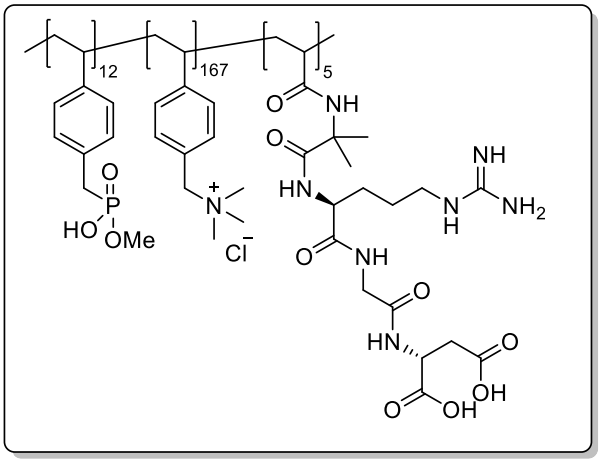

The product of synthesis 6.3.20 (172.5 mg) and ethanolamine (100 µL) were dissolved in water (2 mL). The solution was stirred for 24 h at room temperature and for 19 h at 50 °C. Dialysis and lyophilization of the reaction mixture afforded a colorless solid (141.1 mg).

^{1}H NMR (D_2O, 500 MHz) δ (ppm): 1.11-2.27 (br, C**H**$_2$-C**H**), 2.73-3.13 (br, N-C**H**$_3$), 4.14-4.58 (br, N-C**H**$_2$-Ar and P-C**H**$_2$-Ar), 6.34-7.55 (br, P-CH$_2$-Ar**H** and N-CH$_2$Ar**H**)

^{31}P NMR (D_2O, 283 MHz) δ (ppm): 19.8-24.3 (br, P(OH)(OCH$_3$))

$M_{n(theo., NMR)}$ = 41,000 g/mol

SEC (HFIP + 0.05 M CF_3COOK, calibration with PMMA): M_n = 38,000 g/mol, *D* = 1.75

IR (ATR, ṽ, cm^1, selected bands): 1383 (s, C-H), 1483 (s, C-H), 1624 (s, C=C), 1635 (s, C=C), 2923 (m, C-H), 3026 (m, C-H_{Ar})

6.3.22 P(VSP_{63}-b-$DMVBP_{13}$)

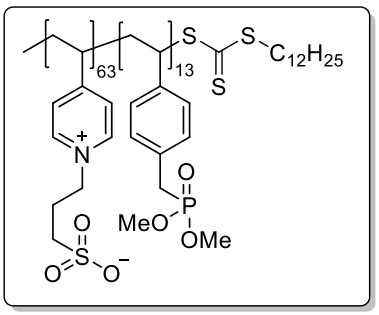

P(VP_{63}-b-$DMVBP_{13}$) (2.0234 g, 0.2 mmol) and 1,3-propane sultone (4.6830 g, 38.3 mmol, 3 eq. per pyridine group) were dissolved in HFIP (20 mL) and stirred at 40 °C bath temperature for 22 h. The solvent was removed in vacuo and 0.5 M NaCl (25 mL) was added. The mixture was dialyzed and lyophilized to yield the product as a colorless solid (2.9853 g, 0.17 mmol, 85 %).

^{1}H NMR (D_2O+NaCl, 500 MHz) δ (ppm): 1.84-2.50 (br, C**H**$_2$-C**H** and N-CH_2-C**H**$_2$), 3.13-3.37 (br, P-C**H**$_2$ and S-C**H**$_2$), 3.51-3.89 (br, P-OC**H**$_3$), 4.77-5.02 (br, N-C**H**$_2$), 6.82-8.28 (br, P-CH_2-Ar**H** and N-CH-C**H**), 8.64-9.11 (br, N-C**H**)

^{31}P NMR (D_2O+NaCl, 283 MHz) δ (ppm): 29.5-33.2 (br, P)

$M_{n(theo., NMR)}$ = 17,700 g/mol

SEC (HFIP + 0.05 M CF_3COOK, calibration with PMMA): M_n = 9,400 g/mol, *Đ* = 1.52

6.3.23 P(VSP_{63}-b-PA_{13})

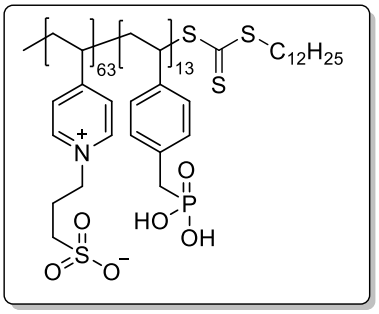

P(VSP_{63}-b-$DMVBP_{13}$) (3.0 g, 0.17 mmol) was dissolved in 1 M NaCl (20 mL) over 6 h. Conc. HCl (10 mL) was added and the mixture was heated to reflux for 3 h. The solution was dialyzed (against 1 M NaCl and distilled water) and lyophilized. Since the ^{31}P NMR spectrum revealed that the conversion was not complete, the polymer was again dissolved in 1 M NaCl (20 mL) and conc. HCl (20 mL) and heated to reflux for 23 h. Dialysis and lyophilization of the reaction mixture afforded the product as a brown solid (1.9646 g, 0.11 mmol, 65 %).

^{1}H NMR (D_2O+NaCl, 500 MHz) δ (ppm): 1.69-2.73 (br, C**H**$_2$-C**H** and N-CH_2-C**H**$_2$), 2.99-3.28 (br, P-C**H**$_2$ and S-C**H**$_2$), 4.70-4.94 (br, N-C**H**$_2$), 6.89-8.13 (br, P-CH_2-Ar**H** and N-CH-C**H**), 8.49-9.05 (br, N-C**H**)

^{31}P NMR (D_2O+NaCl, 283 MHz) δ (ppm): 21.7-25.1 (br, P)

$M_{n(theo., NMR)}$ = 17,300 g/mol

SEC (HFIP + 0.05 M CF_3COOK, calibration with PMMA): the product was not soluble.

6.3.24 P(VP_{64}-b-$DMVBP_{14}$-b-TMA_{64})

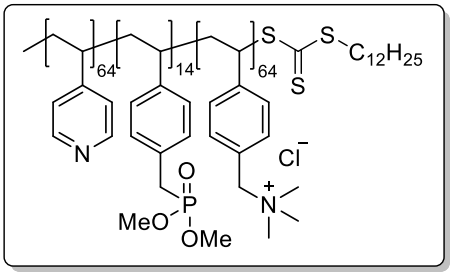

P(VP_{64}-b-$DMVBP_{14}$) (1593.4 mg, 0.15 mmol), TMA (3010.3 mg, 14.2 mmol) and AIBN (5.2 mg, 32 µmol) were dissolved in a mixture of DMF (30 mL) and water (20 mL) in a Schlenk tube with a rubber Septum and a stirring bar. The solution was purged with argon for 30 min and placed in a preheated oil bath at 70 °C afterwards. After stirring for 20 h, the reaction was quenched by freezing the mixture with liquid nitrogen and exposure to air. For the determination of monomer conversion, a sample was taken and examined by ^{1}H NMR spectroscopy. The polymer was precipitated from acetone (600 mL), dissolved in methanol and isolated by removing the solvent in vacuo. P(VP_{64}-b-$DMVBP_{14}$-b-TMA_{64}) with contaminations of DMF, methanol and TMA (4.13 g, 78 % monomer conversion) was obtained as a light-yellow solid. The product was used without further purification.

^{1}H NMR (DMSO-*d6*, 500 MHz) δ (ppm): 0.81-0.87 (br, $C_{11}H_{22}$-C**H**$_3$), 1.16-1.25 (br, C_{10}**H**$_{20}$), 1.25-2.31 (br, C**H**$_2$-C**H**), 2.93-3.30 (br, N-C**H**$_3$ and P-C**H**$_2$), 3.45-3.63 (br, P-OC**H**$_3$), 4.41-5.35 (br, $(CH_3)_3$N-C**H**$_2$), 6.12-7.70 (br, P-CH_2-Ar**H** and N_{Pyr}-CH-C**H** and N-CH_2-Ar**H**), 8.01-8.41 (br, N_{Pyr}-C**H**)

^{31}P NMR (DMSO-*d6*, 202 MHz) δ(ppm): 29.1-29.6 (br, P)

$M_{n(theo., NMR)}$ = 24,000 g/mol

SEC (HFIP + 0.05 M CF_3COOK, calibration with PMMA): M_n = 23,000 g/mol, *Đ* = 1.65

6.3.25 P(VSP_{64}-b-$DMVBP_{14}$-b-TMA_{64})

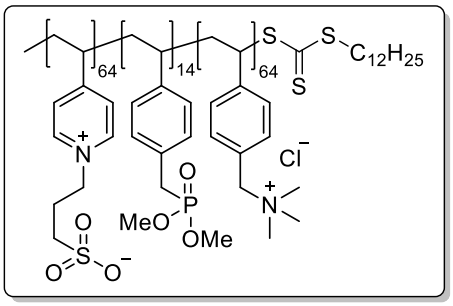

P(VP_{64}-b-$DMVBP_{14}$-b-TMA_{64}) with contaminations of DMF, methanol and TMA (2.985 g) and 1,3-propanesultone (3.051 g, 24.9 mmol, ca. 3.2 eq. per pyridine group) were dissolved in HFIP (21 mL) and placed in a Schlenk flask under argon atmosphere. After stirring at 40 °C for three days, roughly ½ of the solvent was removed in vacuo. It was diluted with 15 mL of 1 M NaCl in water and dialyzed against 1 M NaCl in water and deionized water. Lyophilization of the solution afforded the product as colorless solid (2.796 g, 0.08 mmol, ca. 71 %).

^{1}H NMR (D_2O+NaCl, 500 MHz) δ (ppm): 1.29-1.36 (br, C_{10}**H**$_{20}$), 1.42-2.79 (br, C**H**$_2$-C**H** and N-CH_2-C**H**$_2$), 3.03-3.39 (br, N-C**H**$_3$ and P-C**H**$_2$ and S-C**H**$_2$), 3.69-3.89 (br, P-OC**H**$_3$), 4.44-5.03 (br, $(CH_3)_3$N-C**H**$_2$ and N_{Pyr}-C**H**$_2$), 6.46-8.22 (br, P-CH_2-Ar**H** and N_{Pyr}-CH-C**H** and N-CH_2-Ar**H**), 8.49-9.07 (br, N_{Pyr}-C**H**)

^{31}P NMR (D_2O+NaCl, 202 MHz) δ (ppm): 30.8-32.6 (br, 1P)

$M_{n(theo., NMR)}$ = 33,000 g/mol

SEC (HFIP + 0.05 M CF_3COOK, calibration with PMMA): M_n = 30,000 g/mol, *D* = 1.50

6.3.26 P(VSP_{64}-b-PA_{14}-b-TMA_{64})

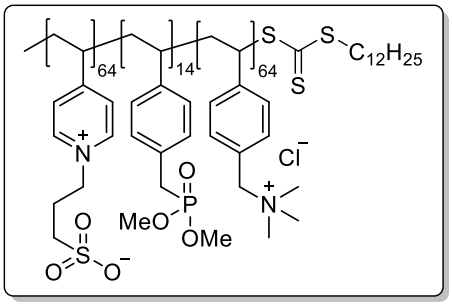

P(VSP_{64}-b-$DMVBP_{14}$-b-TMA_{64}) (2.62 g, 0.08 mmol) and sodium chloride (10.40 g) were dissolved in 6 M hydrochloric acid and stirred under reflux for three hours. The product was isolated by dialyzing the mixture against 1 M NaCl and deionized water. Lyophilization gave P(VSP_{64}-b-PA_{14}-b-TMA_{64}) (2.122 g, 0.06 mmol, 81 %) as colorless solid.

^{1}H NMR (D_2O+NaCl, 500 MHz) δ (ppm): 1.39-2.81 (br, C_{10}**H**$_{20}$ and C**H**$_2$-C**H** and N-CH_2-C**H**$_2$), 2.81-3.64 (br, N-C**H**$_3$ and S-C**H**$_2$), 4.38-5.15 (br, $(CH_3)_3$N-C**H**$_2$ and N_{Pyr}-C**H**$_2$), 6.39-8.41 (br, P-CH_2-**H**$_{Ar}$ and N_{Pyr}-CH-C**H** and N-CH_2-**H**$_{Ar}$), 8.42-9.10 (br, N_{Pyr}-C**H**)

^{31}P NMR (D_2O+NaCl, 202 MHz) δ (ppm): 18.1-22.1 (br, P)

$M_{n(theo., NMR)}$ = 33,000 g/mol

SEC (HFIP + 0.05 M CF_3COOK, calibration with PMMA): M_n = 27,000 g/mol, *D* = 1.50

IR (ATR, ṽ, cm^1, selected bands): 1038 (vs, S=O), 1184 (vs, S=O), 1475 (m, C-H), 1641 (m, C=C), 2926 (w, C-H), 3028 (w, C-H_{Ar})

7 References

[1] B. Ritzert, *Zahnimplantate zunehmend erste Wahl: 1,3 Millionen werden in Deutschland pro Jahr eingepflanzt, abgerufen am 21.01.2023 unter* http://idwf.de/-CsojAA, **2018**.

[2] T. Albrektsson, P. I. Brånemark, H. A. Hansson, J. Lindström, *Acta Orthop. Scand.* **1981**, *52*, 155.

[3] F. Rupp, J. Geis-Gerstorfer, K. E. Geckeler, *Adv. Mater.* **1996**, *8*, 254.

[4] A. G. Gristina, *Science* **1987**, *237*, 1588.

[5] A. Mombelli, N. Müller, N. Cionca, *Clin. Oral Implants Res.* **2012**, *23 Suppl 6*, 67.

[6] P. S. Stewart, J. William Costerton, *Lancet* **2001**, *358*, 135.

[7] J. Grischke, J. Eberhard, M. Stiesch, *Dent. Mater. J.* **2016**, *35*, 545.

[8] M.-T. Tsai, Y.-Y. Chang, H.-L. Huang, J.-T. Hsu, Y.-C. Chen, A. Y.-J. Wu, *Thin Solid Films* **2013**, *528*, 143.

[9] J. Liu, J. Liu, S. Attarilar, C. Wang, M. Tamaddon, C. Yang, K. Xie, J. Yao, L. Wang, C. Liu et al., *Front. Bioeng. Biotechnol* **2020**, *8*, 576969.

[10] R. A. Gittens, R. Olivares-Navarrete, A. Cheng, D. M. Anderson, T. McLachlan, I. Stephan, J. Geis-Gerstorfer, K. H. Sandhage, A. G. Fedorov, F. Rupp et al., *Acta Biomater.* **2013**, *9*, 6268.

[11] Y. Wu, J. Geis-Gerstorfer, L. Scheideler, F. Rupp, *Biofouling* **2016**, *32*, 583.

[12] V. Milleret, S. Tugulu, F. Schlottig, H. Hall, *Eur. Cells Mater.* **2011**, *21*, 430-44; discussion 444.

[13] J. C. Tiller, *Proc. Natl. Acad. Sci. U. S. A.* **2001**, 5981.

[14] R. E. Holmlin, X. Chen, R. G. Chapman, S. Takayama, G. M. Whitesides, *Langmuir* **2001**, *17*, 2841.

[15] A. K. Muszanska, E. T. J. Rochford, A. Gruszka, A. A. Bastian, H. J. Busscher, W. Norde, H. C. van der Mei, A. Herrmann, *Biomacromolecules* **2014**, *15*, 2019.

[16] P. T. Phuong, S. Oliver, J. He, E. H. H. Wong, R. T. Mathers, C. Boyer, *Biomacromolecules* **2020**, *21*, 5241.

[17] W. Hartleb, J. S. Saar, P. Zou, K. Lienkamp, *Macromol. Chem. Phys.* **2016**, *217*, 225.

[18] a) Eduard Simon, *Ann. Pharm.* **1839**, *31*, 265; b) P. Nesvadba in *Encyclopedia of Radicals in Chemistry, Biology and Materials* (Eds.: C. Chatgilialoglu, A. Studer), John Wiley & Sons, Ltd, Chichester, UK, **2012**, p. 2163.

[19] W. A. Braunecker, K. Matyjaszewski, *Prog. Polym. Sci.* **2007**, *32*, 93.

[20] M. Szwarc, *Nature* **1956**, *178*, 1168.

[21] H. Fischer, *Chem. Rev.* **2001**, *101*, 3581.

[22] S. Perrier, *Macromolecules* **2017**, *50*, 7433.

[23] J. Chiefari, Y. K. Chong, F. Ercole, J. Krstina, J. Jeffery, T. P. T. Le, R. T. A. Mayadunne, G. F. Meijs, C. L. Moad, G. Moad et al., *Macromolecules* **1998**, *31*, 5559.

[24] a) H.-G. Elias, *Makromoleküle*, Wiley-VCH, Weinheim, Chichester, **1999-2003**; b) A. H. E. Müller, K. Matyjaszewski, *Controlled and living polymerizations*. *Methods and materials*, Wiley-VCH, Weinheim, **2009**.

[25] G. Moad, E. Rizzardo, S. H. Thang, *Aust. J. Chem.* **2012**, *65*, 985.

[26] C. Barner-Kowollik, *Handbook of RAFT Polymerization*, John Wiley & Sons, **2008**.

[27] A. B. Lowe, C. L. McCormick, *Prog. Polym. Sci.* **2007**, *32*, 283.

[28] G. Moad, E. Rizzardo, S. H. Thang, *Polym. Int.* **2011**, *60*, 9.

[29] M. L. Allegrezza, D. Konkolewicz, *ACS Macro Lett.* **2021**, *10*, 433.

[30] R. N. Carmean, T. E. Becker, M. B. Sims, B. S. Sumerlin, *Chem* **2017**, *2*, 93.

[31] a) A. J. Gormley, J. Yeow, G. Ng, Ó. Conway, C. Boyer, R. Chapman, *Angew. Chem. Int. Ed.* **2018**, *57*, 1557; b) N. G. Engelis, A. Anastasaki, G. Nurumbetov, N. P. Truong, V. Nikolaou, A. Shegiwal, M. R. Whittaker, T. P. Davis, D. M. Haddleton, *Nat. Chem* **2017**, *9*, 171.

[32] a) M. D. Nothling, Q. Fu, A. Reyhani, S. Allison-Logan, K. Jung, J. Zhu, M. Kamigaito, C. Boyer, G. G. Qiao, *Adv. Sci.* **2020**, *7*, 2001656; b) K. Parkatzidis, H. S. Wang, N. P. Truong, A. Anastasaki, *Chem* **2020**, *6*, 1575.

[33] M. Zasloff, *Nature* **2002**, *415*, 389.

[34] J. A. F. Corrêa, A. G. Evangelista, T. d. M. Nazareth, F. B. Luciano, *Materialia* **2019**, *8*, 100494.

[35] R. Bals, *Med. Klin.* **2000**, *95*, 496.

[36] K. Lienkamp, K.-N. Kumar, A. Som, K. Nüsslein, G. N. Tew, *Chem* **2009**, *15*, 11710.

[37] K. A. Brogden, *Nat. Rev. Microbiol* **2005**, *3*, 238.

[38] H.-S. Joo, C.-I. Fu, M. Otto, *Philos. Trans. R. Soc. Lond., B, Biol. Sci.* **2016**, *371*.

[39] A. K. Marr, W. J. Gooderham, R. E. Hancock, *Curr. Opin. Pharmacol* **2006**, *6*, 468.

[40] A. Kanazawa, T. Ikeda, T. Endo, *J. Polym. Sci. Part A: Polym. Chem.* **1993**, *31*, 335.

[41] I. Sovadinova, E. F. Palermo, M. Urban, P. Mpiga, G. A. Caputo, K. Kuroda, *Polymers* **2011**, *3*, 1512.

[42] G. J. Gabriel, A. E. Madkour, J. M. Dabkowski, C. F. Nelson, K. Nüsslein, G. N. Tew, *Biomacromolecules* **2008**, *9*, 2980.

[43] N. Kawabata, M. Nishiguchi, *Appl. Environ. Microbiol.* **1988**, *54*, 2532.

[44] C. H. Kim, J. W. Choi, H. J. Chun, K. S. Choi, *Polym. Bull.* **1997**, *38*, 387.

[45] P. R. Judzewitsch, T.-K. Nguyen, S. Shanmugam, E. H. H. Wong, C. Boyer, *Angew. Chem.* **2018**, *130*, 4649.

[46] B. P. Mowery, A. H. Lindner, B. Weisblum, S. S. Stahl, S. H. Gellman, *J. Am. Chem. Soc.* **2009**, *131*, 9735.

[47] W. Chin, C. Yang, V. W. L. Ng, Y. Huang, J. Cheng, Y. W. Tong, D. J. Coady, W. Fan, J. L. Hedrick, Y. Y. Yang, *Macromolecules* **2013**, *46*, 8797.

[48] K. Kuroda, W. F. DeGrado, *J. Am. Chem. Soc.* **2005**, *127*, 4128.

[49] E. F. Palermo, K. Kuroda, *Appl. Microbiol. Biotechnol.* **2010**, *87*, 1605.

[50] C. Ergene, K. Yasuhara, E. F. Palermo, *Polym. Chem.* **2018**, *9*, 2407.

[51] P. Pham, S. Oliver, E. H. H. Wong, C. Boyer, *Polym. Chem.* **2021**, *12*, 5689.

[52] Z. Si, W. Zheng, D. Prananty, J. Li, C. H. Koh, E.-T. Kang, K. Pethe, M. B. Chan-Park, *Chem. Sci.* **2022**, *13*, 345.

[53] R. Namivandi-Zangeneh, Z. Sadrearhami, D. Dutta, M. Willcox, E. H. H. Wong, C. Boyer, *ACS Infect. Dis.* **2019**, *5*, 1357.

[54] J. Lin, J. C. Tiller, S. B. Lee, K. Lewis, A. M. Klibanov, *Biotechnol. Lett.* **2002**, *24*, 801.

[55] W. Heuer, A. Winkel, P. Kohorst, A. Lutzke, C. Pfaffenroth, H. Menzel, F.-W. Bach, J. Volk, G. Leyhausen, M. Stiesch, *Adv. Eng. Mater.* **2010**, *12*, B609-B617.

[56] a) L. Ringenberg, A. Winkel, O. Kufelt, P. Behrens, M. Stiesch, W. Heuer, *Int. J. Dent.* **2011**, *2011*, 859140; b) T. Calliess, I. Bartsch, M. Haupt, M. Reebmann, M. Schwarze, M. Stiesch, C. Pfaffenroth, M. Sluszniak, W. Dempwolf, H. Menzel et al., *Mater. Sci. Eng. C Mater. Biol. Appl.* **2016**, *61*, 712; c) C. Peng, A. Vishwakarma, S. Mankoci, H. A. Barton, A. Joy, *Biomacromolecules* **2019**, *20*, 1675.

[57] G. Ye, J. Lee, F. Perreault, M. Elimelech, *ACS Appl. Mater. Interfaces* **2015**, *7*, 23069.

[58] E. K. Riga, M. Vöhringer, V. T. Widyaya, K. Lienkamp, *Macromol. Rapid Commun.* **2017**, *38*.

[59] A. E. Madkour, J. M. Dabkowski, K. Nusslein, G. N. Tew, *Langmuir* **2009**, *25*, 1060.

[60] K.-T. Huang, K. Ishihara, C.-J. Huang, *Biomacromolecules* **2019**, *20*, 3524.

[61] L. A. T. W. Asri, M. Crismaru, S. Roest, Y. Chen, O. Ivashenko, P. Rudolf, J. C. Tiller, H. C. van der Mei, T. J. A. Loontjens, H. J. Busscher, *Adv. Funct. Mater.* **2014**, *24*, 346.

[62] F. Siedenbiedel, J. C. Tiller, *Polymers* **2012**, *4*, 46.

[63] R. Kügler, O. Bouloussa, F. Rondelez, *Microbiology* **2005**, *151*, 1341.

[64] L. Hall-Stoodley, J. W. Costerton, P. Stoodley, *Nat. Rev. Microbiol* **2004**, *2*, 95.

[65] A. M. Bieser, Y. Thomann, J. C. Tiller, *Macromol. Biosci.* **2011**, *11*, 111.

[66] S. Jiang, Z. Cao, *Adv. Mater.* **2010**, *22*, 920.

[67] a) Y. He, Y. Chang, J. C. Hower, J. Zheng, S. Chen, S. Jiang, *Phys. Chem. Chem. Phys.* **2008**, *10*, 5539; b) E. Ostuni, R. G. Chapman, R. E. Holmlin, S. Takayama, G. M. Whitesides, *Langmuir* **2001**, *17*, 5605.

[68] S. Kudaibergenov, W. Jaeger, A. Laschewsky in *Advances in Polymer Science*, Springer Berlin Heidelberg, Berlin, Heidelberg, **2006**, pp. 157–224.

[69] A. Laschewsky, *Polymers* **2014**, *6*, 1544.

[70] L. D. Blackman, P. A. Gunatillake, P. Cass, K. E. S. Locock, *Chem. Soc. Rev.* **2019**, *48*, 757.

[71] a) S. Paschke, K. Lienkamp, *ACS Appl. Polym. Mater.* **2020**, *2*, 129; b) Y. Zou, Y. Zhang, Q. Yu, H. Chen, *J. Mater. Sci. Technol.* **2021**, *70*, 24; c) E. Schönemann, A. Laschewsky, E. Wischerhoff, J. Koc, A. Rosenhahn, *Polymers* **2019**, *11*.

[72] a) M. Ezzat, C.-J. Huang, *RSC Adv.* **2016**, *6*, 61695; b) A. C. G. Weiss, H. G. Kelly, M. Faria, Q. A. Besford, A. K. Wheatley, C.-S. Ang, E. J. Crampin, F. Caruso, S. J. Kent, *ACS nano* **2019**, *13*, 4980; c) L. Schardt, A. Martínez Guajardo, J. Koc, J. L. Clarke, J. A. Finlay, A. S. Clare, H. Gardner, G. W. Swain, K. Hunsucker, A. Laschewsky et al., *Macromol. Rapid Commun.* **2022**, *43*, e2100589.

[73] P. Zou, W. Hartleb, K. Lienkamp, *J. Mater. Chem.* **2012**, *22*, 19579.

[74] S. Paschke, R. Prediger, V. Lavaux, A. Eickenscheidt, K. Lienkamp, *Macromol. Rapid Commun.* **2021**, *42*, e2100051.

[75] G. Cheng, H. Xue, Z. Zhang, S. Chen, S. Jiang, *Angew. Chem. Int. Ed.* **2008**, *47*, 8831.

[76] Q. Liu, L. Liu, *Langmuir* **2019**, *35*, 1450.

[77] M. Menzel, W.-L. Chen, K. Simancas, H. Xu, O. Prucker, C. K. Ober, J. Rühe, *J. Polym. Sci. Part A: Polym. Chem.* **2019**, *57*, 1283.

[78] M. Antonietti, A. Briel, S. Förster, *J. Chem. Phys.* **1996**, *105*, 7795.

[79] G. S. Georgiev, E. B. Kamenska, E. D. Vassileva, I. P. Kamenova, V. T. Georgieva, S. B. Iliev, I. A. Ivanov, *Biomacromolecules* **2006**, *7*, 1329.

[80] P. Mary, D. D. Bendejacq, M.-P. Labeau, P. Dupuis, *J. Phys. Chem. B* **2007**, *111*, 7767.

[81] J. Seuring, S. Agarwal, *Macromol. Rapid Commun.* **2012**, *33*, 1898.

[82] M. S. Ganewatta, C. Tang, *Polymer* **2015**, *63*, A1-A29.

[83] U. Hersel, C. Dahmen, H. Kessler, *Biomaterials* **2003**, *24*, 4385.

[84] H. J. Busscher, H. C. van der Mei, G. Subbiahdoss, P. C. Jutte, J. J. A. M. van den Dungen, S. A. J. Zaat, M. J. Schultz, D. W. Grainger, *Sci. Transl. Med.* **2012**, *4*, 153rv10.

[85] R. G. LeBaron, K. A. Athanasiou, *Tissue Eng.* **2000**, *6*, 85.

[86] a) M. D. Pierschbacher, E. Ruoslahti, *Nature* **1984**, *309*, 30; b) S. K. Schmitt, A. W. Xie, R. M. Ghassemi, D. J. Trebatoski, W. L. Murphy, P. Gopalan, *Adv. Healthc. Mater.* **2015**, *4*, 1555.

[87] H. Choi, E. Yildirim, A. Schulte, H. Schönherr, *ACS Appl. Polym. Mater.* **2022**, *4*, 755.

[88] a) D. Delforge, B. Gillon, M. Art, J. Dewelle, M. Raes, J. Remacle, *Lett. Pept. Sci.* **1998**, *5*, 87; b) W. J. Kao, J. A. Hubbell, *Biotechnol. Bioeng.* **1998**, *59*, 2.

[89] A. R. Kuzmyn, A. de los Santos Pereira, O. Pop-Georgievski, M. Bruns, E. Brynda, C. Rodriguez-Emmenegger, *Polym. Chem.* **2014**, *5*, 4124.

[90] Q. Yu, Y. Zhang, H. Wang, J. Brash, H. Chen, *Acta Biomater.* **2011**, *7*, 1550.

[91] Y. Wang, G. Subbiahdoss, J. Swartjes, H. C. van der Mei, H. J. Busscher, M. Libera, *Adv. Funct. Mater.* **2011**, *21*, 3916.

[92] E. J. Tocce, A. H. Broderick, K. C. Murphy, S. J. Liliensiek, C. J. Murphy, D. M. Lynn, P. F. Nealey, *J. Biomed. Mater. Res. A* **2012**, *100*, 84.

[93] S. T. Milner, *Science* **1991**, *251*, 905.

[94] C. Ligoure, L. Leibler, *J. Phys. France* **1990**, *51*, 1313.

[95] W. J. Brittain, S. Minko, *J. Polym. Sci. Part A: Polym. Chem.* **2007**, *45*, 3505.

[96] D. Antonioli, R. Chiarcos, V. Gianotti, M. Terragno, M. Laus, G. Munaò, G. Milano, A. de Nicola, M. Perego, *Polym. Chem.* **2021**, *12*, 6538.

[97] T. Wu, K. Efimenko, J. Genzer, *J. Am. Chem. Soc.* **2002**, *124*, 9394.

[98] M. van der Waarden, *J. Colloid Sci.* **1950**, *5*, 317.

[99] D. Kuckling, K. Moosmann, J. E. S. Schier, A. Britze, *Colloid. Polym. Sci.* **2013**, *291*, 1429.

[100] Q. Wei, X. Pei, J. Hao, M. Cai, F. Zhou, W. Liu, *Adv. Mater. Interfaces* **2014**, *1*, 1400035.

[101] X. Zhang, L. Liu, W. Peng, X. Dong, Y. Gu, Z. Ma, D. Gan, P. Liu, *J. Mater. Chem. B* **2021**, *9*, 4169.

[102] L. Huang, L. Zhang, S. Xiao, Y. Yang, F. Chen, P. Fan, Z. Zhao, M. Zhong, J. Yang, *Chem. Eng. J.* **2018**, *333*, 1.

[103] S. Xiao, B. Ren, L. Huang, M. Shen, Y. Zhang, M. Zhong, J. Yang, J. Zheng, *Curr. Opin. Chem. Eng.* **2018**, *19*, 86.

[104] a) H. Yim, M. S. Kent, S. Mendez, S. S. Balamurugan, S. Balamurugan, G. P. Lopez, S. Satija, *Macromolecules* **2004**, *37*, 1994; b) K. N. Plunkett, X. Zhu, J. S. Moore, D. E. Leckband, *Langmuir* **2006**, *22*, 4259; c) I. N. Haugan, M. J. Maher, A. B. Chang, T.-P. Lin, R. H. Grubbs, M. A. Hillmyer, F. S. Bates, *ACS Macro Lett.* **2018**, *7*, 525.

[105] a) O. Prucker, M. Schimmel, G. Tovar, W. Knoll, J. Rühe, *Adv. Mater.* **1998**, *10*, 1073; b) O. Prucker, J. Rühe, *Macromolecules* **1998**, *31*, 592; c) M. Tirrell, S. Patel, G. Hadziioannou,

Proc. Natl. Acad. Sci. U.S.A. **1987**, *84*, 4725; d) L. K. Ista, S. Mendez, V. H. Pérez-Luna, G. P. López, *Langmuir* **2001**, *17*, 2552.

[106] W. J. Brittain, S. G. Boyes, A. M. Granville, M. Baum, B. K. Mirous, B. Akgun, B. Zhao, C. Blickle, M. D. Foster in *Advances in Polymer Science* (Ed.: R. Jordan), Springer-Verlag, Berlin/Heidelberg, **2006**, pp. 125–147.

[107] a) M. Motornov, R. Sheparovych, R. Lupitskyy, E. MacWilliams, O. Hoy, I. Luzinov, S. Minko, *Adv. Funct. Mater.* **2007**, *17*, 2307; b) J. Draper, I. Luzinov, S. Minko, I. Tokarev, M. Stamm, *Langmuir* **2004**, *20*, 4064.

[108] K. Sparnacci, D. Antonioli, V. Gianotti, M. Laus, F. F. Lupi, T. J. Giammaria, G. Seguini, M. Perego, *ACS Appl. Mater. Interfaces* **2015**, *7*, 10944.

[109] F. Zhou, Z. Zheng, B. Yu, W. Liu, W. T. S. Huck, *J. Am. Chem. Soc.* **2006**, *128*, 16253.

[110] B. Liang, E. Jia, X. Yuan, G. Zhang, Z. Su, *Chem. Eng. J.* **2020**, *401*, 126114.

[111] K. Babu, R. Dhamodharan, *Nanoscale Res. Lett.* **2008**, *3*, 9093.

[112] L. Liu, W. Peng, X. Zhang, J. Peng, P. Liu, J. Shen, *J. Mater. Sci. Technol.* **2021**, *62*, 96.

[113] W. Gao, L. Dickinson, C. Grozinger, F. G. Morin, L. Reven, *Langmuir* **1996**, *12*, 6429.

[114] a) S. Marcinko, A. Y. Fadeev, *Langmuir* **2004**, *20*, 2270; b) G. Guerrero, J. G. Alauzun, M. Granier, D. Laurencin, P. H. Mutin, *Dalton Trans.* **2013**, *42*, 12569.

[115] B. M. Silverman, K. A. Wieghaus, J. Schwartz, *Langmuir* **2005**, *21*, 225.

[116] P. H. Mutin, G. Guerrero, A. Vioux, *J. Mater. Chem.* **2005**, *15*, 3761.

[117] a) P. Thissen, M. Valtiner, G. Grundmeier, *Langmuir* **2010**, *26*, 156; b) S. A. Paniagua, A. J. Giordano, O.'N. L. Smith, S. Barlow, H. Li, N. R. Armstrong, J. E. Pemberton, J.-L. Brédas, D. Ginger, S. R. Marder, *Chem. Rev.* **2016**, *116*, 7117; c) R. Luschtinetz, A. F. Oliveira, J. Frenzel, J.-O. Joswig, G. Seifert, H. A. Duarte, *Surf. Sci.* **2008**, *602*, 1347.

[118] a) A. K. Bhattacharya, G. Thyagarajan, *Chem. Rev.* **1981**, *81*, 415; b) P. Savignac, B. Iorga, *Modern phosphonate chemistry*, CRC Press, Boca Raton, **2003**.

[119] G. Guerrero, P. H. Mutin, A. Vioux, *Chem. Mater.* **2001**, *13*, 4367.

[120] Y. Chen, W. Liu, C. Ye, L. Yu, S. Qi, *Mater. Res. Bull.* **2001**, *36*, 2605.

[121] N. Adden, L. J. Gamble, D. G. Castner, A. Hoffmann, G. Gross, H. Menzel, *Biomacromolecules* **2006**, *7*, 2552.

[122] C. Tudisco, V. Oliveri, M. Cantarella, G. Vecchio, G. G. Condorelli, *Eur. J. Inorg. Chem.* **2012**, *2012*, 5323.

[123] R. Methling, O. Dückmann, F. Simon, C. Wolf-Brandstetter, D. Kuckling, *Macromol. Mater. Eng.* **2023**, accepted.

[124] A. Britze, K. Moosmann, E. Jähne, H.-J. Adler, D. Kuckling, *Macromol. Rapid Commun.* **2006**, *27*, 1906.

[125] B. Boutevin, Y. Hervaud, A. Boulahna, E. M. E. Hadrami, *Polym. Int.* **2002**, *51*, 450.

[126] M. L. Schilling, H. E. Katz, F. M. Houlihan, J. M. Kometani, S. M. Stein, O. Nalamasu, *Macromolecules* **1995**, *28*, 110.

[127] B. Boutevin, B. Hamoui, J.-P. Parisi, B. Améduri, *Eur. Polym. J.* **1996**, *32*, 159.

[128] I. Blidi, O. Coutelier, M. Destarac, *J. Polym. Sci. Part A: Polym. Chem.* **2014**, *52*, 2616.

[129] a) C. Barner-Kowollik, M. Buback, B. Charleux, M. L. Coote, M. Drache, T. Fukuda, A. Goto, B. Klumperman, A. B. Lowe, J. B. Mcleary et al., *J. Polym. Sci. Part A: Polym. Chem.* **2006**, *44*, 5809; b) K. Ponnusamy, R. P. Babu, R. Dhamodharan, *J. Polym. Sci. Part A: Polym. Chem.* **2013**, *51*, 1066.

[130] S. R. Gondi, A. P. Vogt, B. S. Sumerlin, *Macromolecules* **2007**, *40*, 474.

[131] V. Sambhy, B. R. Peterson, A. Sen, *Angew. Chem. Int. Ed.* **2008**, *47*, 1250.

[132] J. Salamone, B. Snider, W. Fitch, *Macromolecules* **1970**, *3*, 707.

[133] a) M. Hernández-Orta, E. Pérez, L. E. Cruz-Barba, M. A. Sánchez-Castillo, *J. Mater. Sci. (Journal of Materials Science)* **2018**, *53*, 8766; b) K. Mavronasou, A. Zamboulis, P. Klonos, A. Kyritsis, D. N. Bikiaris, R. Papadakis, I. Deligkiozi, *Polymers* **2022**, *14*.

[134] E. J. Cornel, S. van Meurs, T. Smith, P. S. O'Hora, S. P. Armes, *J. Am. Chem. Soc.* **2018**, *140*, 12980.

[135] a) S. Rauch, K.-J. Eichhorn, D. Kuckling, M. Stamm, P. Uhlmann, *Adv. Funct. Mater.* **2013**, *23*, 5675; b) M. K. Corbierre, N. S. Cameron, R. B. Lennox, *Langmuir* **2004**, *20*, 2867.

[136] M. Laus, R. Chiarcos, V. Gianotti, D. Antonioli, K. Sparnacci, G. Munaò, G. Milano, A. de Nicola, M. Perego, *Macromolecules* **2021**, *54*, 499.

[137] a) L. Michalek, K. Mundsinger, C. Barner-Kowollik, L. Barner, *Polym. Chem.* **2019**, *10*, 54; b) J. Glasing, J. Bouchard, P. G. Jessop, P. Champagne, M. F. Cunningham, *Polym. Chem.* **2017**, *8*, 6000.

[138] N. Horn, M. Kreiter, *Plasmonics* **2010**, *5*, 331.

[139] B. P. Tripathi, P. Das, F. Simon, M. Stamm, *Eur. Polym. J.* **2018**, *99*, 80.

[140] a) S. Roessler, R. Zimmermann, D. Scharnweber, C. Werner, H. Worch, *Colloids Surf. B: Biointerfaces* **2002**, *26*, 387; b) K. Cai, M. Frant, J. Bossert, G. Hildebrand, K. Liefeith, K. D. Jandt, *Colloids Surf. B: Biointerfaces* **2006**, *50*, 1.

[141] B. Łosiewicz, P. Osak, J. Maszybrocka, J. Kubisztal, S. Stach, *Materials* **2020**, *13*, 4154.

[142] B. Feng, J. Y. Chen, S. K. Qi, L. He, J. Z. Zhao, X. D. Zhang, *J. Mater. Sci. Mater. Med.* **2002**, *13*, 457.

[143] F. Kaiser, D. Scharnweber, S. Bierbaum, C. Wolf-Brandstetter, *Bioelectrochemistry* **2020**, *133*, 107485.

[144] M. Waßmann, A. Winkel, K. Haak, W. Dempwolf, M. Stiesch, H. Menzel, *J. Biomater. Sci. Polym. Ed.* **2016**, *27*, 1507.

[145] a) K. Suga, M. Murakami, S. Nakayama, K. Watanabe, S. Yamada, T. Tsuji, D. Nagao, *ACS Appl. Bio Mater.* **2022**, *5*, 2202; b) S. Kliewer, S. G. Wicha, A. Bröker, T. Naundorf, T. Catmadim, E. K. Oellingrath, M. Rohnke, W. R. Streit, C. Vollstedt, H. Kipphardt et al., *Colloids Surf. B: Biointerfaces* **2020**, *186*, 110679.

[146] a) Y. U. D. Semchikov, *Macromol. Symp.* **1996**, *111*, 317; b) E. V. Chernikova, S. D. Zaitsev, A. V. Plutalova, K. O. Mineeva, O. S. Zotova, D. V. Vishnevetsky, *RSC Adv.* **2018**, *8*, 14300.

[147] Y. Oda, S. Kanaoka, T. Sato, S. Aoshima, K. Kuroda, *Biomacromolecules* **2011**, *12*, 3581.

[148] J. Li, X. Yu, A. Herberg, D. Kuckling, *Macromol. Rapid Commun.* **2019**, *40*, e1800674.

[149] J. Li, C. Ji, X. Yu, M. Yin, D. Kuckling, *Macromol. Rapid Commun.* **2019**, *40*, e1900189.

[150] a) V. Vassileva, E. M. Georgiev, K. Troev, D. M. Roundhill, *Phosphorus Sulfur Silicon Relat. Elem.* **1994**, *92*, 101; b) D. E. Bryant, C. Kilner, T. P. Kee, *Inorganica Chim. Acta* **2009**, *362*, 614.

[151] a) D. Scharnweber, S. Bierbaum, C. Wolf-Brandstetter, *FEBS Lett.* **2018**, *592*, 2181; b) P. H. E. Hamming, J. Huskens, *ACS Appl. Mater. Interfaces* **2021**, *13*, 58114; c) W. L. Hurley, E. Finkelstein, B. D. Holst, *J. Immunol. Methods* **1985**, *85*, 195.

[152] a) M. H. Heggeness, J. F. Ash, *J. Cell Biol.* **1977**, *73*, 783; b) D. A. Noppl-Simson, D. Needham, *Biophys. J.* **1996**, *70*, 1391.

[153] N. Zhao, Z. Yang, B. Li, J. Meng, Z. Shi, P. Li, S. Fu, *Int. J. Nanomedicine* **2016**, *11*, 5595.

[154] E. Jäger, J. Humajová, Y. Dölen, J. Kučka, A. Jäger, R. Konefał, J. Pankrác, E. Pavlova, T. Heizer, L. Šefc et al., *Adv. Healthc. Mater.* **2021**, *10*, e2100304.

[155] Y. Wang, J. Wu, D. Zhang, F. Chen, P. Fan, M. Zhong, S. Xiao, Y. Chang, X. Gong, J. Yang et al., *J. Mater. Chem. B* **2019**, *7*, 5762.

[156] R. Balzarotti, C. Cristiani, L. F. Francis, *Surf. Coat. Technol.* **2017**, *330*, 1.

[157] a) V. M. Monroy Soto, J. C. Galin, *Polymer* **1984**, *25*, 121; b) A. Venault, M.-W. Lai, J.-F. Jhong, C.-C. Yeh, L.-C. Yeh, Y. Chang, *ACS Appl. Mater. Interfaces* **2018**, *10*, 17771.

[158] D. R. Bloch, *Polymer handbook*, Wiley-Interscience, Hoboken, N.J., **1999**.

[159] a) N. S. Andreeva, M. N. James, *Adv. Exp. Med. Biol.* **1991**, *306*, 39; b) H. S. Sundaram, J.-R. Ella-Menye, N. D. Brault, Q. Shao, S. Jiang, *Chem. Sci.* **2014**, *5*, 200.

[160] J. Vörös, *Biophys. J.* **2004**, *87*, 553.

[161] M. van de Lagemaat, A. Grotenhuis, B. van de Belt-Gritter, S. Roest, T. J. A. Loontjens, H. J. Busscher, H. C. van der Mei, Y. Ren, *Acta Biomater.* **2017**, *59*, 139.

[162] D. J. Phillips, J. Harrison, S.-J. Richards, D. E. Mitchell, E. Tichauer, A. T. M. Hubbard, C. Guy, I. Hands-Portman, E. Fullam, M. I. Gibson, *Biomacromolecules* **2017**, *18*, 1592.

[163] D. A. Shirley, *Phys. Rev. B* **1972**, *5*, 4709.

[164] E. Yildirim, H. Choi, A. Schulte, H. Schönherr, *Eur. Polym. J.* **2021**, *148*, 110370.

8 Appendix

8.1 Antibacterial polymer brushes on titanium via "grafting to"

Table 8.1: SPR simulation parameters after coating of P(VPPr$_{65}$-b-PA$_{16}$).

layer	thickness /nm	EpsX-real	EpsX-imag
LaSFN9	0	3.408	0
Cr	1	-6.3	10
Au	44.5	-12.049	1.269
TiO_2	3.7	3.33	0.34
Polymer	9.3	2.06	0
Water	0	1.773	0

Table 8.2: SPR simulation parameters after exposure of substrates coated with P(VPPr$_{65}$-b-PA$_{16}$) to aqueous NaOH.

layer	thickness /nm	EpsX-real	EpsX-imag
LaSFN9	0	3.408	0
Cr	1	-6.3	10
Au	44.5	-12.049	1.269
TiO_2	3.7	3.33	0.34
Polymer	4.9	2.06	0
Water	0	1.773	0

Determination of bacteria surviving in solution close to the surface (planktonic bacteria):

Samples were prepared by dropping 25 µl of each polymer dissolved in methanol (2 mM) on each titanium disc, covering it completely and dried until solvent was evaporated completely. At such prepared samples more than 80 % of immobilized polymer amounts are redissolved in water-based solvents within 5 min of contact.

Onto coated samples lying in a 48 well plate (for suspension culture, Nunc) 50 µl of a bacterial solution containing 10^7 CFU/mL was dropped, while all outer wells and spaces between wells were filled with sterile water to generate an atmosphere saturated with water vapor. After 2 h incubation time 450 µl of fresh LB was added to each well and the plates were vigorously

shaken for 5 min. Next, 300 µl of each original suspension and serial dilutions in LB medium were transferred into 96-cell culture plates (TPP) for quantification of CFU equivalents using the proliferation assay.

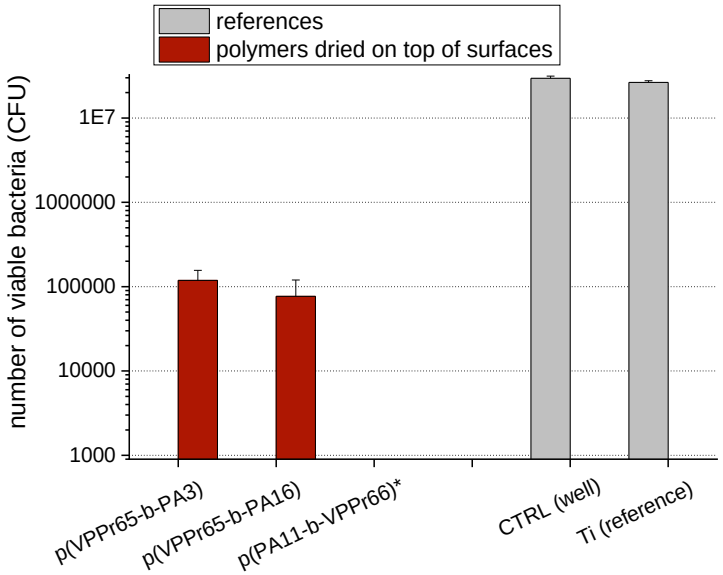

*Figure 8.1: Numbers of viable bacteria surviving in close vicinity to the samples surface coated with 50 nmol of each polymer dried on top of the samples (without washing): Antimicrobial activity of the studied compounds was much higher under these test conditions than for adsorbed polymers. *No surviving bacteria were detected for P(PA_{11}-b-$VPPr_{66}$).*

Light microscopy of human gingival cells cultured with soluble polymers diluted in cell culture medium

Cells were seeded at a density of 5000 cells per well and left for 2 h to settle down. Then medium was exchanged and a fresh solution containing 2 mM solution of each polymer dissolved in methanol and further diluted 1:100 in cell culture medium was added to each well. After 24 h the treated cells as well as control, incubated with medium containing the same extent of methanol, were analysed with a cell culture microscope (magnification 10x).

a **b**

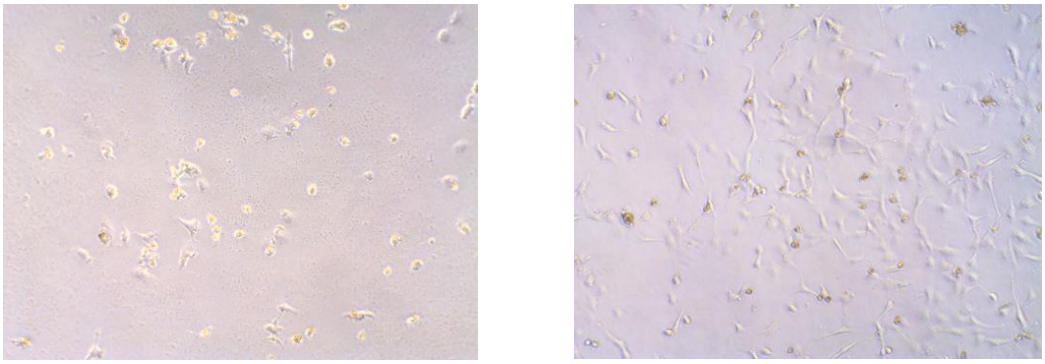

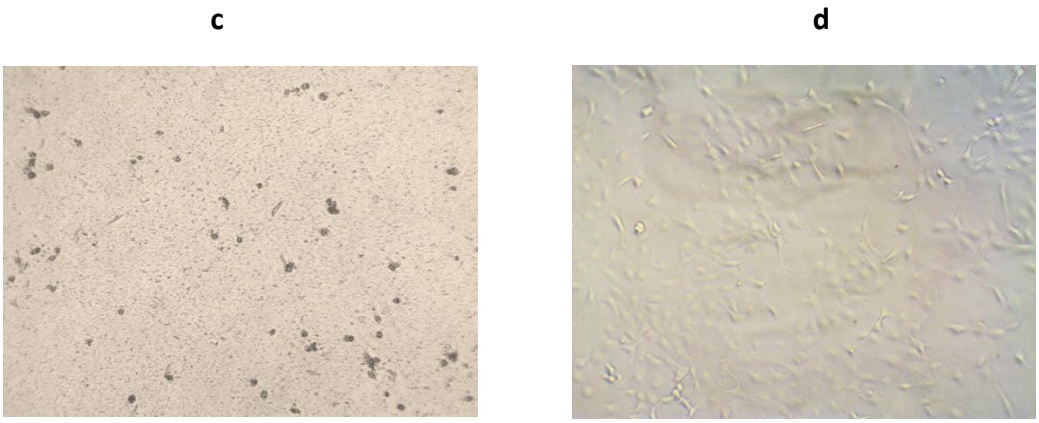

Figure 8.2: Cytotoxicity of dissolved polymers diluted in cell culture medium (1:100) analysed 24 h after exchange of normal medium by medium containing the polymers; a) P(VPPr$_{65}$-b-PA$_3$), b) P(VPPr$_{65}$-b- PA$_{16}$), c) P(PA$_{11}$-b-VPPr$_{66}$), d) control (cell culture medium with similarly added pure methanol).

Table 8.3: Relative elemental compositions of reference and polymer coated samples as derived from XPS survey spectra.

	C 1s	N 1s	O 1s	Al 2s	Si 2p	P 2p	S 2p	Cl 2p	K 2p	Ti 2p3/2	Pb 4f
Reference (Ti)	48.25	1.01	37.26	0.73	0.28	0.38	0.1			11.94	0.05
p(VPPr$_{65}$-b-PA$_3$)	58.84	2.35	29.05	0.33	0.23	1.03	0.25	0.22	0.33	7.35	0.02
p(VPPr$_{65}$-b-PA$_{16}$)	59.73	2.97	27.56	0.53	0.51	1.49	0.33	0.16		6.7	0.02
p(VPPr$_{65}$-b-PA$_{21}$)	64.78	2.93	23.79	0.26	0.42	2.02	0.1	0.21		5.45	0.02
p(PA$_{11}$-b-VPPr$_{66}$)[a]	55.12	2.56	31.05	0.65	0.44	1.31	0.31	0.13		8.41	0.02

Table 8.4: Relative elemental compositions of reference and polymer coated samples as derived from XPS high resolution spectra. Ti reference ΔE = 3.755 eV

Peak	Position BE (eV)	FWHM (eV)	Raw Area (CPS)	Height	Atomic Conc %	Mass Conc %
C 1s *A*	285.000	1.110	9950.6	8176	72.84	72.84
C 1s *B*	286.008	1.242	1629.1	1196	11.92	11.92
C 1s *C*	286.835	1.222	1113.8	831	8.15	8.15
C 1s *D*	288.185	1.242	434.1	319	3.18	3.18

C 1s *E*	289.017	1.242	535.2	393	3.91	3.91
N 1s *L*	400.336	1.617	319.9	180	69.52	69.52
N 1s *M*	402.645	1.179	140.3	108	30.48	30.48
P $2p_{3/2}$ *O*	133.689	1.300	141.1	99	50.00	50.00
P $2p_{1/2}$ *O*	134.529	1.300	70.6	49	50.00	50.00

Titanium with P($VPPr_{65}$-b-PA_3 ΔE = 3.783 eV

Peak	Position BE (eV)	FWHM (eV)	Raw Area (CPS)	Height	Atomic Conc %	Mass Conc %
C 1s *Ph*	284.780	1.036	1803.2	1588	10.19	10.19
C 1s *A*	285.000	1.207	9092.5	6869	51.36	51.36
C 1s *B1*	285.395	1.036	2121.9	1869	11.98	11.98
C 1s *B2*	286.001	1.036	1759.6	1550	9.94	9.94
C 1s *C*	286.747	1.184	2114.1	1628	11.94	11.94
C 1s *D*	288.007	1.184	530.7	409	3.00	3.00
C 1s *E*	289.120	1.184	282.9	218	1.59	1.59
N 1s *L*	399.843	1.656	610.8	336	51.13	51.13
N 1s *M*	402.281	1.126	584.0	473	48.87	48.87
P $2p_{3/2}$ *O*	132.944	1.302	338.7	237	50.00	50.00
P $2p_{1/2}$ *O*	133.784	1.302	169.4	119	50.00	50.00

Titanium with P($VPPr_{65}$-b-PA_{16}) ΔE = 3.867 eV

Peak	Position BE (eV)	FWHM (eV)	Raw Area (CPS)	Height	Atomic Conc %	Mass Conc %
C 1s *Ph*	284.706	1.030	2594.8	2299	14.99	14.99
C 1s *A*	285.000	1.270	6961.8	4995	40.22	40.22
C 1s *B1*	285.327	1.030	2594.8	2299	14.99	14.99

C 1s *B2*	285.923	1.030	2233.6	1979	12.90	12.90
C 1s *C*	286.748	1.184	2505.0	1929	14.47	14.47
C 1s *D*	288.013	1.184	342.4	264	1.98	1.98
C 1s *E*	288.877	1.184	77.1	59	0.45	0.45
N 1s *L*	399.889	1.604	619.5	352	41.85	41.85
N 1s *M*	402.387	1.145	861.2	686	58.15	58.15
P $2p_{3/2}$ *O*	133.226	1.302	487.6	341	50.00	50.00
P $2p_{1/2}$ *O*	134.066	1.302	243.8	171	50.00	50.00

Titanium with P($VPPr_{65}$-b-PA_{21}) ΔE = 3.85 eV

Peak	Position BE (eV)	FWHM (eV)	Raw Area (CPS)	Height	Atomic Conc %	Mass Conc %
C 1s *Ph*	284.611	1.024	3515.5	3128	18.73	18.73
C 1s *A*	285.000	1.294	6620.5	4666	35.27	35.27
C 1s *B1*	285.226	1.024	2536.9	2258	13.51	13.51
C 1s *B2*	285.832	1.024	2205.3	1963	11.74	11.74
C 1s *C*	286.535	1.194	2865.7	2187	15.26	15.26
C 1s *D*	288.238	1.194	804.6	614	4.28	4.28
C 1s *E*	288.601	1.194	227.4	174	1.21	1.21
N 1s *L*	399.712	1.441	590.1	373	39.02	39.02
N 1s *M*	402.334	1.114	922.9	755	60.98	60.98
P $2p_{3/2}$ *O*	133.074	1.302	635.2	445	50.00	50.00
P $2p_{1/2}$ *O*	133.914	1.302	317.6	222	50.00	50.00

Titanium with reversed block order: P(PA_{11}-b-$VPPr_{66}$) ΔE = 3.859 eV

Peak	Position	FWHM	Raw Area	Height	Atomic Conc %	Mass

	BE (eV)	(eV)	(CPS)			Conc %
C 1s *Ph*	284.714	1.037	2173.7	1912	14.27	14.27
C 1s *A*	285.000	1.294	6112.3	4303	40.13	40.13
C 1s *B1*	285.329	1.037	2123.1	1867	13.94	13.94
C 1s *B2*	285.935	1.037	1848.0	1625	12.13	12.13
C 1s *C*	286.746	1.184	2581.8	1988	16.94	16.94
C 1s *D*	288.133	1.184	291.6	225	1.91	1.91
C 1s *E*	288.709	1.184	102.9	79	0.68	0.68
N 1s *L*	399.857	1.540	495.7	294	38.78	38.78
N 1s *M*	402.327	1.134	782.9	629	61.22	61.22
P $2p_{3/2}$ *O*	133.140	1.302	437.4	306	50.00	50.00
P $2p_{1/2}$ *O*	133.980	1.302	218.7	153	50.00	50.00

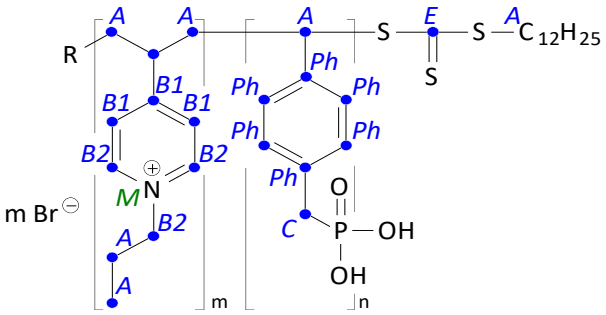

Figure 8.3: Assignment of the component peaks shown in the XPS high-resolution C 1s and N 1s spectra recorded from the polymer-coated titanium samples (Fig. 2) to the structural units of the P(VPPr-b-PA) copolymers. The contributions of carbon atoms assigned with C and E to the C 1s spectrum recorded from the polymer coated samples is marginal. The majority contributing to component peaks C results from the presence of C–O bonds (alcohols, ethers and/or alcohol-sided carbon atoms of carboxylic esters). Photoelectrons from carbonyl carbon atoms of carboxylic ester and/or ketone groups were collected as component peak D, and carbonyl carbon atoms of carboxylic acids were identified as component peak E. Component peak B in the C 1s spectrum of the titanium reference sample summarizes photoelectrons escaped from nitrogen-bonded carbon atoms and carbon atoms in the α-position to carbonyl carbon atoms.

8.2 Salt-responsive polymer brushes with antibacterial and antifouling properties

Table 8.5: SPR simulation parameters for substrates coated with P(VSP_{63}-b-PA_{13}). No significant adlayer of pepsin was detected after the kinetic adsorption measurements.

layer	thickness /nm	EpsX-real	EpsX-imag
LaSFN9	0	3.4036	0
Cr	1	-6.3	10
Au	46.2	-12.0108	1.401
TiO_2	3.7	2.97	0.11
Polymer	4.4	2.519	0
Water	0	1.773	0

Table 8.6: SPR simulation parameters for substrates coated with P(PA_{16}-b-TMA_{101}) and pepsin adlayer after kinetic measurements. Pepsin layer thickness depends on the refractive index chosen (= √(EpsX-real)).

layer	thickness /nm	EpsX-real	EpsX-imag
LaSFN9	0	3.4036	0
Cr	1	-6.3	10
Au	46.8	-11.9987	1.5976
TiO_2	3.7	3.02	0
Polymer	8	2.5	0
Pepsin adlayer	0.6 or 7.2	2.56 or 1.8225	0
Water	0	1,773	0

Table 8.7: SPR simulation parameters for substrates coated with P(VSP_{64}-b-PA_{14}-b-TMA_{64}). No significant adlayer of pepsin was detected after the kinetic adsorption measurements.

layer	thickness /nm	EpsX-real	EpsX-imag
LaSFN9	0	3.4036	0
Cr	1	-6.3	10
Au	45.82	-12.0965	1.526
TiO_2	3.4	3.35	0.268
Polymer	5.1	2.64	0
Water	0	1.783	0

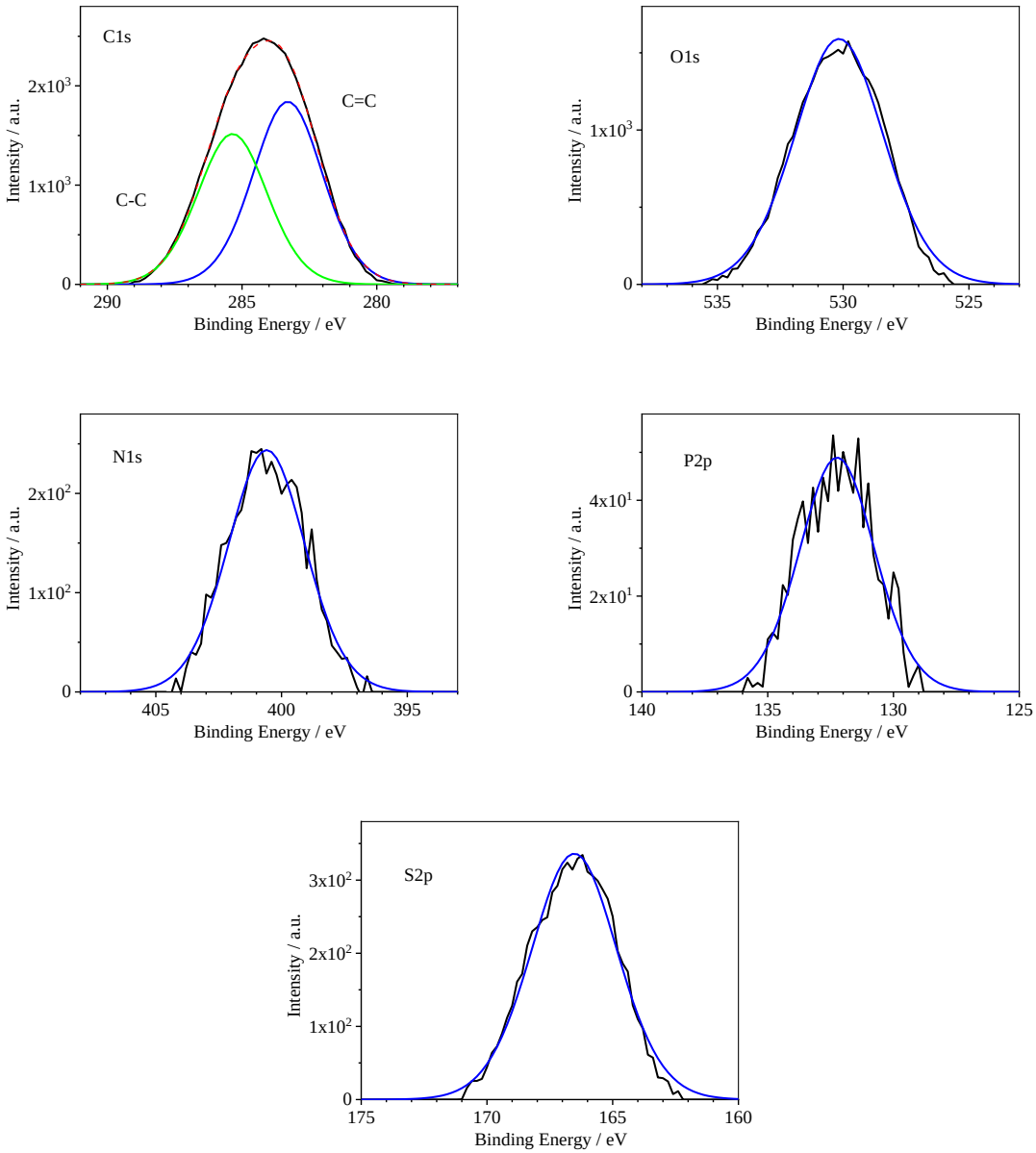

Figure 8.4: High resolution XPS spectra of titanium oxide surfaces coated with P(VSP$_{63}$-b-PA$_{13}$) with measured data in black and peak fitting in color.

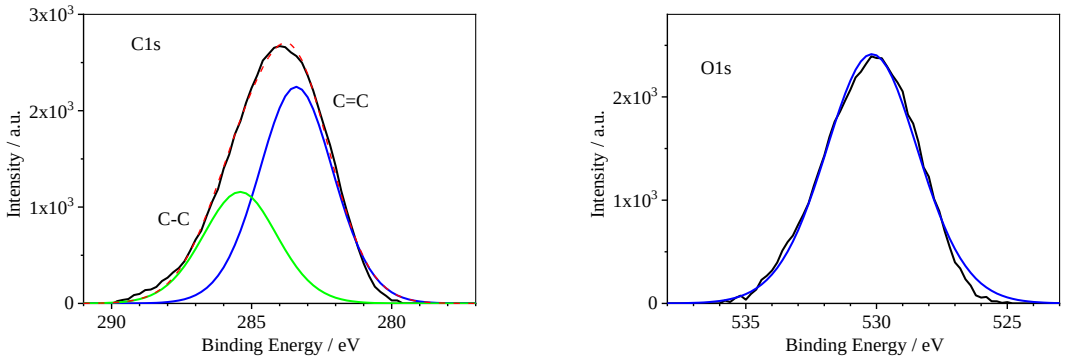

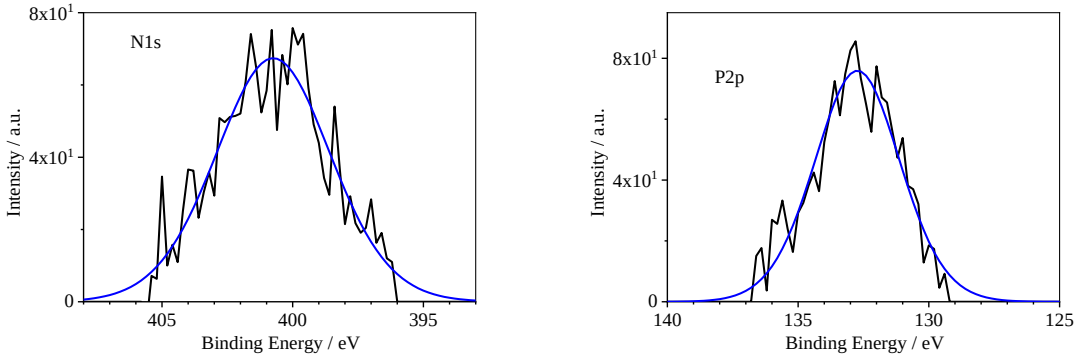

Figure 8.5: High resolution XPS spectra of titanium oxide surfaces coated with P(PA_{16}-b-TMA_{101}) with measured data in black and peak fitting in color.

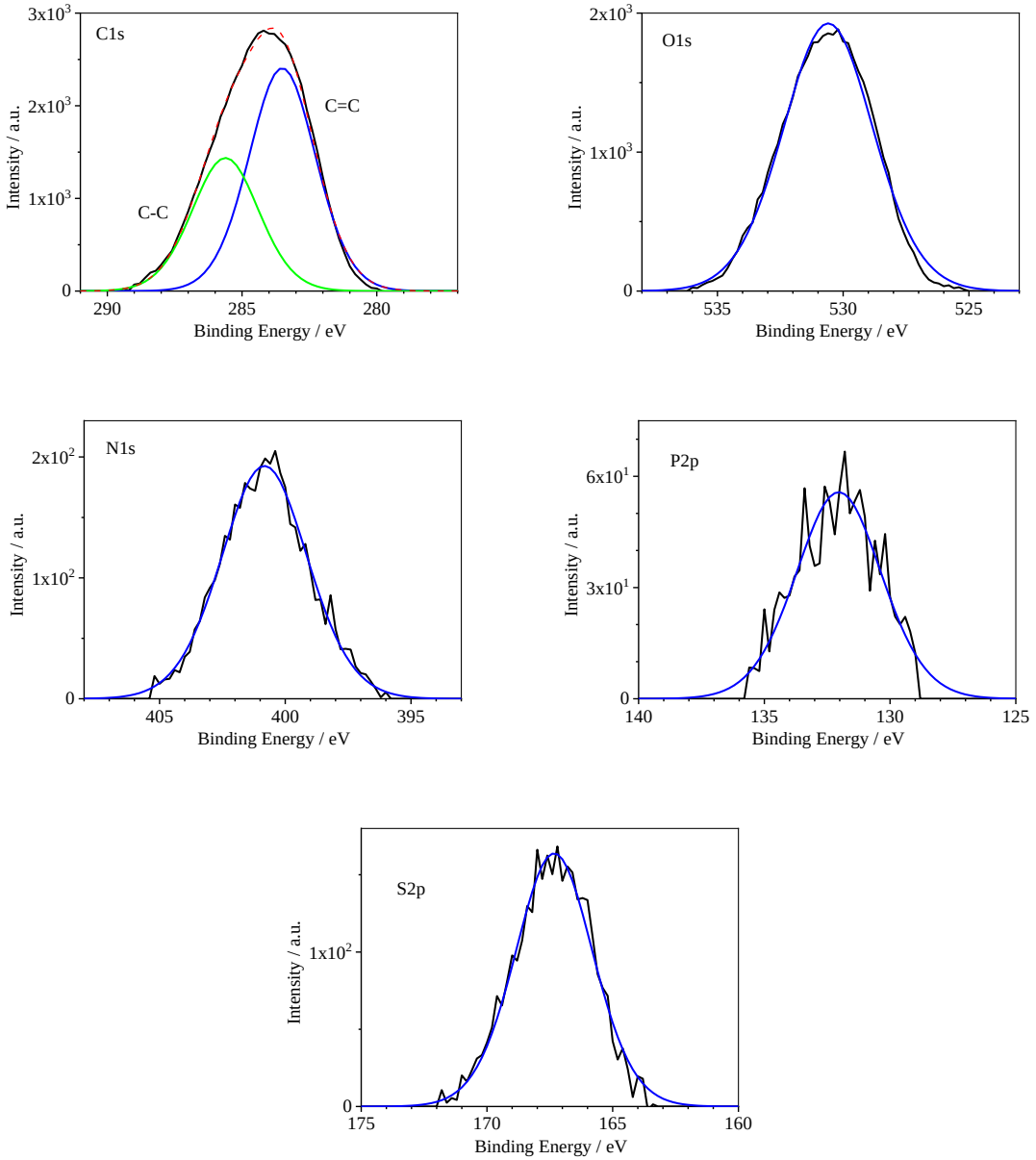

Figure 8.6: High resolution XPS spectra of titanium oxide surfaces coated with P(VSP_{64}-b-PA_{14}-b-TMA_{64}) with measured data in black and peak fitting in color.

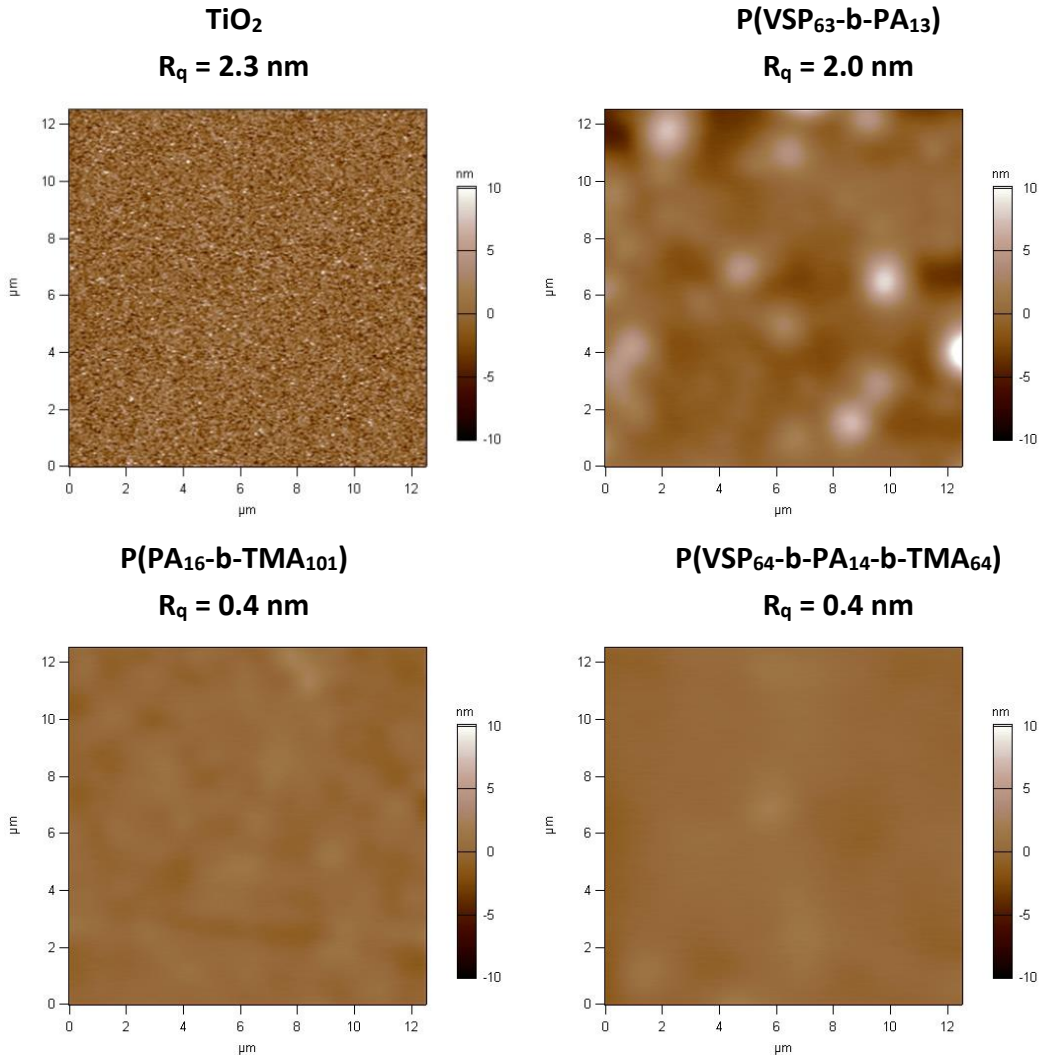

Figure 8.7: AFM images of native and coated substrate surfaces with root mean square roughness (R_q).

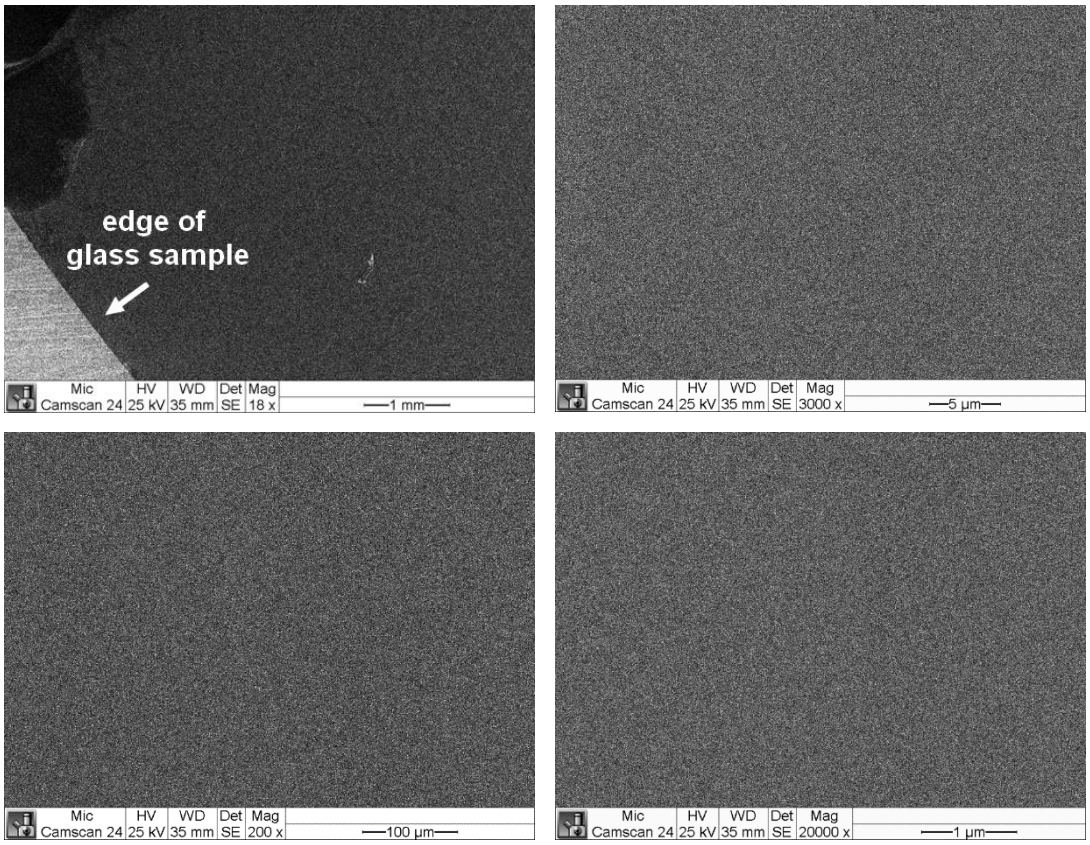

Figure 8.8: SEM images of sample coated with P(VSP_{64}-b-PA_{14}-b-TMA_{64}) at different magnifications (18x, 200x, 3000x, 20000x).